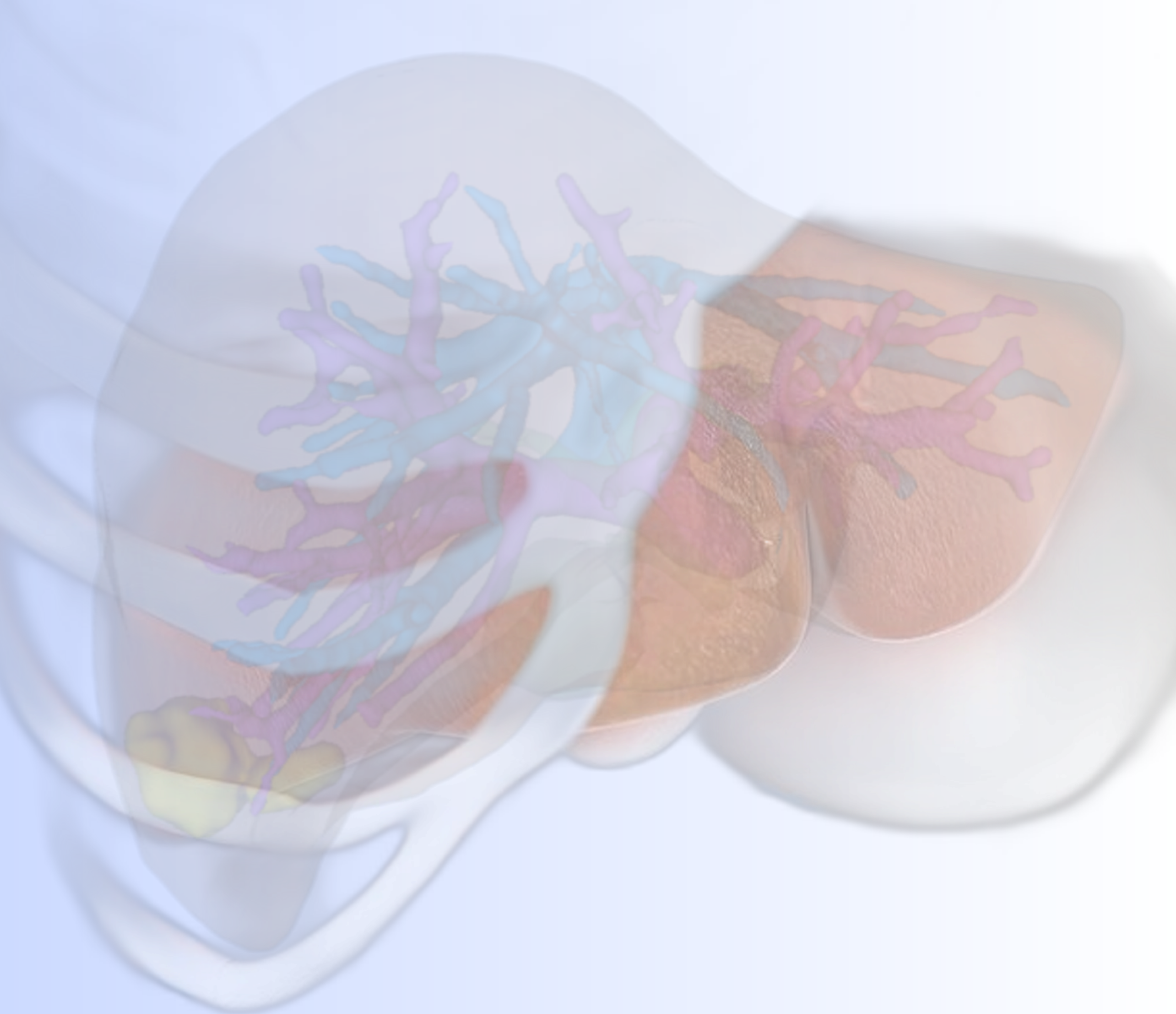

Evaluating surgeon experience to improve AR in liver surgery

Maaike Pruijt

Surgical oncology, Antoni van Leeuwenhoek Hospital
Master thesis Technical Medicine

September 2024

Evaluating surgeon experience to improve Augmented Reality in liver surgery

Maaike Pruijt

MSc Technical Medicine

Student number: 4670698

9 September 2024

Thesis in partial fulfilment of the requirements for the joint degree of Master of Science in *Technical Medicine*

Leiden University; Delft University of Technology; Erasmus University Rotterdam

Master thesis project (TM30004 ; 35 ECTS)

Department of Surgical Oncology, Netherlands Cancer Institute – Antoni van Leeuwenhoek (NKI-AvL)

December 2023 - September 2024

Supervisors:

Medical supervisors: MD, PhD K. Kuhlmann and MD, PhD J.S.D. Mieog
Technical supervisor: Dr. M. Fusaglia
Daily supervisor: K.A. Olthof, MSc

Thesis committee members:

Dr. Ir. T. van Walsum, EMC (chair)
MD, PhD K. Kuhlmann, NKI-AvL MD, PhD J.S.D. Mieog, LUMC, and
Dr. M. Fusaglia, NKI-AvL

An electronic version of this thesis is available at http://repository.tudelft.nl/

SUMMARY

Introduction Accurate intrahepatic anatomical localization remains challenging for laparoscopic liver resection (LLR) of patients with colorectal liver metastases (CRLMs). Image-guided surgery (IGS) systems utilizing augmented reality (AR) visualizations have been developed to assist in these procedures by projecting virtual models onto the laparoscopic view. However, AR visualization, often presented as a comprehensive model, requires improvements to achieve an effective and positive experience for surgeons. A user study was performed to develop and evaluate multiple AR and VR visualizations and identify the most promising and effective visualizations based on feedback from surgeons. Additionally, adapters with EM sensors are required to track the 30° laparoscopes and enable AR. The secondary objective was to develop and calibrate these adapters.

Methods Multiple visualizations, categorized into three classes, were developed and assessed on a phantom and patients. The user study consisted of two phases. Phase 1 focused on the development and evaluation of these visualizations. Feedback from three surgeons was gathered using a custom-made survey that assessed experience, effectiveness, and usability. Phase 2 involved evaluating clinical usage of the visualizations and their applications by showing videos of these tests to seven surgeons from two hospitals.

Results In Phase 1, five patients were included for AR-guided laparoscopic resection. Improvements were made compared to the gold standard whole liver model in AR experience, effectiveness, depth perception, and information balance. In Phase 2, the most promising visualizations from Class 1 were the depth shader and target structures visualization, both preferred by six surgeons. Additionally, all seven surgeons wanted the ability to augment a predefined virtual resection plan. For class 2, all seven surgeons found the US view promising and only one surgeon indicated they would use the virtual painter. Five surgeons indicated they would use the third-person and target view of class 3 during liver procedures. Furthermore, adapters with EM sensors were developed and calibrated to track the 30° laparoscopes and enable AR.

Conclusion AR is promising in liver surgery when surgeons can easily interpret the visualization and have a positive experience. To be effective, AR systems should accurately localize and define vessels and tumor margins, provide clear depth perception, and offer well-balanced information. Several aspects of AR visualization for the entire liver model have been improved. Future research should further improve these visualization aspects, implement non-rigid registration techniques and on-demand patient-specific activation of structures. These advancements can enable AR integration into the surgical workflow, enhancing precision and effectiveness.

ACKNOWLEDGMENTS

This thesis was my final project for the joint-degree Master in Technical Medicine with TU Delft, Leiden University Medical Center (LUMC), and Erasmus Medical Center (EMC). Throughout my master's journey, I followed the track imaging and intervention, combining medical knowledge with medical technology. I completed four hospital internships across various departments at LUMC, EMC, and NKI-AvL, after which I enthusiastically returned to NKI-AvL for my final project.

In the first place, I would like to thank my supervisors for their enthusiasm, time, and guidance throughout the period. Their support made my thesis experience both educational and also a lot of fun. Without them, I would not have achieved this result. I want to thank my daily supervisor, Karin, a clinical technologist. Her in-depth expertise in navigation during liver surgeries and constant availability for questions were invaluable throughout these months. I also wish to thank my technical supervisor, Matteo, a technical postdoc with extensive knowledge in Augmented Reality and the Unity software. His expertise was essential for this thesis, and his excitement about AR technology also helped to amplify my enthusiasm. Moreover, thanks go to my medical supervisors, Koert Kuhlmann and Sven Mieog, for their critical perspectives from a surgeon's point of view and for connecting me with other surgeons. Surgeon participation was important to bridge the gap between this novel technology and clinical relevance in my results. Finally, I am grateful to everyone in the research group "Group Ruers" for the enjoyable times, outings, and coffee breaks, which made my thesis a memorable and pleasant period.

Amsterdam, August 2024
Maaike Pruijt

List of Abbreviations

2D Two-dimensional.
3D Three-dimensional.
AR Augmented reality.
CRC Colorectal cancer.
CRLM Colorectal liver metastases.
CT Computed tomography.
ED Euclidean distance.
EM Electromagnetic.
FG Field Generator.
FOV Field of view.
ICG Indocyanine green fluorescence imaging.
IGS Image-guided surgery.
IOUS Intraoperative ultrasound.
LLR Laparoscopic liver resection.
MIS Minimally invasive surgeries.
MRI Magnetic resonance imaging.
NKI-AvL Netherlands Cancer Institute – Antoni van Leeuwenhoek.
RLR Robotic liver resection.
RMS Root Mean Squared.
SCU System Control Unit.
SD Standard deviation.
6DOF Six degrees of freedom
SIU Sensor Interface Unit.
US Ultrasound.
VR Virtual Reality.

CONTENTS

INTRODUCTION

1.1 Colorectal liver metastases

Colorectal cancer (CRC) is the third most common cancer and one of the major causes of cancer-related deaths worldwide, with approximately 1.9 million new cases and 0.9 million deaths reported in 2020 [1], [2]. Among these patients, colorectal liver metastases (CRLMs) occur in at least 50% of the cases [3]. The high incidence of CRLMs is mainly attributed to the liver's role in draining blood from the colon and rectum through the portal vein system, making it a primary site for metastases.

1.1.1 Diagnostics

CRLMs should be identified in patients with a confirmed diagnosis of CRC. Among them, synchronous CRLMs appear in approximately 10-15% of the patients, while the metastases may also develop in months, if not years, after treatment [4]. Therefore, extensive examination of the liver is advised. Standard diagnostics involves contrast-enhanced computed tomography (CT) with iodine contrast to enhance contrast-to-noise between healthy liver tissue and malignant lesions. However, lesions smaller than 10 mm can be missed on CT and may be difficult to distinguish from benign ones [5]. Magnetic Resonance Imaging (MRI) is often acquired for its high sensitivity in detecting liver lesions, especially smaller ones with diameters less than 1cm. At the Netherlands Cancer Institute – Antoni van Leeuwenhoek (NKI-AvL), multi-phase MRI sequences with a gadolinium-based hepatospecific contrast agent (Gd-EOBDTPA, Primovist) are routinely used for diagnostic imaging. This scan visualizes the complete hepatic vascular and biliary anatomy, including small lesions [6]. Furthermore, Positron-emission tomography using the radiotracer 18F-fluorodeoxyglucose can be performed with CT (18F-FDG PET/CT) to screen for extrahepatic tumor activity. However, this technique has limited resolution for detecting small lesions [5].

1.1.2 Liver anatomy

The liver, the largest internal organ of the human body, plays an important role in various physiological processes, including metabolism, immunity, digestion, detoxification, and vitamin storage. Its dual blood supply from the portal vein (approximately 75%) and the hepatic artery (approximately 25%) ensures efficient functioning [7]. This anatomical complexity is further described by the Couinaud classification, which divides the liver into eight distinct functional segments (Figure 1). Each liver segment has its vascular inflow via the portal vein and hepatic artery and outflow through the hepatic vein, as well as biliary drainage [8], [9]. This segmentation facilitates surgical procedures by delineating distinct regions within the liver, ensuring precise removal of tumors while minimizing damage to adjacent structures and reducing the risk of excessive bleeding [8], [9].

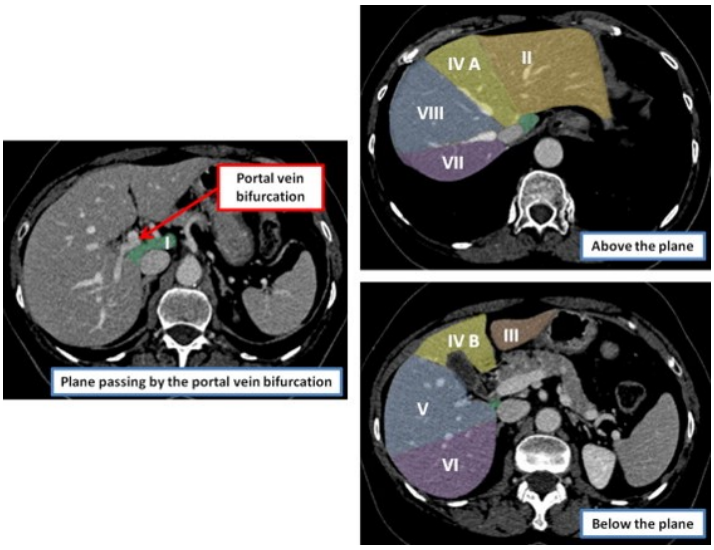

Figure 1: Couinaud's classification of eight liver segments on MRI-scan [8].

1.1.3 Minimal invasive surgery

For CRLMs, treatment decisions are determined based on the location and stage of the tumor. Treatment options include radiation, chemotherapy, resection, local ablation, or a combination of treatments. Surgical resection is the gold standard for patients with CRLM and has witnessed a shift toward minimally invasive surgeries (MIS) in recent decades. Since the first laparoscopic liver resection (LLR) in the early 1990s, it is rapidly increasing, and certain types of resection are considered standard procedures for liver resection [10], [11]. LLR includes various resection types, including wedge resections, segmentectomies, and hemi-hepatectomies. Wedge resections involve the removal of a small, wedge-shaped portion of the liver containing the tumor, with segmentectomies involving the removal of a larger segment of the liver containing the tumor along with its corresponding vascular and biliary structures [12].

LLR offers numerous patient benefits compared to open liver resection. The smaller incisions result in shorter hospital stays and recovery times, reduced morbidity, less intraoperative blood loss, and better cosmetic outcomes [10], [11], [13]. However, LLR presents several technical challenges. The two-dimensional (2D) laparoscopic view lacks depth perception of the liver's complex three-dimensional (3D) anatomy and removes tactile feedback of liver parenchyma [14]. Additionally, LLR faces issues related to operating space, the small field-of-view, and suboptimal viewing angles of the scope [15]. Robotic liver resection (RLR) addresses some challenges of LLR, such as the incorporation of wristed instruments and tremor removal, which enhance dexterity compared to LLR [15]. Nevertheless, both LLR and RLR have limitations in palpating the liver parenchyma and interpreting its 3D anatomical context during surgery. Therefore, complex cases like deep-seated tumors involving major blood vessels or multiple tumors in both liver lobes are usually performed with open surgery instead of MIS. Overcoming these challenges could enable more complex surgeries to be performed laparoscopically.

1.1.4 Intraoperative guidance during laparoscopic surgery

To address the challenges of LLR, it is necessary to support accurate tumor localization to achieve negative resection margins and spare healthy liver parenchyma, bile ducts, and vessels. Intraoperative ultrasound (IOUS) is considered a "gold standard" for detecting liver tumors, resection margins, and guiding surgical procedures [16]. At the NKI-AvL, surgeons use IOUS in combination with diagnostic imaging to determine tumor borders on the liver surface and mark them with diathermy before resection. However, accurately determining deep resection margins remains challenging with IOUS, because it is limited by its low resolution, reduced sensitivity post-ablation or chemotherapy, and 2D representation of the liver's complex 3D anatomy. Additionally, distinguishing tumors that appear isoechoic from healthy tissue is challenging [17], [18]. An alternative technique, indocyanine green (ICG) fluorescence imaging, offers potential advantages by enabling real-time visualization of tumor borders and resection boundaries during surgery. Despite these benefits, ICG fluorescence is not used at the NKI-AvL. It has a high false-positive rate and limited tissue penetration (5-10 mm), which restricts its effectiveness in visualizing deeply located tumors [19], [20].

Image-guided surgery (IGS) addresses these challenges. An IGS system is already implemented as standard clinical practice at the NKI-AvL during open procedures, and this workflow is emerging toward clinical implementation in a laparoscopic setting. It offers a virtual representation of the surgery, displaying the intraoperative situation and the surgical instruments in spatial relation to a patient-specific virtual model of the organ. This aids the surgeon in better lesion localization and visualization of surrounding anatomical structures, thus supporting decision-making during surgery.

1.2 Image-Guided Liver Surgery

The IGS workflow involves four main steps: reconstructing a 3D virtual model, tracking the instruments, performing registration, and visualizing the virtual representation of the surgery.

1.2.1 3D model reconstruction

The interactive 3D models used in IGS are manually [11], [21] or automatically [6], [13] delineated from diagnostic CT or MRI scans (See Figure 2).

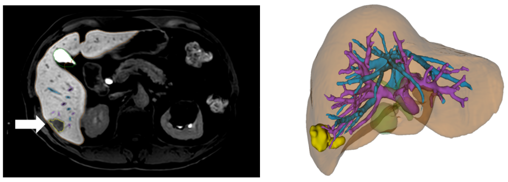

(a) Diagnostic MRI-scan including a CRLM in the left liver lobe (white arrow).

(b) Reconstructed virtual model including anatomical structures, based on MRI-scan.

Figure 2: 3D model reconstruction. The liver is brown, the tumor is yellow, the gallbladder is green, the hepatic artery is blue, and the portal vein is purple.

1.2.2 Tracking

Tracking enables the real-time alignment of the diagnostic model with the surgical environment. It precisely determines the position and orientation of surgical instruments within a known coordinate system [22].
Two primary methods used for tracking are optical and electromagnetic (EM) tracking. EM tracking measures the magnetic field strength at precise locations, generated by a field generator (FG). EM sensors attached to the surgical instruments create disturbances in this magnetic field, allowing the instruments to be accurately localized. In contrast, optical tracking identifies the pose of a tracked instrument by measuring light emitted or reflected by the instruments, typically achieved through infrared reflecting markers attached to the instruments [23], [24].

Furthermore, recent studies have shown that self-localization systems, such as simultaneous localization and mapping tracking [14], can be used for camera position tracking. These systems operate autonomously, without relying on external signals like EM fields or visual markers, and instead utilize internal sensors.
EM tracking is preferred for flexible laparoscopic IOUS probes [25], however, the main drawback of EM tracking is its sensitivity to ferromagnetic interference, which can occur in environments with metallic objects or electronic components. This interference can disrupt the tracking accuracy, leading to potential errors in instrument localization [23]. Optical tracking faces challenges due to line-of-sight issues [23], making it difficult to track the distal end of instruments during MIS, because they operate inside the abdominal cavity.

In the current workflow at the NKI-AvL, EM tracking is integrated into the surgical procedures for open surgery, and this integration is progressing toward clinical implementation in laparoscopic settings. To generate the EM field, a planar FG (Figure 3a) is used, and signals from the six degrees of freedom (6DOF) EM sensors (NDI, Waterloo, ON, Figure 3b) are amplified and digitized by a Sensor Interface Unit (SIU) (Figure 3c) [26]. The System Control Unit (SCU) controls the FG and collects information from the SIUs. It calculates the position and orientation of each sensor and connects with the computer (Figure 3d). The EM sensors are integrated into a surgical pointer and adapters, attached to the IOUS probe and the laparoscope. These adapters have a reproducible and calibrated positioning on the instruments. An EM sensor is also attached near the liver lesion to track its position during surgery. This sensor minimizes navigation errors during surgical manipulation and compensates for intraoperative organ deformations [27].

(a) The Aurora NDI planar 20-20 low-intensity electromagnetic (EM) field generator (FG).

(b) 6DOFs, including Positional data (X, Y, Z) and rotational data (roll, pitch, and yaw).

(c) Sensor Interface Unit (SIU), to amplify and digitize the signals from the EM sensors.

(d) System Control Unit, to control the FG and collect information from the SIUs to the computer.

Figure 3: Components used during Electromagnetic (EM) tracking of surgical instruments [26].

1.2.3 Registration

Registration is performed after tracking has determined the positions and orientations of the liver, laparoscope (Chapter 3), and instruments within a coordinate system. It involves transforming data coordinates from one coordinate system to another to align the preoperative 3D model to the tracking coordinate system. Registration during liver surgery is a challenging step that significantly affects navigation accuracy. This is due to the absence of fixed rigid landmarks and due to the non-rigid deformations of the liver caused by respiratory and cardiac motions, as well as increased intra-abdominal pressure from the pneumoperitoneum and surgical manipulation [25].
At the NKI-AvL, a landmark-based registration approach was proposed to align the virtual and

real anatomy. During this approach, both internal and external landmarks are selected. For LLR, external landmarks (e.g., distinctive liver ridges) are indicated by the tracked pointer on the laparoscopic video screen and matched with corresponding locations of a diagnostic liver model in the IGS software. Subsequently, internal landmarks (e.g., vessel bifurcations) from the virtual model are matched with corresponding landmarks on the IOUS in the IGS software. This software obtains the indicated coordinates through active tracking of the IOUS and aligns the coordinates of both the real liver and virtual liver within the IOUS's coordinate system. This alignment results in a screen that displays tracked instruments, the IOUS, and the model (Figure 4).

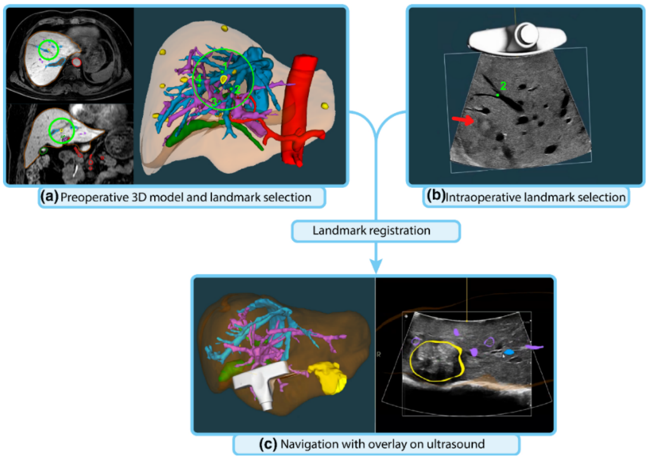

Figure 4: Internal landmark-based registration workflow at the NKI-AvL [22]. Additionally, external landmarks (e.g., distinctive liver ridges) are used for registration during LLR.

1.3 Augmented Reality

1.3.1 Navigation workflow

Various methods exist for the visualization of surgical liver navigation. The use of the laparoscopic video camera not only enables the integration of virtual reality (VR) on a separate screen (Figure 4) next to the US and laparoscopic view but also allows the implementation of Augmented Reality (AR) onto one integrated screen within the workflow, thereby reducing focus switching for the surgeon. AR involves the real-time superimposition of the virtual world directly onto the real surgical field. Figure 5 shows a schematic overview of all transformations required for AR navigation.

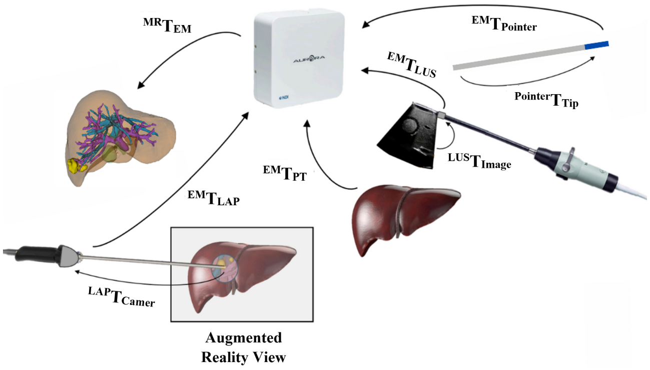

Figure 5: Schematic overview of all transformations required for navigation. The real and diagnostic liver, the laparoscope, the US, and the pointer contains an EM sensor and were tracked and aligned within the same coordinate system [28]

A virtual environment is developed in the software Unity 3D (Unity Technologies, US, version 2022.3.13f1) for visualizing the surgical instruments, virtual model, and laparoscopic video in a virtual 3D coordinate system. Unity is a software commonly used for creating video-games and is also employed for AR applications. The software connects with the NDI Aurora tracking system using a software called NDI Track. The 30° laparoscopic view is then integrated into the environment, and the position and orientation of the laparoscope in 3D space are measured in real-time by tracking the EM sensor and incorporating the extrinsic camera parameters. The virtual object scene, which includes a liver and the tracked instruments, is merged with the real laparoscopic video view (Figure 6). This object scene is captured by a virtual laparoscope whose intrinsic parameters are the same as those from the laparoscope used during surgery (Figure 7). Both intrinsic- and extrinsic parameters are determined as described in Chapter 3.

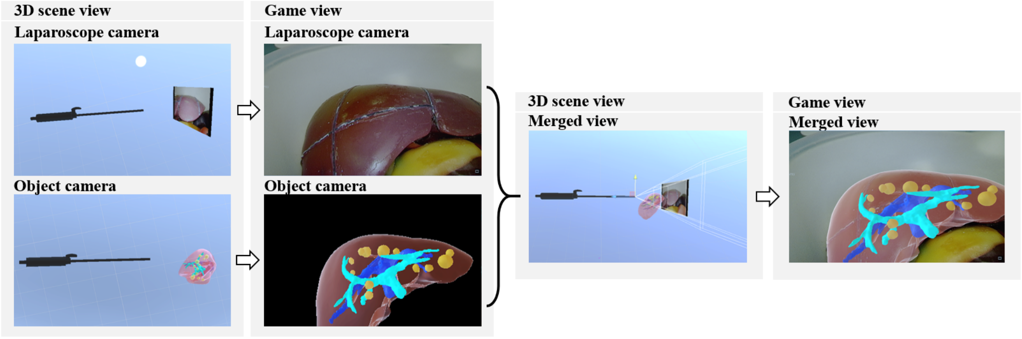

Figure 6: A laparoscopic camera view and virtual object camera view including a liver model are merged to enable AR within one integrated view.

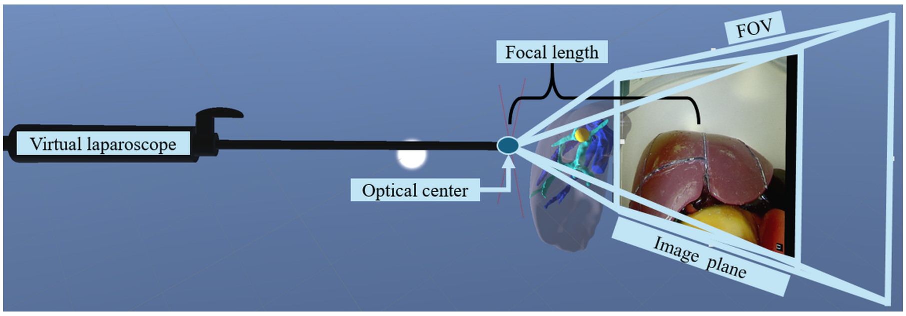

Figure 7: Virtual representation of laparoscope, laparoscopic image plane, optical center, focal length, and field of view (FOV). The focal length and FOV of the virtual laparoscope are the same as those of the surgical laparoscope.

In addition to these views, Unity includes a hierarchy window to list all models and cameras, a project window to show all folders and assets, and an inspector window to display properties of selected objects. It also provides play and pause controls and tools for transforming, scaling, and rotating objects in the scene. All components are shown in Figure 8. Furthermore, C# scripts can be created to automate steps, make shader effects, control the models and cameras, or implement custom functionality.

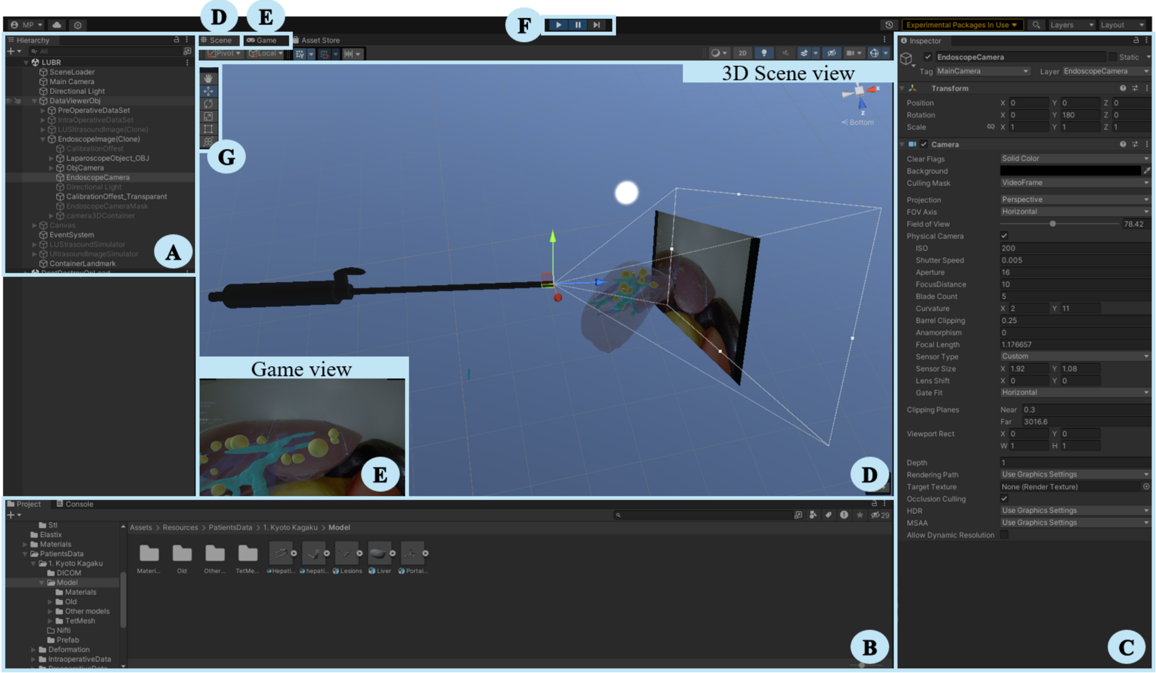

EndoscopeCamera Static
Tag MainCamera Layer EndoscopeCamera

Transform
Position X 0 Y 0 Z 0
Rotation X 0 Y 180 Z 0
Scale X 1 Y 1 Z 1

Camera
Clear Flags: Solid Color
Background
Culling Mask: VideoFrame
Projection: Perspective
FOV Axis: Horizontal
Field of View: 78.42
Physical Camera: ✓
ISO: 200
Shutter Speed: 0.005
Aperture: 16
FocusDistance: 10
Blade Count: 5
Curvature: X 2 Y 11
Barrel Clipping: 0.25
Anamorphism: 0
Focal Length: 1.176657
Sensor Type: Custom
Sensor Size: X 1.92 Y 1.08
Lens Shift: X 0 Y 0
Gate Fit: Horizontal
Clipping Planes: Near 0.3 Far 3016.6
Viewport Rect: X 0 Y 0 W 1 H 1
Depth: 1
Rendering Path: Use Graphics Settings
Target Texture: None (Render Texture)
Occlusion Culling: ✓
HDR: Use Graphics Settings
MSAA: Use Graphics Settings
Allow Dynamic Resolution: ☐

Figure 8: Unity scene components. (a) A hierarchy window listing all models, instruments, and the laparoscopic and virtual camera. (b) Project window listing all folders and assets. (c) An inspector window to display the settings and properties of selected objects. (d) 3D Scene tab for visualization and interaction with the virtual environment. (e) Game tab, representing the surgeon's perspective. (f) Play and Pause controls. (g) Tools for transforming, scaling, and rotating objects in the scene.

1.3.2 AR visualization options and benefits

To investigate the state-of-the-art AR visualizations during liver surgery and identify the potential benefits, current limitations, and future recommendations for improving AR visualization, a literature review was conducted before this study [29] (Appendix A). The review indicated that AR visualizes anatomical structures (lesions, vessels, and bile ducts) normally hidden within the depth of the liver parenchyma onto the laparoscopic video. Additionally, AR can localize disappearing [30], deeply seated [31], or small liver lesions, broadening surgical options for previously undetectable lesions [32]. Furthermore, AR may improve the surgeon's confidence in decision-making without focus-switching [24], [29], [33], [34].

AR can be visualized as a virtual model overlaid onto the laparoscopic video (Figure 9a-9e) [30]–[32] or as a virtual representation of the surgical instruments [35], [36] (Figure 9f-9g). Moreover, a visualization of VR onto the laparoscopic screen that shows the liver (in the example game objects) from a side perspective or tumor-to-instrument distances was found in literature [27] (Figure 9h-9j).

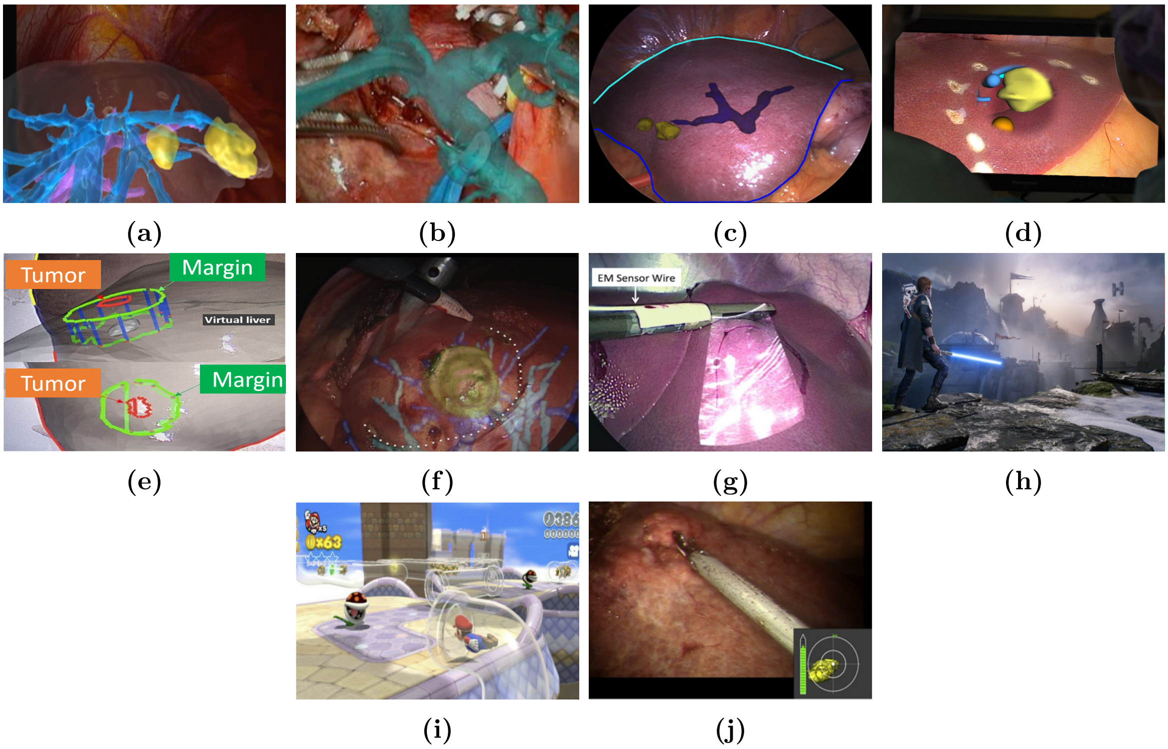

Figure 9: Intraoperative Augmented Reality visualizations [29]. (a) Whole liver model at the NKI-AvL, (b-c) Target vessel(s) and lesion [31], [32]. (d) Window view [30], (e) Resection plan visualization [37], (f) A surgical pointer draws a virtual resection plan onto the liver surface [35], (g) virtual US overlay [36], (h-i) Third person view to enhance depth perception and spatial awareness for interactions with the environment [38]. (j) Virtual Reality projected onto the laparoscopic screen visualizes tumor-to-instrument distances within a bull's eye [27].

1.3.3 Pitfalls of AR

AR in LLR is not standard of care, primarily due to challenges in achieving accurate AR of a deformable liver and limitations in AR visualization. AR should provide additional information about the patient's anatomy or the surgical plan without degrading the surgeon's view. However, an overload of information is visualized in the most common AR visualization of the entire liver model (Figure 9a) [39]. Additionally, projecting a 3D model onto the 2D laparoscopic view causes the occlusion of structures and instruments, and limits depth perception of objects that are close or distant from the perspective view [24], [40]–[42]. This affects the surgeons' interpretation and experience of AR, potentially leading to ineffective localization of anatomy, tumor margins determination, and resection planning.

1.4 Research objectives

For patients with CRLMs, a navigation workflow at the NKI-AvL is emerging towards clinical implementation in a laparoscopic setting, where the video screen can be used to superimpose AR. AR can give the surgeon real-time improved comfort about the localization of anatomical structures within the liver parenchyma in an already known view. However, improvements in visualization are required to achieve an effective and positive experience for surgeons before it can be implemented in the navigation workflow. The following objectives need to be accomplished:

1.4.1 Primary objective

The primary objective of this thesis is to improve the AR visualization projected onto the laparoscopic video during LLR at the NKI-AvL, aiming to augment rather than degrade the surgeons' perception of the surgical scene. A user study was performed to develop and evaluate multiple AR visualizations of virtual models, AR information from tracked instruments, and VR integration, based on feedback from surgeons (Chapter 2).

1.4.2 Secondary objective

To enable AR during LLR, tracking of the position and orientation of the 30° laparoscope in the EM field is required. The secondary objective of this thesis is tracking the 30° laparoscopes used in this hospital, by developing and calibrating adapters containing EM sensors (Chapter 3).

2.1 Introduction

The surgeon's experience is important for the successful improvement and implementation of AR in liver surgery. Various AR and VR visualizations investigated in literature (Appendix A and Figure 9) and the gaming industry were developed and compared to assess their effectiveness for surgeons in guiding liver resections. This user study assessed multiple developed AR and VR visualizations based on surgeon's feedback to evaluate them on several visualization aspects (Phase 1) and identify the most promising and effective visualizations (Phase 2).

2.2 Methods

2.2.1 List of requirements

A list of the most important requirements for AR and VR visualizations was created based on the current visualization limitations (Table 1, Section 1.3.3). This list could subsequently be used for visualization development and evaluation.

Table 1: The requirements for AR and VR visualization

No.	Requirement	Explanation
1.0	Easy interpretation	The visualization should be easy to interpret (intuitive) without extensive explanation.
2.0	Positive experience	The surgeon's experience with the visualization should be positive.
3.0	Effective	The visualization should be effective in: • Localization of hidden structures within the liver parenchyma. • Determination of tumor margins to accurately resect tumor tissue. • Determination of the resection plan to spare healthy tissue.
4.0	Depth perception	The visualization should provide clear depth perception: • Objects should not occlude each other. • There should be a clear understanding of the order and perspective of the real and virtual models in the augmented scene. • Use of depth cues such as shadows, semi-transparencies, shaders, and colors should enhance depth perception.
5.0	Information balance	The visualization should balance displaying sufficient information without overwhelming the user with excessive data.

2.2.2 Visualization development

Based on the literature (Appendix A) and the requirements of Table 1 nine visualizations for liver navigation were developed. Three classes were identified to categorize the visualizations: AR of virtual anatomic models (class 1), interaction with tracked instruments (class 2), and VR (class 3). See Table 2 for a detailed overview of the visualization classes.

Table 2: Included visualization classes

Visualization	**Explanation**	**Example**
Class 1. Augmented Reality of virtual anatomical models		
Whole liver model (gold standard)	Semi-transparent visualization of all hepatic structures (parenchyma, vessels, gallbladder, bile duct, and lesion(s)) in different colors superimposed onto the laparoscopic scene. [21].	Fig. 9a
Target lesion and vessel(s)	Visualization that highlights the target lesion and important vessels near the lesion, aimed to reduce information overload [31], [32].	Fig. 9b-9c
Window view	Window mask within the camera's field of view, which allows for displaying only the anatomical structures within the surgeon's focal range [30]. This approach aims to enhance depth perception and reduce information overload.	Fig. 9d
Hole view	Visualization of holes in the virtual model, aiming to enhance depth perception of the lesions and vessels concerning the liver surface.	-
Resection plan	Visualization of the resection margin or plan. For this visualization, preoperative discussions with surgeons were held to assess which resection approach is preferred (e.g. a diamond, chip, or cake-shaped resection) [37].	Fig. 9e
Class 2. Instrument interaction*		
Painter resection plan*	Tool to draw a virtual resection plan directly onto the liver surface using a tracked surgical pointer. This method replaces the traditional diathermy technique, where the surgeon marks the resection plan onto the tissue [35].	Fig. 9f
US view	Projection of the US image onto the laparoscopic video image, corresponding with the actual location of the US probe. This aims to reduce focus switching between the US and laparoscopic view and enhance depth perception [36].	Fig. 9g
Class 3. Virtual Reality		
Third-person view*	Additional third-person camera view allows visualization of the patient's anatomy from a virtual side camera perspective to provide more depth perception. This third-person view is commonly used in video-games to expand information about the 3D scene [38].	Fig. 9h-9i
Target view*	Target view with a camera perspective from the pointer's tip, allowing for an assessment of the distance between the tumor and the instrument. This view aims to improve the surgeon's ability to locate lesions accurately and establish safe tumor margins [27].	Fig. 9j

***Comment 1**: In class 2, the virtual US and pointer registration do not consider tissue motion and deformation because they are independent of 3D models.

***Comment 2**: The virtual painter, the third-person- and the target views are intended to be combined with the AR views. The US view can be displayed separately or together with the virtual models.

2.2.3 Qualitative evaluation

The study evaluation was divided into two phases.
Phase 1: Prospective Surgeon Evaluation on AR and VR Visualization aspects
Phase 1 involved a prospective evaluation of AR and VR visualization aspects and was conducted over 5 months (from March to July). This Phase included 1) phantom tests and 2) a patient study for evaluation. In both approaches, the AR and VR visualizations of the virtual liver model were overlaid on a laparoscopic video screen.

In the phantom experiments, all nine visualizations were displayed to three hepatobiliary surgeons from the NKI-AvL (two men and one woman) in a single session per surgeon within a simulated clinical operation room setting (Left Figure 10). The experiments used the 'IOUS-FAN' phantom (Kyoto Kagaku Co., Ltd, Kyoto, Japan), including abdominal organs to provide a realistic experience. The liver of this phantom includes a hepatic vein, portal vein, and several superficial and deep-located tumors.
For the patient study, a prospective patient study researching AR-guided LLR was conducted at NKI-AvL after approval from the Medical Ethics Review Committee. For each patient undergoing LLR in this phase, two to three of the nine developed visualizations were chosen and visualized on the laparoscopic screen. One to three surgeons at the NKI-AvL evaluated them per procedure. See Figure 10 (right image) for the clinical setup.

A phantom/patient-specific 3D model was automatically segmented from CT or MRI and modified in the software 3D Slicer (https://www.slicer.org/, version 5.0.3) [6]. A registration process was performed as mentioned in section 1.2.3 and visualized in a virtual environment in Unity as described in section 1.3.1.

A custom-made 5-item qualitative survey was used to evaluate the surgeons' visualization experience, effectiveness, and usability (Appendix B.1). Since, as far as is known, no validated user experience and usability questionnaires existed for AR visualization in LLRs, this survey was designed to integrate all visualization requirements according to a Likert scale (1-5) (Table 1). The survey was administered at multiple points throughout Phase 1 to refine the visualizations. Only the most recent evaluations were included in the final analysis, regardless of whether they were from clinical or phantom tests.
The three classes were compared separately to ensure a fair comparison. For class 1, the different variable was the virtual model, with the whole liver model overlay used as the baseline visualization (Figure 9a). Classes 2 and 3 were more challenging to compare but were combined based on their class.

Furthermore, it is important to note that this study focused on visualization improvement and did not address accurate alignment. Therefore, the alignments of the overlays were optimized through manual adjustments, as misalignment complicates visualization assessment.

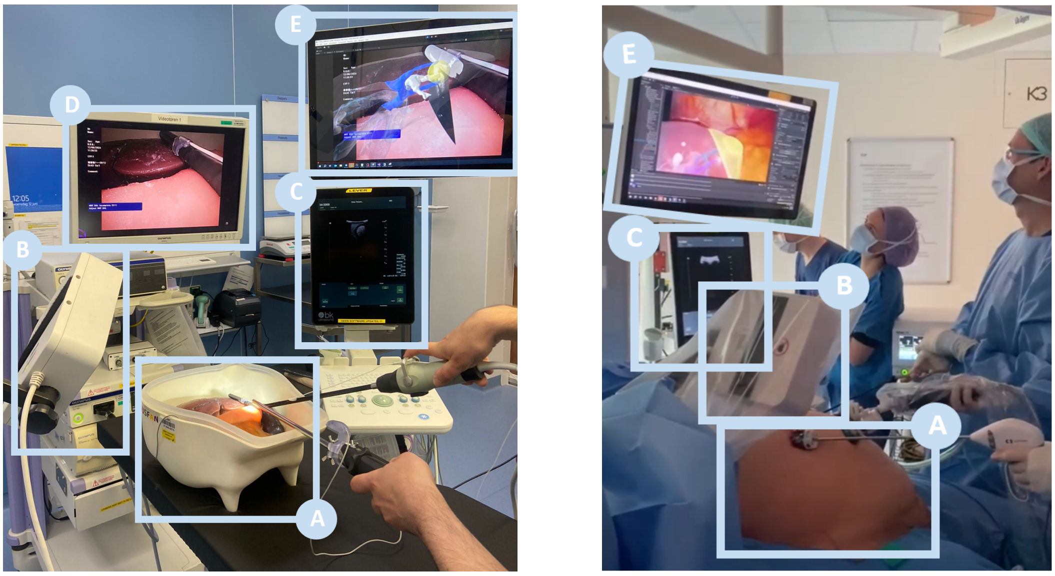

Figure 10: Simulated operation room (left image) and clinical (right image) set-up to test AR and VR visualizations in Phase 1: (a) Liver phantom simulating the patient (left image) and real patient (right image). (b) Planar Field Generator. (c) Ultrasound system. (d) Laparoscopic video screen. (e) Navigation trolley including AR visualization in the Unity game view.

Phase 2: Surgeon evaluation of clinical use and potential

Phase 2, conducted at the end of the study, focused on evaluating the clinical use and potential of the AR and VR visualizations. This phase involved presenting videos from Phase 1 assessments to seven surgeons across two hospitals. A custom-made survey evaluated the surgeons' preferences regarding the most promising visualizations, assessed the potential usage of these visualizations, and identified possible applications for them. Additionally, the surgeons rated the most important anatomical liver structures to visualize during AR using a Likert scale ranging from 1 to 3 (Appendix B.2). The participants included three hepatobiliary surgeons and two fellows from NKI-AvL, comprising two men and three women. Additionally, three hepatobiliary surgeons from Leiden University Medical Center (LUMC), all men, participated.

2.3 Results

2.3.1 Included patients

Five patients were included for AR-guided LLR. Table 3 shows the included patient characteristics.

Table 3: Patient characteristics

Patient	Sex	Age (y)	No. of Lesions	Segment lesion(s)	Largest Diameter Lesion(s) (mm)	Procedure	Visualizations Evaluated
1	Male	58	2	VI	14, 24	Segmentectomy	Whole liver model, target lesions and vessels and US overlay
2	Female	74	1	III	53	Segment II-III Resection	Target lesion and vessels with resection plan, and virtual painter
3	Male	69	1	III	25	Segment II-III Resection	Target lesion and vessels, hole view, and target view
4	Male	73	1	VII	15	Wedge Resection	US as VR and depth shader
5	Female	51	2	III, VII	11, 12	Two wedge resections	Window view and depth shader

2.3.2 Class 1: AR of virtual anatomical models

Phase 1

All developed visualizations of this class were shown in Figure 11. Questionnaire results of the first phase can be found in Figure 12. This figure shows that all visualizations were easy to interpret (mean score of 4.6 out of 5.0), provided a positive experience for surgeons (mean score of 3.7), and effectively localized anatomical structures (mean score of 3.6). The visualization specifically depicting vessels toward the tumor received the highest scores for experience and localization (4.0 for both components). However, this visualization and the whole liver model overlay posed challenges in determining tumor margins and planning resections, with both visualizations scoring 1.7 and 2.3 on these aspects. Visualization of the resection plan received higher scores on these aspects (Scores of 3.3 and 3.3, respectively), as could a hole view (3.5 and 3.0, respectively). Depth perception when visualizing the whole liver model, the target structures, or an additional resection plan was scored low (1.3, 2.0, and 2.0, respectively), however, the hole view showed a better depth perception, especially between the liver surface and lesions (Score of 4.0). The target structures view (score 3.5 out of 5.0) and the hole view (score 4.0 out of 5.0) provided the best information balance.

The lack of depth perception between superficial and deeply-seated vascular structures (Figure 13a) was addressed by developing a new shader in C# (Appendix C.1) and testing it in a clinical setting. This shader transitions from less transparent to transparent and light to dark based on the distance from the camera center to the virtual model (Figure 13) [43].

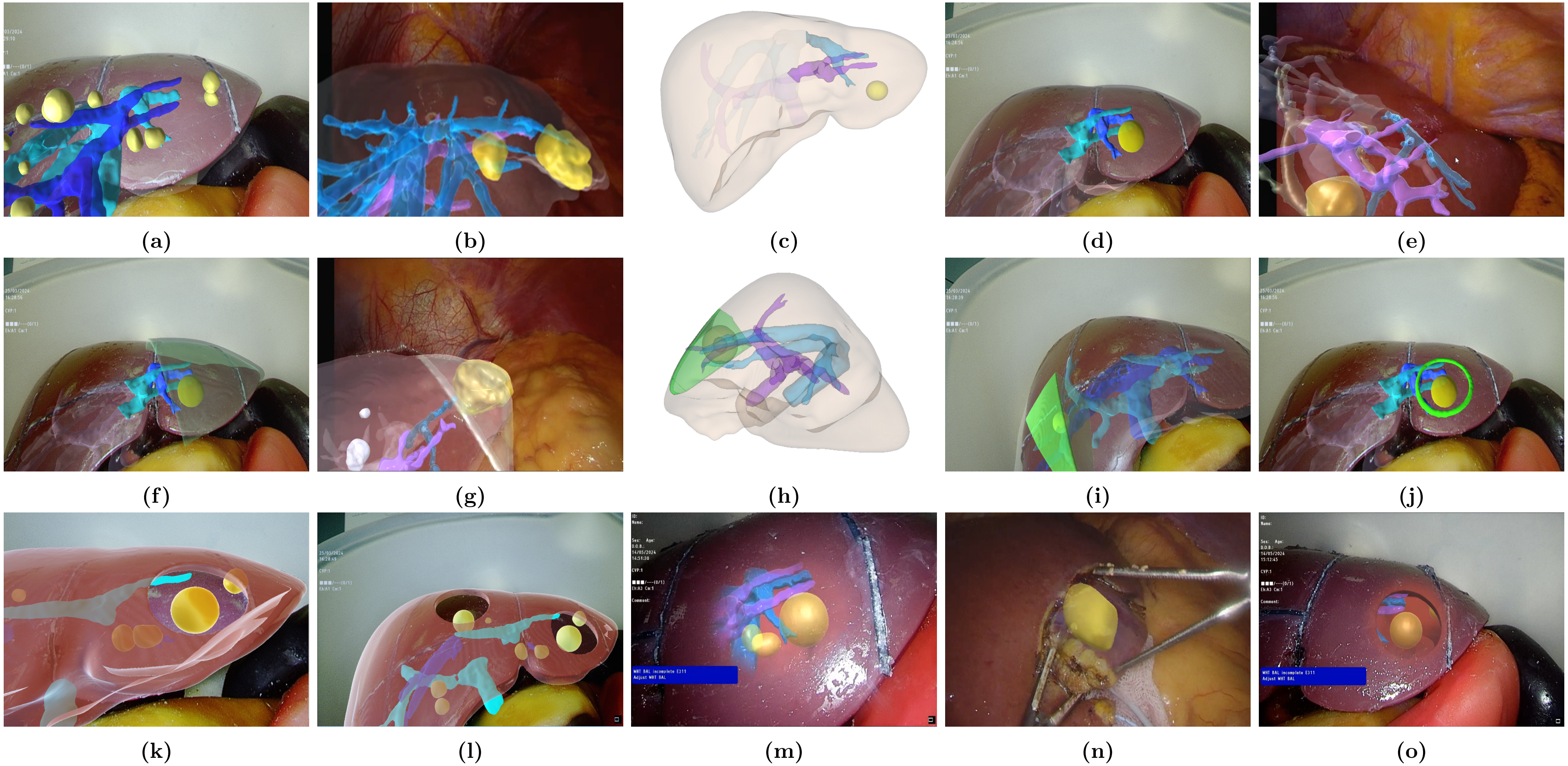

(a) (b) (c) (d) (e)

(f) (g) (h) (i) (j)

(k) (l) (m) (n) (o)

Figure 11: Visualizations of class 1: Augmented Reality of virtual anatomical models. Veins in blue and purple and tumors in yellow. (a) The gold standard whole liver model is visualized during phantom tests and (b) during surgery, showing an overload of information and lack of depth perception between structures, making resection planning difficult. (c-d) 3D Slicer scene and phantom test visualization of the vessels to segment II-III. (e) Clinical test of patient 3. The vessels to the CRLM in Segment III are less transparent than the whole vessel model aimed at reducing information overload. (f) Phantom test of a visualized resection plan for a CRLM located at the tip of the liver (segments II-III). Only the vessels to segments II-III are visualized to reduce information overload. (g) The same case was tested during LLR on patient 2. (h-i) Phantom test of a patient with a cake-shaped resection of a CRLM in segment V. (j) Resection plan visualized on the surface without depth information. A diamond-shaped visualization is more effective due to rigid surgical instruments. (k-l) Holes created in the liver surface enhance depth perception between the liver surface and lesions. (m) Window visualization [30] to reduce information overload in phantom and (n) in a clinical setting on patient 5 during a wedge resection of segment III. (o) Window view combined with a hole in the liver surface, aimed to enhance depth perception and reduce information overload. However, the surgeons lost their overall perspective in the window views.

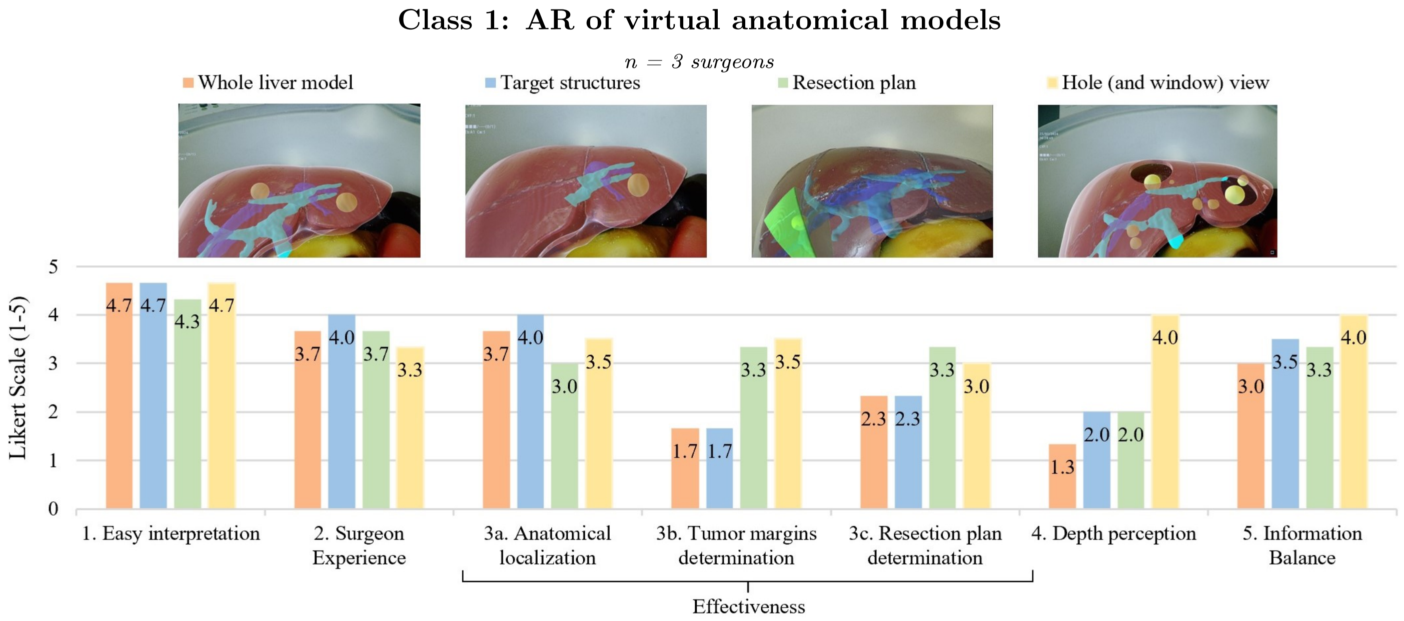

Figure 12: Results of the custom-made qualitative survey for Class 1 visualizations in Phase 1.

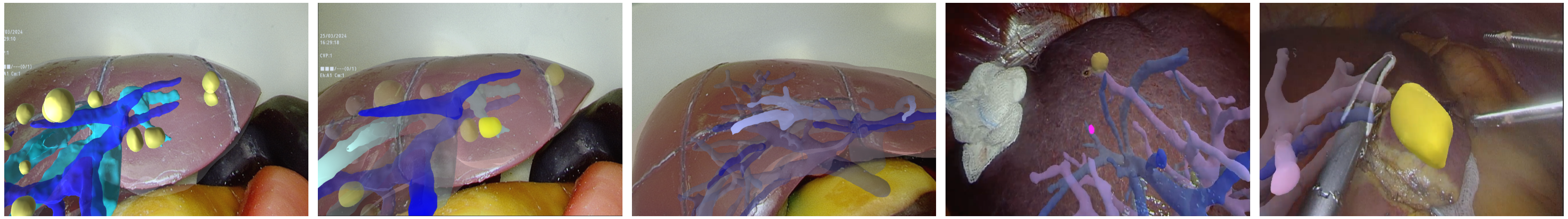

(a) (b) (c) (d) (e)

Figure 13: Further depth perception improvement. The hepatic vein is light blue or purple, the portal vein is dark blue, and the lesions are yellow. (a) Standard shader with limited depth perception. (b) A depth shader was created and tested on the phantom. The shader transitions from less transparent to transparent and light to dark based on the distance from the camera center to the 3D model. (c) The depth shader was tested on a phantom with the vessel model of patient 4. (d) The depth shader was validated in a clinical setting on patient 4, who was positioned in the left lateral position with a tumor in segment VII, and (e) on patient 5 in the supine position during a wedge resection of a CRLM in segment III.

Phase 2

The survey conducted in the second phase showed that the most promising visualizations of class 1 were the depth shader (Figure 13) and target structures visualization (Figure 11c- 11e), both chosen by six surgeons (Figure 14a). Two surgeons were interested in the whole liver view (Figure 11a-11b) and hole view (Figure 11k-11l), while none found the window view appealing (Figure 11m-11n). Additionally, all seven surgeons wanted the ability to activate the resection plan during surgery (Figure 11f- 11j). All surgeons noted that they would use the anatomical virtual models during LLR, and two surgeons would also use it during ablation (Figure 14b). The tumor (maximum score of 21), vena hepatica (score of 20), vena porta (score of 20), and bile duct (score of 19) received the highest scores for visualization importance during AR in liver surgery (Figure 15).

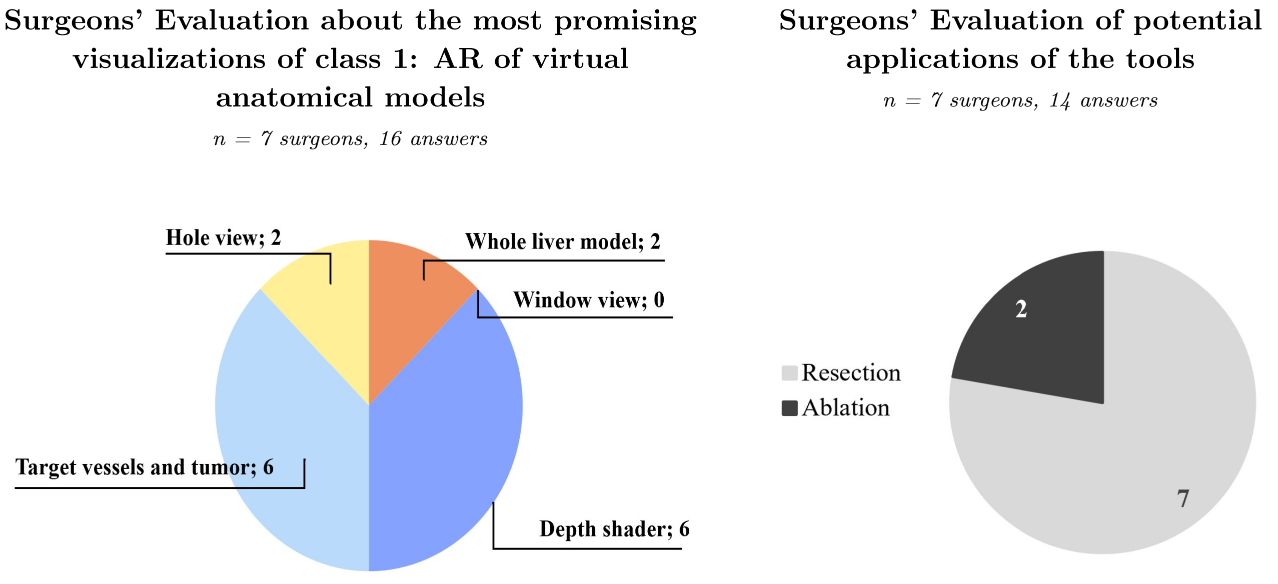
Surgeons' Evaluation about the most promising visualizations of class 1: AR of virtual anatomical models

n = 7 surgeons, 16 answers

Surgeons' Evaluation of potential applications of the tools

n = 7 surgeons, 14 answers

(a) (b)

Figure 14: Results of Phase 2. (a) Most promising visualizations of class 1. Furthermore, all 7 surgeons would like to visualize an additional resection plan. (b) Potential applications of AR of virtual anatomical models. The pie chart shows the distribution of answers for each application where 'yes' (1) indicates interest and 'no' (0) indicates no interest in the tool for that application.

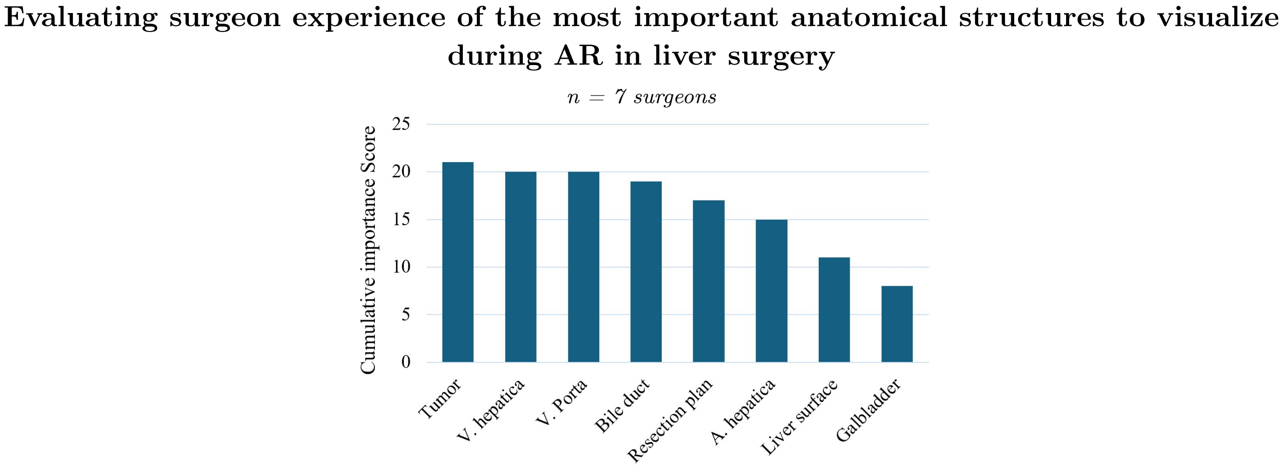
Evaluating surgeon experience of the most important anatomical structures to visualize during AR in liver surgery

n = 7 surgeons

Figure 15: Results of Phase 2. Scoring the importance of anatomical structures for visualization during AR was based on a Likert scale ranging from 1 (not important) to 3 (very important), with cumulative scores ranging from a minimum of 7 to a maximum of 21.

2.3.3 Class 2: Instrument interaction

Phase 1

Figure 16 displays all the visualizations developed for class 2. The virtual resection plan painter was developed in C# (Appendix C.2). This tool received higher scores for ease of interpretation (4.3 vs. 2.5), surgeon experience (4.0 vs. 2.5), resection plan determination (2.3 vs. 1.5), depth perception (3 vs. 2.5), and information balance (3.7 vs. 3) than the US overlay. However, the virtual resection plan painter scored 0 for anatomical structure localization and tumor margin determination, whereas the US view scored 2.5 for anatomical localization and 2.0 for tumor margin determination (Figure 17).

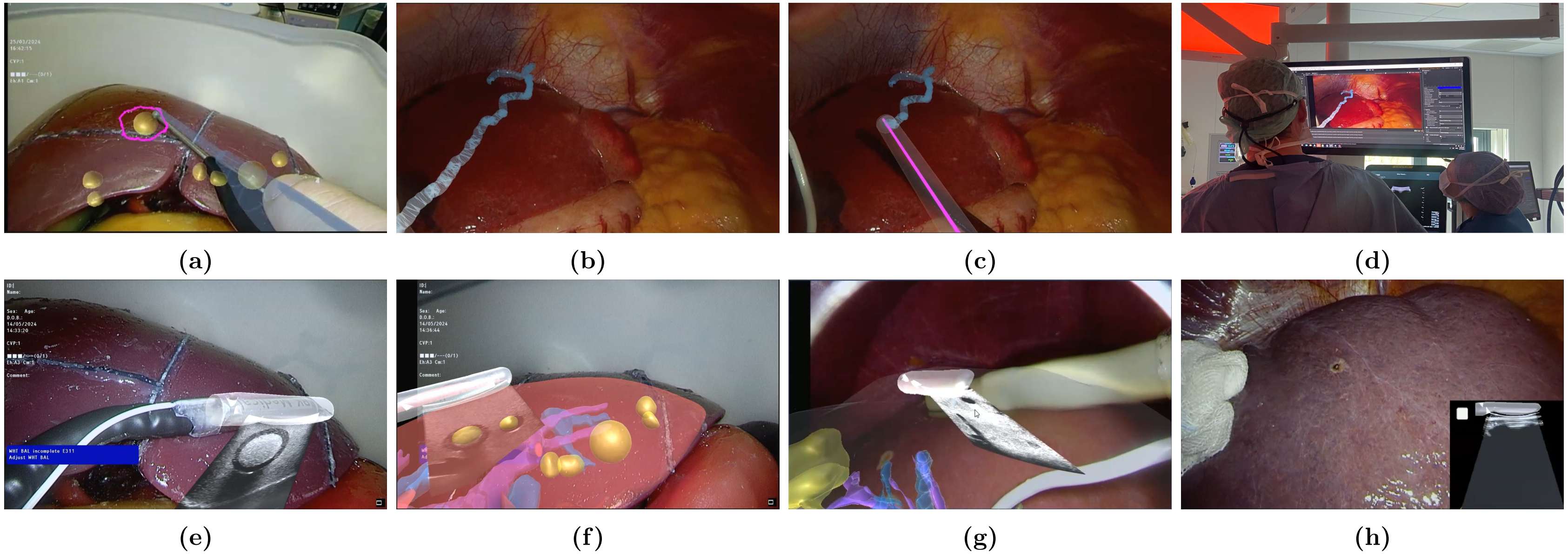

Figure 16: AR visualizations of class 2: Instrument interaction. (a) The surgical pointer draws a virtual resection plan on the phantom. This tool allows for the real-time generation of a virtual line on the laparoscopic video image of the liver when using a surgical pointer. This enables the creation of a virtual resection plan on the liver surface before the resection. The pointer is equipped with an EM sensor, enabling real-time location tracking. (b-d) A clinical test of the virtual resection plan on patient 2 undergoing segment II-III resection. (e) This visualization enables real-time projection of the US image at the exact position of the US probe through EM tracking. This allows for real-time US information visualization within the laparoscopic view and reduces focus switching. (f) US projection in combination with a whole liver model AR view (class 1). (g) US view tested with cysts (in white) during surgery of patient 1. (h) US view visualized as VR in laparoscopic view during OR of patient 4 to reduce focus switching.

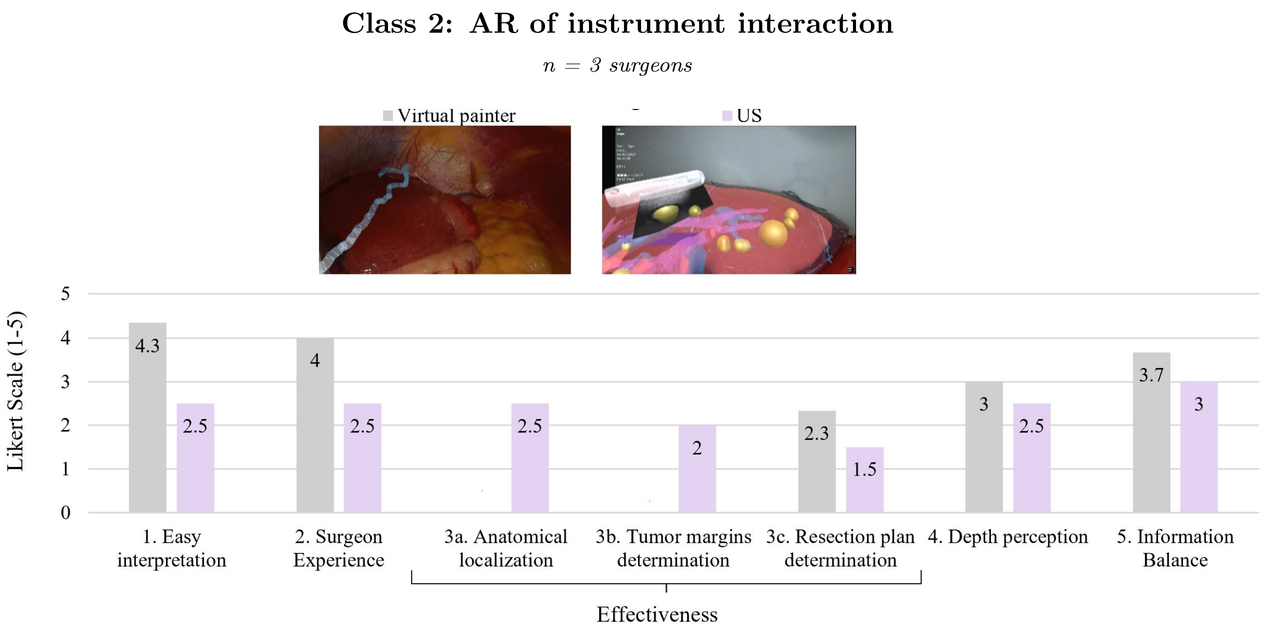

Figure 17: Results of the custom-made qualitative survey for Class 2 visualizations in Phase 1.

Phase 2

All seven surgeons found the US view a promising visualization. Of these, the US-only view (Figure 16e) and the US in the corner as VR (Figure 16h) were favored by one surgeon, and the US in combination with AR of a virtual anatomical model (class 1) was preferred by five surgeons (Figure 16f). Conversely, only one surgeon indicated they would use the virtual painter (Figure 16a-16d) during LLR (Figure 18).

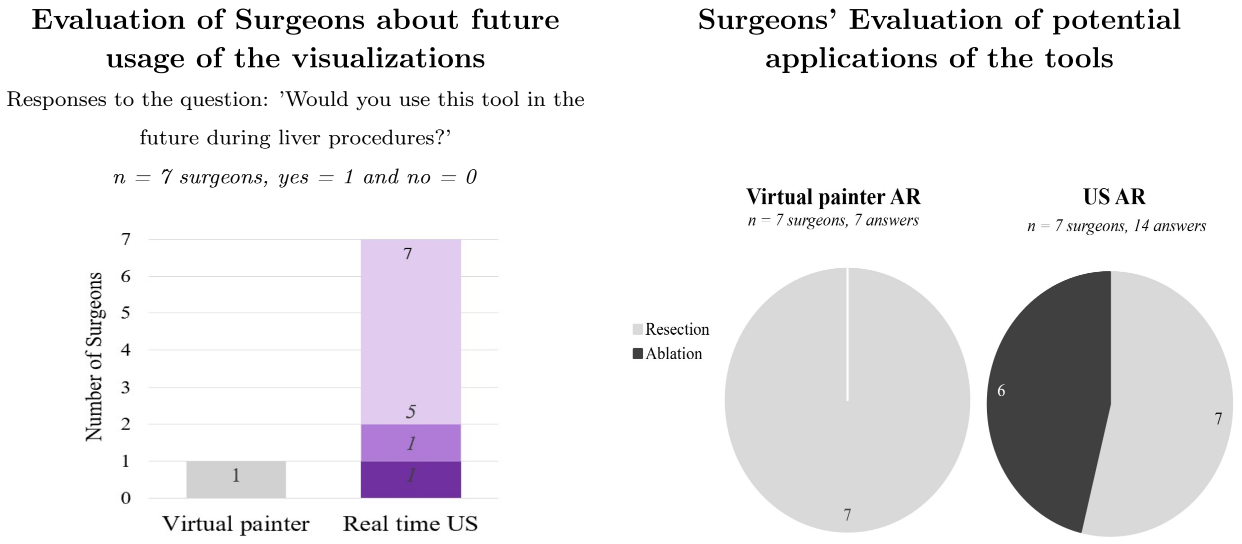

(a) (b)

Figure 18: Results of Phase 2. (a) Surgeon evaluation about future usage of the tools from class 2. (b) Potential applications of the visualizations. The pie chart shows the distribution of answers for each application where 'yes' (1) indicates interest and 'no' (0) indicates no interest in the tool for that application.

2.3.4 Class 3: Virtual Reality

Phase 1

Figure 19 presents the developed visualizations for class 3. The target view (Figure 19c-19f), developed in C# (Appendix C.3), achieved higher scores in all aspects compared to the third-person view (Figure 19a-19b). Specifically, it scored higher on ease of interpretation (4.5 vs. 1), surgeon experience (4.5 vs. 1), anatomical localization (3.5 vs. 2), tumor margin determination (3.5 vs. 2.3), resection plan determination (3.5 vs. 2), depth perception (4 vs. 2.5), and information balance (4.5 vs. 2.5) (Figure 20).

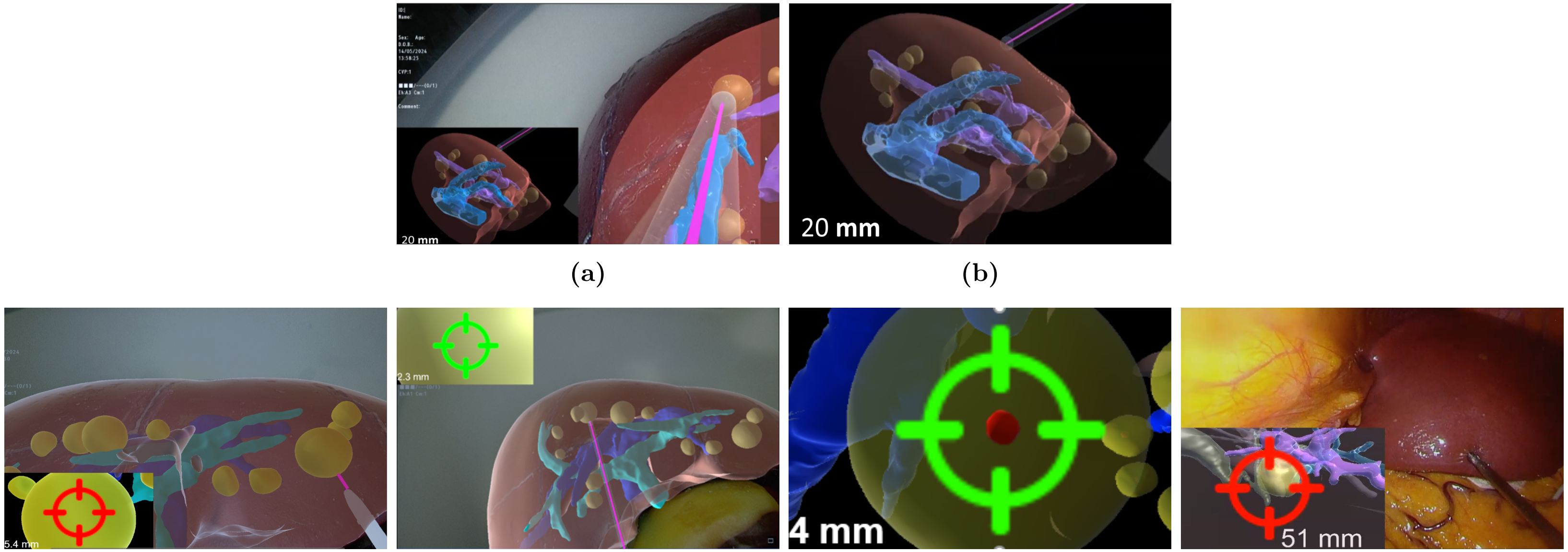

(a) **(b)**

(c) **(d)** **(e)** **(f)**

Figure 19: Visualizations of class 3: Virtual Reality (VR). (a) In the AR view, it appears as if the pointer is superficially touching the tumor. However, the third-person VR view in the left corner offers a lateral perspective of the liver, demonstrating that the tumor is located deeper (20 mm) within the liver. (b) Close-up VR view of the lateral perspective of the liver. (c-d) A target view is added as VR. In this view, the surgeon can localize the lesions with a tracked surgical pointer and visualize their relative position and orientation within a bull's eye. (e) Close-up VR view of the target view. The tumor-to-instrument distance was shown in the corner of the image. The colors of the bull's eye indicated the distance from the instrument's tip to the tumor's center, displaying green when the target was within 5 mm and red when the depth to the target was exceeded. A red dot was added in the center to indicate the center of the lesion for accurate targeting. (f) Target view during a clinical test of patient 3, where the CRLM is located 51 mm from the tip of the pointer.

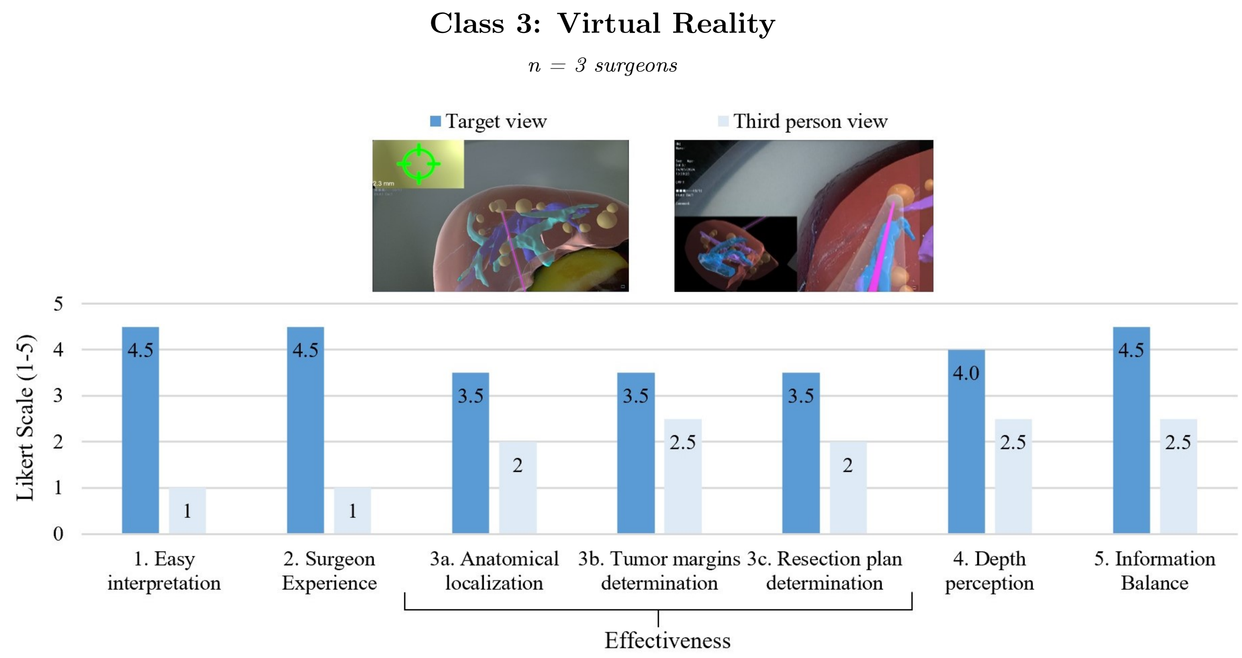
Class 3: Virtual Reality

n = 3 surgeons

Figure 20: Results of the custom-made qualitative survey for Class 3 visualizations in Phase 1.

Phase 2

Five surgeons indicated they would use the third-person view, with four finding it suitable for both resection and ablation, one considering it more appropriate for ablation, and two for resection. Additionally, five surgeons would use the target view tool during ablation (Figure 21).

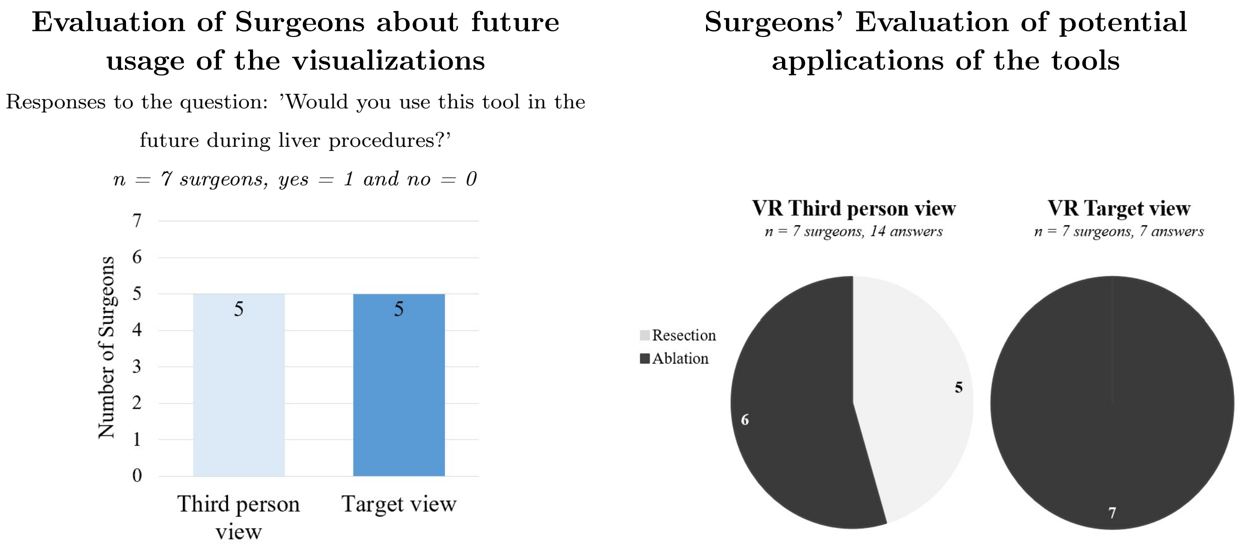
Evaluation of Surgeons about future usage of the visualizations

Responses to the question: 'Would you use this tool in the future during liver procedures?'

n = 7 surgeons, yes = 1 and no = 0

Surgeons' Evaluation of potential applications of the tools

(a)

(b)

Figure 21: Results of Phase 2. (a) Surgeon evaluation about future usage of the tools from class 3. (b) Potential applications of the visualizations. The pie chart shows the distribution of answers for each application where 'yes' (1) indicates interest and 'no' (0) indicates no interest in the tool for that application.

2.4 Discussion

This user study aimed to improve the AR visualization during LLR at NKI-AvL. Nine AR and VR visualizations inspired by literature and the gaming industry were developed and evaluated by surgeons. Phase 1 assessed their experience, effectiveness, and usability during phantom tests and five LLRs. Phase 2 gathered preferences from surgeons on the most promising visualizations and their potential applications.

2.4.1 Interpretation of Results

Class 1: AR of virtual anatomical models

The visualization focusing solely on critical liver vessels and the target lesion provided a more targeted and less overwhelming representation ($3.5 > 3$), and improved the overall surgeon experience ($4.0 > 3.7$) compared to the whole liver model. It slightly enhanced anatomical localization ($4.0 > 3.7$), aligning with Zhang et al. [32], who investigated that targeted AR projection aids in identifying important anatomical structures. Depth perception improved minimally compared to the whole liver model ($2.0 > 1.3$) but remained challenging. Six out of seven surgeons rated this visualization as one of the most promising, while the whole liver model was considered promising by only two surgeons (Figure 14a).

Two surgeons found the hole view promising, because it showed better depth perception between the liver surface and lesions compared to the whole liver view ($4.0 > 1.3$).
While the window view reduced visual clutter, aligning with Prevost et al. [30], it was not considered promising by any surgeons. This was due to its compromise of the overall surgical perspective and because it can be inconvenient since the camera is often operated by someone other than the surgeon.

All seven surgeons would use an additional resection plan visualization, with higher scores for tumor margin (3.3 vs. 1.7) and resection plan determination (3.3 vs. 2.3) compared to the whole liver model. They emphasized the need to consider rigid instrument placement and scope entry under the ribs, making a perfectly round resection plan visualization impractical (Figure 11j). Adballah et al. [37] found that AR overlay of resection margins provided more accurate margins compared to US navigation, especially for deep tumors.

All visualizations of anatomical structures face challenges in accurately depicting vessel depth within the liver surface during surgery, making it hard for surgeons to decide which vessels to cut first during resection. The depth shader was developed to improve this and was also chosen as the most promising AR visualization by six surgeons (Figure 14a). Nevertheless, the depth shader lacks precise distance information between structures.

In addition, Phase 2 identified the portal vein, hepatic vein, and tumor(s) as the most important structures to visualize during resection (Figure 15). However, the preferences of the surgeons vary with tumor location. Although the gallbladder and liver surface scored lower for visualization importance, they might be necessary for AR orientation.

Class 2: Instrument Interaction

AR visualizations with instrument interaction have the major advantage of maintaining accuracy despite registration errors, as the overlay relies on EM sensor coordinates at the US probe [36] and pointer tip, rather than on the virtual model.

The US overlay scored low on experience, effectiveness, and usability (Figure 17), but all surgeons still found it promising for AR visualization. It provides continuous imaging guidance, which allows real-time resection adjustments without diverting attention from the laparoscopic screen. However, surgeons require more experience with this new technique, a point supported

by Lau et al. [36]. Lau et al. also noted that AR with anatomical virtual models (class 1) can lose effectiveness and reliability as rigid overlays become inaccurate during resection. However, they suggested that diagnostic MRI or CT models could be valuable for visualizing vanishing lesions or those invisible on conventional US. Therefore, the most popular view (chosen by five surgeons) was the US combined with the virtual anatomical model (Figure 16f), as it provides dual validation of tumor and vessel localization within a single view.
The US view without the AR model (Figure 16e) and the US view in the corner as VR (Figure 16h) were both considered promising by one surgeon, with the latter being similar to US visualization in robotic surgery within the surgeon's FOV [44].

The virtual resection plan painter needs a virtual model for resection plan determination, has room for depth perception improvement (Figure 17), and was regarded as promising by only one surgeon (Figure 18a). The remaining six surgeons preferred diathermy due to the painter's inability to adjust in real-time with liver manipulation. Additionally, surgeons noted the lack of shadow artifacts in the US view, visible with diathermy for localization confirmation. The results indicate that refinements of the tool and additional investigation into the usability are required.

Class 3: VR
Additional VR techniques were investigated in this study to enhance depth perception of the anatomical virtual model overlay. The target view visualized tumor-to-instrument distances within a bull's-eye, similar to the approach used by Buchs et al. [27]. Five surgeons evaluated this tool as a promising technique. It also scored high on experience, effectiveness, and usability, potentially offering a valuable solution for ablation procedures. However, while the target view has been tested in LLR, surgeons must evaluate it in ablation settings.

The third-person view offers additional lateral depth information but lacks straightforward positioning and rotation controls. Despite its lower scores in various visualization aspects, five surgeons showed interest in using it for liver procedures. Implementing a more user-friendly button system and an option to toggle the view on and off could enhance its information balance, interpretation, and effectiveness (Figure 20).

2.4.2 Strengths

This study is as far as is known the first to evaluate different AR visualizations during LLR in a clinical setting from a surgeon's perspective. In current literature, this information is scarce. Furthermore, the study developed new visualizations inspired by non-medical industries, where aspects such as depth perception are more advanced.
In addition, including surgeons from two hospitals reduced selection bias and broadened the evaluation beyond NKI-AvL's familiarity with the AR technique.

Another strength was the development of two custom-made surveys, specifically designed to evaluate AR in liver surgery. These surveys identified visualization aspects and assessed clinical potential, enhancing the clinical relevance and applicability of the findings.

Furthermore, the visualizations were tested during LLR, providing realistic validation for clinical implementation. Phantom tests offered accurate overlays without surgical obstacles and allowed direct comparison with minimal time gaps. In addition, a strength was the diverse group of five patients and seven surgeons, encompassing different ages and genders. The patients had tumors of varying depths, sizes, and locations, allowing visualization tests of varying types of resections in both lateral and supine positions.

2.4.3 Limitations

A limitation was the small number of clinical tests, which, while covering some diversity, did not encompass all patient cases and tumor locations. LLR for CRLMs at NKI-AvL is not a routine procedure, often performed by open surgery for complex cases or when combined with other abdominal procedures (e.g., colorectal surgery). This highlights the need to explore AR's potential to expand laparoscopic options for challenging scenarios.

Another limitation was the small number of surgeons participating in the first survey. However, prioritizing the input of the most experienced staff during development was chosen. For extra perspectives, Phase 2 also included fellows and surgeons from LUMC. Their interviews were based on videos instead of live tests.

Additionally, although registration accuracy was not addressed in this study, it could impact surgeons' assessment of the visualizations due to potential overlay misalignments caused by liver movements.

Another important limitation of this study is the heterogeneity of comparisons, as different classes of visualizations were evaluated, making it challenging to draw uniform conclusions, mainly for the class 2 and 3 visualizations of the instrument interaction and VR integration.

Moreover, the study did not employ standardized and validated questionnaires like the System Usability Scale (SUS) [45] and NASA Task Load Index (NASA-TLX) [46], which provide reliable comparable data on usability and cognitive and emotional workload. However, these tools are not specifically made for evaluating AR visualizations in liver surgery.

2.4.4 Future prospects

Further improvements in visualization aspects are essential to enhance the interpretation and experience of AR for surgeons, particularly focusing on the most promising visualizations. Ultimately, this will enable surgeons to localize anatomy and determine tumor margins more effectively.

Interpretation of AR
To make the promising US overlay easier for surgeons to understand, research should focus on simplifying the learning curve and enhancing the surgical experience. Additionally, intuitive control buttons must be implemented for the third-person view.

Effectiveness
AR should be effective in the localization of anatomical structures, tumor margins determining to resect tumor tissue accurately, and resection plan determination to spare healthy tissue. However, results have shown that accurately determining tumor margins with the tested AR visualizations remains challenging (Figure 12). Specifically, continuous visualization of resection margins during surgery is not feasible with the current AR techniques. Integrating ICG imaging into AR systems could significantly enhance surgical precision through real-time fluorescence guidance of tumor margins throughout the procedure. Bijlstra et al. [44] employ a fluorescence approach during RLR, where a VR model of the liver is displayed alongside the robotic view in the surgeon's console. This approach can potentially shorten operation times, reduce intraoperative blood loss, and improve patient outcomes [47], [48].

A dual approach combining AR and ICG might enhance accurate localization and precise delineation of tumor margins. Pessaux et al. [35], [49] have demonstrated this dual approach in robotic duodenopancreatectomy. The study demonstrates precise and safe recognition of vascular and biliary structures. However, fluorescence imaging has limitations, including a high false-positive rate and limited tissue penetration (5-10 mm), which diminishes its effectiveness for visualizing deeply located tumors [19], [20]. Additionally, ICG is unable to identify vessels. AR can complement this by providing navigational support for visualization of vessels and deeply seated tumors. This can be achieved through visualization methods such as the third-person view, US overlay, or a liver model with the depth shader.

Information balance

Currently, a significant amount of information is displayed simultaneously, which can be overwhelming. Implementing an activation-on-demand (AOD) approach can help balance this. This technique, already used in robotic surgeries with foot pedals [50], allows important structures to be toggled on and off only when needed, minimizing potential disruptions during surgery (Example figure 22a - 22c). AOD can also switch between visualization classes and make AR more adaptable to patient-specific tumor locations and relevant adjacent structures.

Depth perception

Viewing 3D models on a 2D screen limits the surgeon's depth perception, making it difficult to estimate distances between structures and decide which vessels to cut first during resection. The 2D laparoscopic view is static, offering a single, fixed perspective, whereas 3D models can be rotated and viewed from multiple angles. To further improve depth perception between superficial and deeply located structures, the instrument occlusion problem must be resolved (Figure 22d) [41], [42]. This can be achieved by overlaying instruments on the virtual model with an additional object camera (Figure 22e) or by using binary masks [51] or depth maps [52] to automatically segment the instruments within the laparoscopic image. These visualization improvements require further research, particularly regarding surgeon experience.

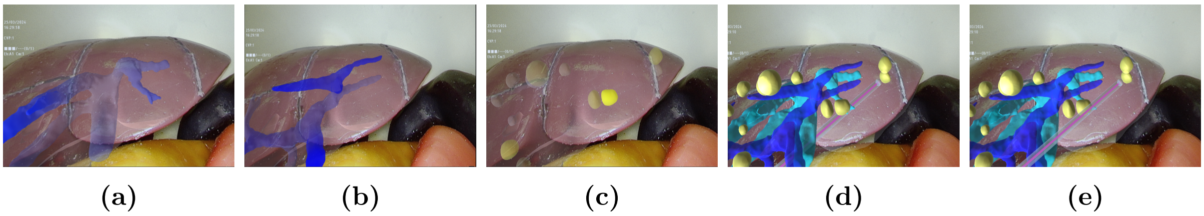
(a) (b) (c) (d) (e)

Figure 22: Further depth perception and information balance improvements. The hepatic vein is light blue, the portal vein is dark blue, and the lesions are yellow. (a-c) Activation-on-demand can be implemented in the workflow by toggling structures on and off based on the surgeons' preferences. This reduces information overload. (d) Standard shader and visualization where the virtual model occludes the surgical pointer. (e) The surgical pointer is overlaid on top of the virtual model. This improves the understanding of the order of the objects in the augmented scene.

Deformable AR

Due to limited registration accuracy, AR mostly serves as additional navigational support at the start rather than a reliable resection guide throughout the whole procedure [21]. Future research on AR in liver surgery should focus on developing dynamic registration processes for real-time interaction between instruments and the AR model. AR and VR views can then adapt dynamically to the resection process, offering real-time visibility of the resected critical structures. Some studies have explored real-time deformable registration [31], [37], [41], [53], and a study by Nam et al. [54] developed IOUS segmentation with a live virtual model.

Impact on long-term patient outcomes

Further research should focus on large-scale clinical trials to validate the long-term patient benefits of AR in liver procedures. This involves assessing its effects on patient outcomes, surgical precision, and limited surgical risks. Also, exploring the potential of AR visualizations in additional applications beyond LLR, such as RLR and ablations could be valuable. For instance, if the target view can improve and support needle localization during ablation, the ablation could potentially offer similar patient outcomes with reduced morbidity, mortality, length of hospital stay, and costs compared to LLR [55].

2.5 Conclusion

AR is promising in liver surgery when surgeons can easily understand the visualization and have a positive experience. It should effectively localize and define vessels and tumor margins, provide clear depth perception, and present well-balanced information. Additionally, the overlays must be accurate. Multiple AR visualizations were developed and tested in five patient cases with the depth shader, target structures, and US overlay emerging as the most promising visualizations. Only two surgeons favored the whole liver view and the view including holes in the liver surface, while none of the surgeons found the window view and virtual resection plan painter promising. Furthermore, adding VR into the laparoscopic view might enhance depth perception and require further research, especially in ablation procedures.

Looking ahead, integrating non-rigid registration techniques and depth shaders onto a balanced liver model, combined with AOD for selective visualization of critical structures and ICG for precise tumor margin delineation, holds significant promise for AR in liver surgery. These advancements could enable AR to be integrated into the surgical workflow. Ultimately, the successful implementation of AR could enhance precision and effectiveness in surgical procedures, leading to patient benefits.

Laparoscope tracking

3.1 Introduction

To enable AR during LLR, accurate tracking of the position and orientation of the laparoscope is required. Initially, the NKI-AvL utilized an Olympus Endoeye 0° laparoscope (Figure 23a) for liver surgeries, for which an adapter was developed in a previous project [56]. This adapter, attached to the camera handle integrates an EM sensor, which can track the movements of the laparoscope.
However, this institute has transitioned to an oblique 30° laparoscope (Figure 23b and 23c), in which the viewing direction is tilted 30 degrees from the axial direction of the scope cylinder. This tilt can be adjusted by rotating the scope cylinder around its axis while maintaining a constant position and orientation of the camera head. Oblique scopes offer a significant advantage over 0° scopes because they provide a broader range of viewing directions [57].

Nevertheless, there are in this hospital no adapters to track the movements of the 30° laparoscope. Consequently, surgeons are required to switch laparoscopes to visualize AR during surgery, which is time-intensive. This tracking is particularly challenging because the 30° scope introduces an additional degree of freedom, resulting in a total of 7-DoF. A single 6-DoF sensor cannot track all the possible parameters. Therefore, the secondary objective of this thesis is tracking both 30° laparoscopes used in this hospital, by developing and calibrating adapters containing 6-DoF EM sensors. Additionally, a solution must be found to track the extra degree of freedom.

This chapter describes the design, calibration, and validation of adapters for tracking the movement of the 30° laparoscope.

(a) Laparoscope (Endoeye 0°, Olympus).

(b) Laparoscope (Endoeye 30° HD, Olympus), horizontally orientated buttons.

(c) Laparoscope (Endoeye 30° HD, Olympus), vertically orientated buttons.

Figure 23: Different laparoscopes used during laparoscopic surgery at the NKI-AvL.

3.1.1 Camera calibration

The EM sensors cannot be positioned at the exact camera location at the laparoscopic tip. Thus, calibration is required to determine the unknown geometric relationship between the coordinate systems of the laparoscopic camera and the EM sensor in the adapter.

The intrinsic and extrinsic camera parameters must be calibrated to map a virtual liver to the laparoscopic video (to map camera coordinates to pixel coordinates in the image plane). A schematic overview of the components involved in camera calibration is shown in Figure 24.

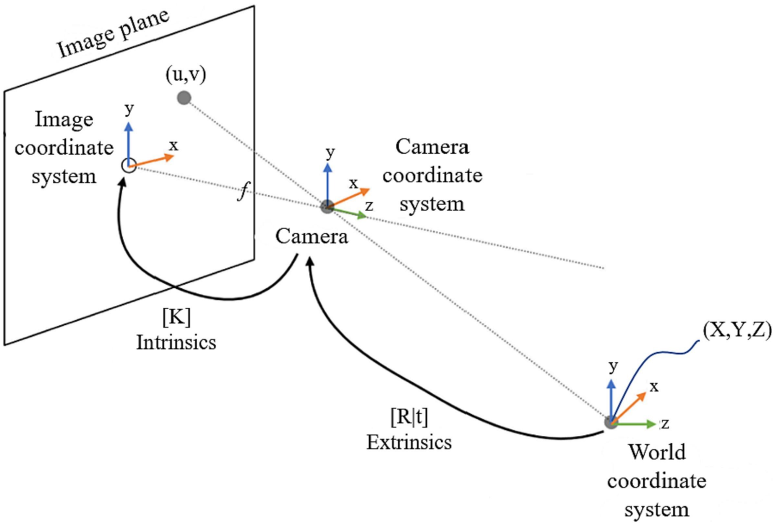

Figure 24: Transformation from world coordinate system to image coordinate system to find the geometric relationship between the coordinate systems of the laparoscopic camera tip and the EM sensor. Image copied from Poorghasem et al. [58].

The 2D points (u,v) in the image plane (laparoscopic video) can be mapped to 3D points (X, Y, Z) in the world coordinate system (e.g. virtual liver or instruments) by solving equation 1 [59]. In this equation, $[R\ t]$ are the extrinsic camera parameters (R represents the rotation and t represents the translation of the camera's position relative to the world coordinate system). Additionally, K corresponds to the constant intrinsic camera parameters, with f representing the focal length in the x and y directions and $(u_0,\ v_0)$ representing the principal point [59].

$$\begin{pmatrix} u \\ v \\ 1 \end{pmatrix} = K \cdot [Rt] \begin{pmatrix} X \\ Y \\ Z \\ 1 \end{pmatrix} = \begin{pmatrix} f_x & 0 & u_0 \\ 0 & f_y & v_0 \\ 0 & 0 & 1 \end{pmatrix} \cdot [Rt] \cdot \begin{pmatrix} X \\ Y \\ Z \\ 1 \end{pmatrix} \tag{1}$$

The general approach to solving this equation involves capturing several images of a checkerboard (image plane) from different angles and extracting the corners. This data is then used to solve the equation and determine the camera parameters [59].

3.2 Methods

3.2.1 Adapter design

A list of requirements was developed during the design of the adapters (Table 4). The adapters were designed using the open source software packages Meshmixer (V3.5, https://meshmixer.en.softonic.com/) and Blender (V4.1, https://www.blender.org/). These designs were based on 3D optical scans of the 30° scopes, created using a high-resolution Artec Space Spider 3D scanner (with a 0.1 mm 3D resolution and 0.05 mm accuracy) [60].

The adapters were printed using the Formlabs Form 3B 3D printer, which employs Stereolithography (SLA) technology. SLA involves a laser solidifying photopolymer resin, with an ultraviolet laser accurately reproducing the shape of each layer from the 3D model. Subsequently, the photopolymers are hardened under UV light exposure. The final version was printed in Biomed clear resin (Requirements 1.1-1.2 and 2.1-2.3, Table 4), making it suitable for clinical use. Furthermore, a screw mechanism, similar to the one used for a previously developed 0° adapter [56], was implemented.

3.2.2 Adapter location and sensor position

Optimal EM sensor positioning is important in the designing process. The design should contain an Aurora 6-DOF EM sensor (Figure 3b), including optimal sensor position for tracking (requirement 3.1, Table 4). Positioning the sensor at the tip increases the probability of being within the EM field. Besides, a radial distance of 4 cm from the handle allows for free rotation of the laparoscope in the trocar without hindering the surgeon with the adapter. This position of the sensor part of the adapter was replicated for the 30° scope to maintain consistency across the different designs [56].

3.2.3 Reproducibility assessment

A reproducibility assessment was performed to assess the fitting and secure attachment of the adapter and its EM sensor (Requirement 1.1 and 1.3, Table 4). Achieving high reproducibility requires a stable and consistent connection between the EM sensor and the laparoscopic optical center.

The following experimental set-up was conducted for both 30° scopes including corresponding final adapters to confirm the adapter's reproducibility:

- Three 6-DOF EM sensors were attached to the scope. The sensor of the adapter is glued, while two reference sensors are taped — one at the tip of the scope and the other below the adapter sensor, on the instrument's shaft (Figure 25).
- A FG was placed next to the laparoscope, with the three sensors within the EM field.
- The tracking system calculated the position and orientation of each sensor while interfacing with the host computer.
- To minimize ferromagnetic interference during the experiments, the measurements were obtained on a plastic table.

This test aimed to estimate the transformations between the two reference sensors and between the sensor of the adapter and the two reference sensors. The set-up for this test is shown in Figure 25.

Table 4: List of requirements for adapter design and development

No.	Requirement	Explanation
1. Usability		
1.1	Unique fit	• There should be no movement between the adapter and scope after the attachment. • The adapter should be attached and detached easily without the need for extensive training.
1.2	No hinder	• The adapter should not hinder the laparoscope movements or the surgeon's access to controls during surgery. • The adapter should be as compact as possible. • The adapter should be free of sharp edges to prevent damage to equipment.
1.3	Fixed	• The adapter should be fixed to the scope similarly for each attachment, to ensure accurate calibration. • The adapter attachment should be reproducible to eliminate necessity of recalibration.
2. Durability and materials		
2.1	Sterilizable	• The design should be made from sterilizable material and should not contain any holes, except for the opening for sensor placement. Any remaining space should be entirely filled with glue to prevent bacteria and microorganisms from entering.
2.2	Non-ferromagnetic	• The material of the adapter should be non-ferromagnetic, to minimize ferromagnetic interference with the EM field.
2.3	Reusable	• The adapter material should be strong enough to withstand attachment and detachment without breaking.
3. Precision		
3.1	Sensor position	• The design should contain an Aurora 6DOF EM sensor (NDI, Waterloo, ON). • Optimal sensor position is required to maximize the accuracy of the tracking.

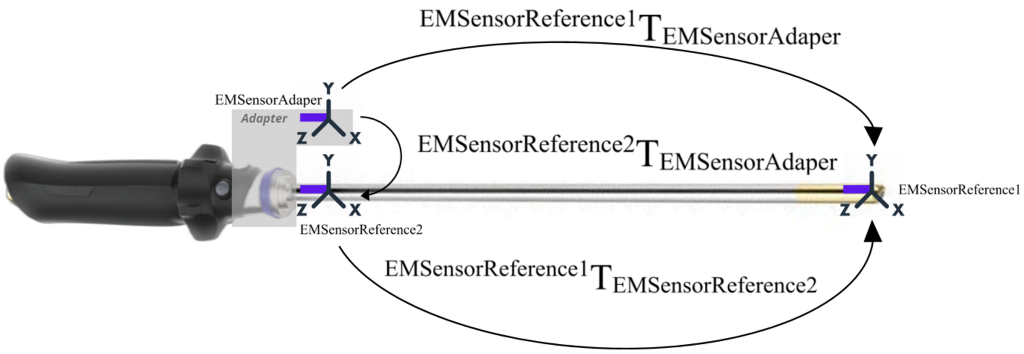

Figure 25: Set-up for the reproducibility test of attaching and detaching the adapter to test the fixation onto the 30° scope.

Two individuals performed the test five times, resulting in ten measurements per adapter. The experiment consists of the following steps for each measurement:

1. Attachment of the adapter onto the scope.
2. Positioning of the scope in the center of the EM field. Positions may differ per measurement because the goal is to determine the sensors' position and orientation relative to each other.
3. Recording of sensors' position and orientation for five seconds to filter jitter errors.
4. Detachment of the adapter.

From the ten measurements, Euclidean distances (ED) and three Euler angles (Rx, Ry, Rz) between the sensors were calculated per adapter. The ED between two points $p_1 = \begin{bmatrix} x_1 \; y_1 \; z_1 \end{bmatrix}$ and $p_2 = \begin{bmatrix} x_2 \; y_2 \; z_2 \end{bmatrix}$ in 3D space can be computed using Equation 2. The ED and Euler angles were normalized by subtracting the median value from each data point and were plotted. Additionally, standard deviations (SD) of ED and Euler angles were calculated to assess the variation across the ten measurements. These SD values were then compared with the tracking accuracy of the attached Aurora 6DoF EM sensors, as presented in Table 5 [26].

$$d(p_1, p_2) = \sqrt{(x_1 - x_2)^2 + (y_1 - y_2)^2 + (z_1 - z_2)^2} \tag{2}$$

Table 5: Root Mean Squared (RMS) errors of the Aurora 6DoF sensor in orientation and position, used for tracking with a field generator (FG) [26].

Accuracy (6DOF sensor)	Dome Volume FG (RMS)
Position (mm)	0.70
Orientation (°)	0.30

3.2.4 Calibration and validation

The calibration was done after the reproducibility tests. The goal was to eliminate the need for recalibration during each AR visualization by performing a calibration once. Therefore, the transformation between the center of the laparoscopic camera and the EM sensor needs to be estimated (${}^{\text{Adapter}}T_{\text{Cam}}$). Figure 26 shows a schematic overview of the calibration setup. The transformation ${}^{\text{EMsensorCk}}T_{\text{Ck}}$ has already been determined in a previous study conducted by

NKI-AvL using a tracked pointer to identify the coordinates of the corners of the checkerboard [15], [59], [61].

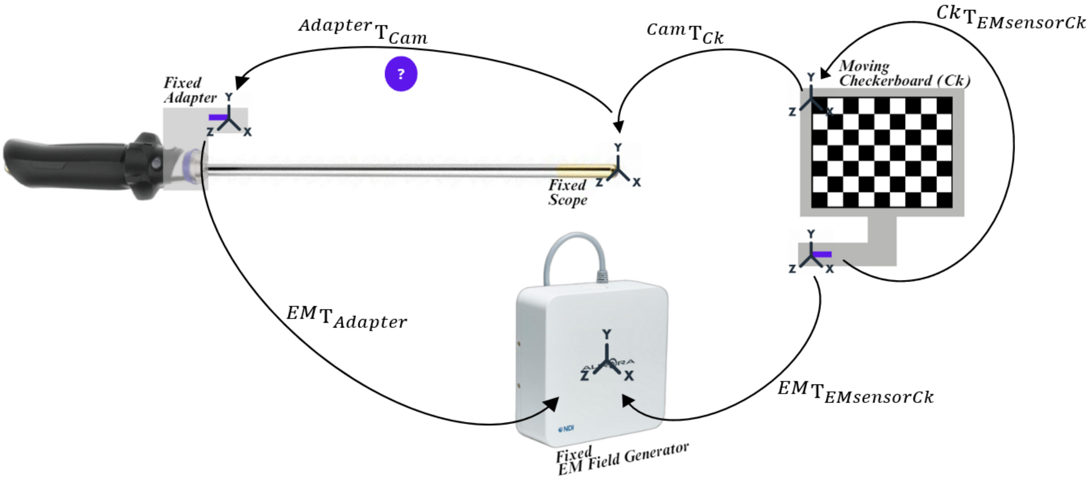

Figure 26: Coordinate systems with corresponding transformations for the hand-eye calibration of the 30° adapters.

The camera parameters were determined in MATLAB (Release 2024A). An intrinsic camera parameter calibration was performed to find the intrinsic camera parameters of the 30° scopes and a hand-eye calibration was done to find the transformation ${}^{\text{Adapter}}T_{\text{Cam}}$ to position the camera in the 3D space of the tracking system (See equation 3) [15], [59], [61].

$${}^{\text{Adapter}}T_{\text{Cam}} = {}^{\text{Adapter}}T_{\text{EM}} \cdot {}^{\text{EM}}T_{\text{EMsensorCk}} \cdot {}^{\text{EMsensorCk}}T_{\text{Ck}} \cdot {}^{\text{Ck}}T_{\text{Cam}} \tag{3}$$

The experimental setup to determine the extrinsic and intrinsic camera parameters involved taking twenty images while varying the position and orientation of the checkerboard, which contained an EM sensor. The 30° scope and its adapter remained stationary. During this process, the stationary FG tracked the position and orientation of each EM sensor.

The corners of the checkerboards in the acquired images were extracted to determine the camera parameters. Subsequently, the 2D points (u,v) of these corners in the image plane were mapped to 3D points (X, Y, Z) in the world coordinate system by solving equation 1 [59].

The constant intrinsic camera parameters (K) were based on the images and calculated once. Based on K, the focal length (f_x) and the horizontal field of view (FOV) can be calculated and implemented in Unity. The formula for calculating the FOV is given by Equation 4.

$$\text{FOV}_{\text{horizontal}} = 2 \times \arctan\left(\frac{\text{sensor width}}{2 \times F_x}\right) \tag{4}$$

To find the transformation ${}^{\text{Adapter}}T_{\text{Cam}}$, the twenty images including their tracked positions and orientations of the adapter and the checkerboard were used. As this transformation remains constant for all checkerboard positions, the final transformation matrix was determined by averaging the measurements. The resulting ${}^{\text{Adapter}}T_{\text{Cam}}$ for both scopes enables their tracking.

It is important to note that this research did not account for the tracking and calibration of the cylinder rotation (See cylinder in Figure 23b and 23c). Therefore, this rotation was manually adjusted in Unity during the validation of the AR visualizations.

3.3 Results

3.3.1 Adapter design

The final designs of the adapters were printed in Biomed clear resin (Figure 27 and 28). The final designs did not obstruct the movements of the laparoscope or the surgeon's ability to reach the controls during surgery, were as compact as possible, and were free of sharp edges. The EM sensors were inserted into the holes of the superior adapter parts, and any remaining space was filled with glue to prevent bacteria and microorganisms from entering. The designs have screw components on both sides to secure the adapter to the scope.

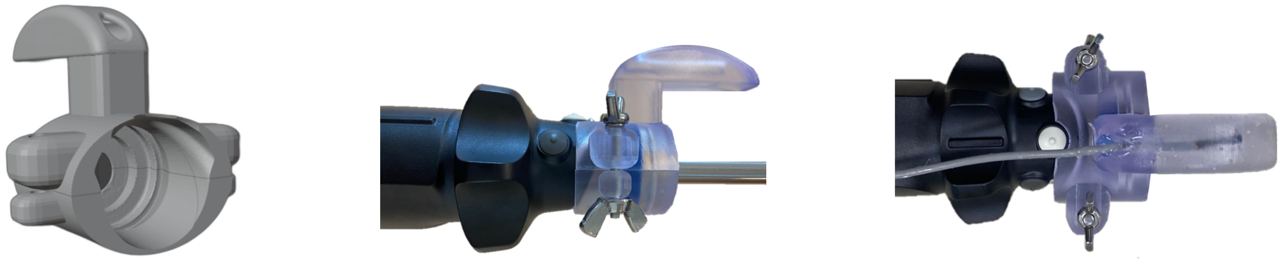

(a) Final 3D model of the adapter.

(b) Final adapter in Biomed Clear, attached to the 30° scope.

(c) Final adapter including EM sensor.

Figure 27: Final design of the adapter of the horizontally positioned buttons 30° scope.

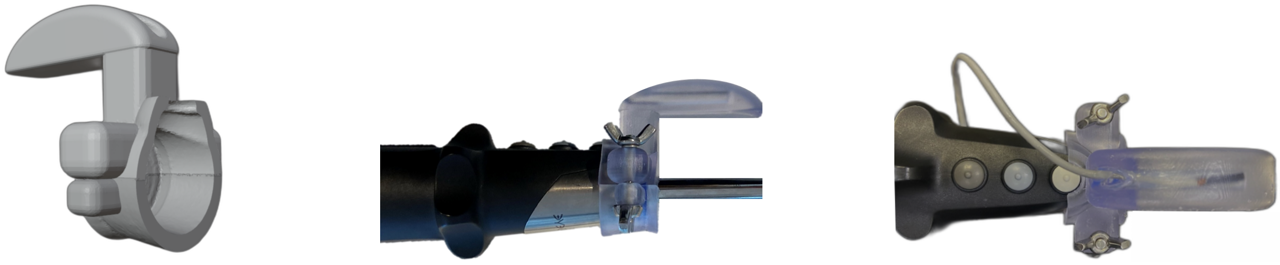

(a) Final 3D model of the adapter.

(b) Final adapter in Biomed Clear, attached to the 30° scope.

(c) Final adapter including EM sensor.

Figure 28: Final design of the adapter of the vertically positioned buttons 30° scope.

3.3.2 Reproducibility

A reproducibility test was performed and the SDs of ED and Euler angles of the repeated adapter attachment onto the 30° scopes are shown in Table 6. Furthermore, the ED and Euler angles between the sensors were plotted in Figure 29 for both 30° scopes.

The adapter's positional accuracy remains consistently within the sensors' tracking accuracy (0.70 mm), as outlined in Table 5. This indicates a reliable and consistent attachment (Requirement 1.1 and 1.3, Table 4). Furthermore, the SDs of the rotation angles were the least constant around the x-axis (>0.30°), and are outlined in Table 5.

Table 6: Standard deviations of Euclidean distances and Euler angles for repeated adapter attachment onto scopes with vertically- and horizontally positioned buttons

	Sensor tip and adapter	Sensor near handle and adapter	Reference sensors
30° scope adapter horizontally orientated buttons			
SD Euclidean Distance (mm)	0.53	0.31	0.44
SD Rx (°)	2.92	3.92	2.05
SD Ry (°)	0.36	0.36	0.09
SD Rz (°)	0.33	0.82	0.2
30° scope adapter orientated vertically buttons			
SD Euclidean Distance (mm)	0.32	0.11	0.27
SD Rx (°)	2.52	0.31	2.62
SD Ry (°)	0.82	0.14	0.72
SD Rz (°)	0.83	0.15	0.32

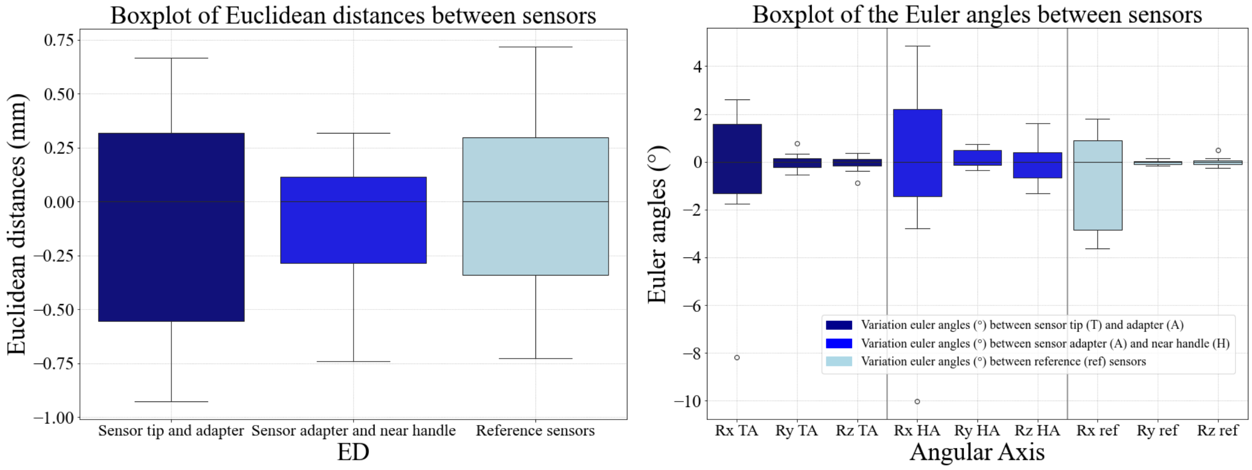

(a) Euclidean distances **(b)** Euler angles

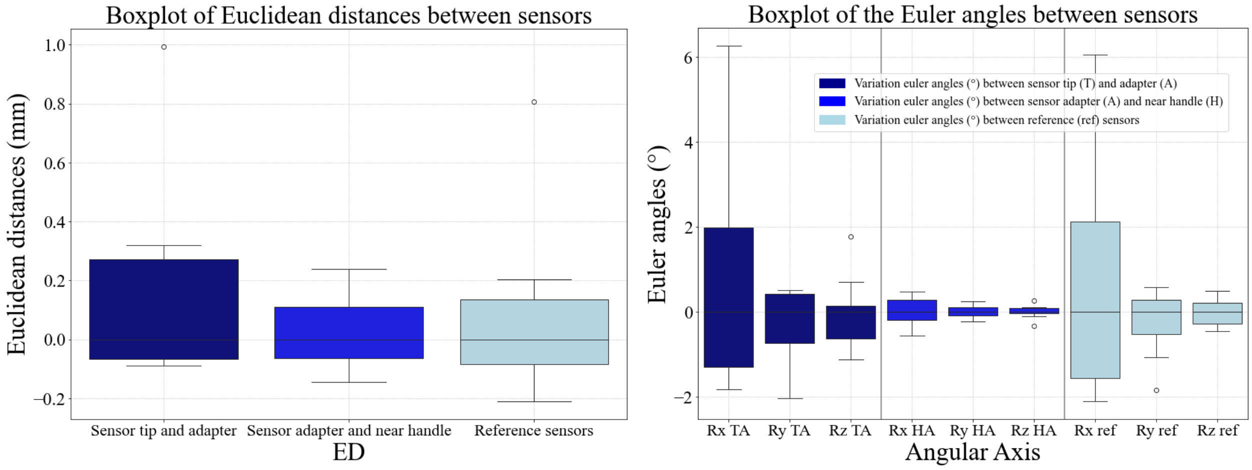

(c) Euclidean distances **(d)** Euler angles

Figure 29: Boxplot depicting the Euclidean distances (a and c) and Euler angles (b and d) for repeated adapter attachment onto laparoscope with horizontally (a-b) and vertically (c-d) orientated buttons. The boxplots are centered around y=0, with each box representing 10 measurements.

3.3.3 Calibration and validation

The transformation matrices obtained from the calibration of the adapters are shown in equations 5 and 6, and were subsequently loaded into Unity. Loading the obtained camera calibrations into Unity resulted in the AR visualization of the virtual model onto the phantom in the camera view, as shown in Figures 30a and 30b. The image size was 1920 × 1080 pixels, the FOV and F_x were determined using Equation 4 (see Equation 7 and 8). All values are manually adjusted in the Unity settings. To compensate for the additional degree of freedom, corresponding to the tilt angle (cylinder rotation), a z-axis rotation was manually applied in the software. To further improve the visualization, the z-axis of the virtual model was slightly adjusted by approximately the f_x value, as the virtual liver appeared larger than the real liver in both views. Additionally, the x- and y-axis were slightly adjusted to improve visualization.

$$K \cdot [Rt] \cdot \begin{pmatrix} X \\ Y \\ Z \\ 1 \end{pmatrix} = \begin{pmatrix} 1176.6 & 0 & 967.6 \\ 0 & 1178.6 & 550.4 \\ 0 & 0 & 1 \end{pmatrix} \cdot \begin{pmatrix} 0.70 & -0.67 & 0.23 & 12.6 \\ 0.70 & 0.60 & -0.39 & -42.0 \\ 0.12 & 0.44 & 0.89 & 325 \\ 0 & 0 & 0 & 1 \end{pmatrix} \cdot \begin{pmatrix} X \\ Y \\ Z \\ 1 \end{pmatrix} \tag{5}$$

$$K \cdot [Rt] \cdot \begin{pmatrix} X \\ Y \\ Z \\ 1 \end{pmatrix} = \begin{pmatrix} 1117.8 & 0 & 973.1 \\ 0 & 1122.7 & 562.8 \\ 0 & 0 & 1 \end{pmatrix} \cdot \begin{pmatrix} -0.11 & 0.96 & 0.25 & -12.9 \\ -0.85 & 0.04 & -0.53 & -65.8 \\ -0.52 & -0.27 & 0.81 & 292 \\ 0 & 0 & 0 & 1 \end{pmatrix} \cdot \begin{pmatrix} X \\ Y \\ Z \\ 1 \end{pmatrix} \tag{6}$$

$$\mathrm{FOV}_{\text{horizontally orientated buttons}} = 2 \times \arctan\left(\frac{1920}{2 \times 1176.6}\right) = 78.42^\circ \tag{7}$$

$$\mathrm{FOV}_{\text{vertically orientated buttons}} = 2 \times \arctan\left(\frac{1920}{2 \times 1117.7}\right) = 81.32^\circ \tag{8}$$

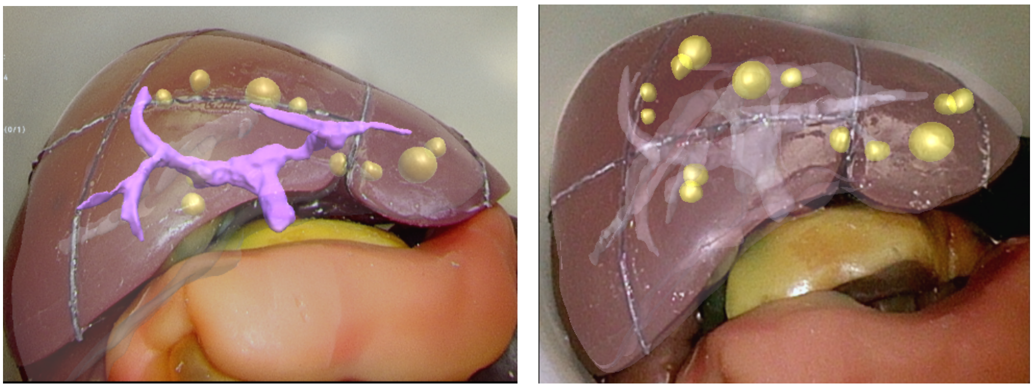

(a) AR overlay adapter horizontally orientated buttons.

(b) AR overlay adapter vertically orientated buttons.

Figure 30: Results of the AR overlay after calibration.

3.4 Discussion

This chapter described tracking the position and orientation of two different 30° laparoscopes, enabling AR during LLR. The adapters met all the 7 requirements (Table 4), implying the adapters have a unique fit, do not hinder the laparoscope movements or the surgeon's access to controls, are reproducibly fixed, and are made of a sterilizable, non-ferromagnetic, and reusable material. They are designed for easy attachment by surgeons and integrate Aurora 6DOF sensors positioned as optimally as possible relative to the camera. Additionally, intrinsic and hand-eye calibrations eliminate the need for recalibration during surgery. Ultimately, AR visualization was achieved (Figure 30).

3.4.1 Reproducibility

Both reproducibility tests were performed to test the fixation of the adapters and showed inaccuracies in the positions of the adapters within the sensors' tracking accuracy (<0.70 mm, Table 5). This indicates the adapter's reliability and consistent position after reattachment. Nevertheless, the SD for rotation showed larger deviations (>0.30°), especially along the x-axes. This might be because the Rx direction (roll) measurement is less accurate when both x-axes are aligned in the same direction for both sensors.

The minimum deviated values and outliers of the positional and rotational errors could be attributed to several factors: 1) inconsistencies in attachment. While the adapters are firmly secured to the scope with screws, ensuring they do not move, errors may still arise if the adapters are not positioned correctly. Even with secure attachment, improper placement can result in high error. 2) Displacement of the reference sensors; the reference sensors were secured with tape to the laparoscope's shaft, whilst glue is more reliable. Nevertheless, this explanation seems improbable, as the outliers occurred in the middle of the measurements. Given that the setup remained unchanged and the measurements returned to their initial values after the outliers, it is unlikely that the outliers were caused by sensor displacement. 3) The sensors may be positioned at varying distances from the FG, resulting in lower tracking accuracy at greater distances.

Nonetheless, minor rotational discrepancies may not affect the usability of the adapter, whereas positional errors could lead to significant misalignments of the AR visualization. Thus, the reliability of the adapter's placement is considered sufficient despite the rotational inaccuracies.

3.4.2 Overlay/ AR inaccuracies

Both laparoscopes are tracked within the same coordinate system of the virtual model and the 2D laparoscopic view of the liver. However, overlay inaccuracies were addressed by slight adjustments in the rotation and translation along the x, y, and z axes of the object camera. These inaccuracies can be ascribed to various factors.

First, parallax or perspective errors may occur because the 3D virtual overlay might not align perfectly with the 2D real-world scene at all distances and perspectives [62]. Additionally, the placement of the adapter and sensor at the handle, far from the camera at the tip, can lead to larger errors. Tracking inaccuracies can also play a role, as reduced tracking accuracy at certain positions or distances can limit the visualization of the overlay. However, an analysis of the tracking errors per second per measurement showed no significant tracking errors. Calibration inaccuracies can also cause misalignments. Furthermore, non-rigid deformations of the liver due to intraoperative organ deformations and surgical manipulation can affect registration, even with the EM sensor near the liver lesion. Lastly, lens distortion, if not properly corrected, can cause distortions in the overlay [63]. Some of these factors are explained in more detail below.

3.4.2.1 Sensor placement

The adapter is placed at the handle to avoid hindering the laparoscope movements or the surgeon's access to controls during surgery. However, this positioning may create a lever effect due to the large distance between the adapter and the camera's optical center, which can magnify calibration errors (Figure 26). Further research is needed to confirm. Positioning and designing an adapter at the tip of the laparoscope tip limits the distance between the sensor and the camera's optical center and could enhance final accuracy. Furthermore, it provides a better chance of being visible in the EM field, as the adapter sometimes disappears from view. Nevertheless, the perspective error still needs to be addressed. Additionally, this approach presents challenges, as the adapter would need to be tracked within the abdomen, complicating its implementation due to more strict sterilization requirements.

3.4.2.2 Calibration

Calibration inaccuracies can also cause misalignments. Firstly, the calibration is more accurate at a specific distance, resulting in errors when deviating from this distance. To mitigate this, the calibration was performed using a checkerboard positioned at various distances and orientations from the camera to ensure accuracy across different distances. Additionally, slight inaccuracies in intrinsic or extrinsic parameter estimation can lead to registration errors and differences in FOV calculations, affecting alignment accuracy. Moreover, the tracking and calibration of the laparoscope's cylinder rotation were not considered in this research. Consequently, this rotation was manually adjusted during the validation of the AR visualizations. To eliminate the need for manual adjustment, it is recommended to design and develop an extra adapter to track the cylinder rotation of the scopes. Cylinder rotation extends the FOV of oblique scopes but also complicates the calibration process due to the need for complex calibrations and additional devices [64]. Several solutions have been proposed in the literature to address this issue. One approach is to use rotary encoders [57][65] or markers [64], [66] by attaching an optical or magnetic marker to the cylinder to track the angular position with respect to the camera. The rotary encoder is effective, as shown in the literature, because it is not subject to the line-of-sight issues of an optical tracker or the magnetic field distortions of a magnetic tracker, and is thus most recommended. Despite the absence of cylinder rotation tracking, the adapters were usable for AR, and manual rotational adjustment was fast.

3.5 Conclusion

The developed adapters enhance the implementation of AR as a visualization method for the virtual representation of IGS. Despite reproducibility, calibration, and registration inaccuracies, AR visualization in the navigation workflow yields satisfactory results. Furthermore, with the new adapters, there is no need for a laparoscope switch during surgery, as AR can be used throughout the entire procedure rather than only when a 0°laparoscope is used. Addressing the limitations is recommended by reducing perspective errors, implementing an adapter at the laparoscope tip, and tracking cylinder rotation to improve performance during LLR. Optimizing these aspects holds the potential to enhance the accuracy of the AR overlay in the future, facilitating its implementation during surgery.

References

[1] Y. Xi and P. Xu, “Global colorectal cancer burden in 2020 and projections to 2040,” en, *Transl. Oncol.*, vol. 14, no. 10, p. 101 174, 2021-10.

[2] U. Testa, E. Pelosi, and G. Castelli, “Colorectal cancer: Genetic abnormalities, tumor progression, tumor heterogeneity, clonal evolution and tumor-initiating cells,” en, *Med. Sci. (Basel)*, vol. 6, no. 2, p. 31, 2018-04.

[3] D. Hu, Y. Pan, and G. Chen, “Colorectal cancer liver metastases: An update of treatment strategy and future perspectives,” en, *Surg. Pract. Sci.*, vol. 7, no. 100042, p. 100 042, 2021-12.

[4] H. Zhou, Z. Liu, Y. Wang, *et al.*, “Colorectal liver metastasis: Molecular mechanism and interventional therapy,” en, *Signal Transduct. Target. Ther.*, vol. 7, no. 1, p. 70, 2022-03.

[5] E. Van Cutsem, H. M. W. Verheul, P. Flamen, *et al.*, “Imaging in colorectal cancer: Progress and challenges for the clinicians,” en, *Cancers (Basel)*, vol. 8, no. 9, p. 81, 2016-08.

[6] O. V. Ivashchenko, E.-J. Rijkhorst, L. C. Ter Beek, *et al.*, “A workflow for automated segmentation of the liver surface, hepatic vasculature and biliary tree anatomy from multiphase MR images,” en, *Magn. Reson. Imaging*, vol. 68, pp. 53–65, 2020-05.

[7] A. Kalra, E. Yetiskul, C. J. Wehrle, and F. Tuma, *Physiology, Liver.* StatPearls Publishing, 2023-05.

[8] T. Germain, S. Favelier, J.-P. Cercueil, A. Denys, D. Krausé, and B. Guiu, “Liver segmentation: Practical tips,” en, *Diagn. Interv. Imaging*, vol. 95, no. 11, pp. 1003–1016, 2014-11.

[9] B. Rasuli and J. Jones, “Couinaud classification of hepatic segments,” in *Radiopaedia.org*. Radiopaedia.org, 2008-08.

[10] J. Martin, A. Petrillo, E. C. Smyth, *et al.*, “Colorectal liver metastases: Current management and future perspectives,” *World J. Clin. Oncol.*, vol. 11, no. 10, pp. 761–808, 2020-10.

[11] C. Conrad, M. Fusaglia, M. Peterhans, H. Lu, S. Weber, and B. Gayet, “Augmented reality navigation surgery facilitates laparoscopic rescue of failed portal vein embolization,” en, *J. Am. Coll. Surg.*, vol. 223, no. 4, e31–e34, 2016-10.

[12] B. Lee and H.-S. Han, “Laparoscopic anatomical resection of the liver: Segmentectomy and sub-segmentectomy,” in *The IASGO Textbook of Multi-Disciplinary Management of Hepato-Pancreato-Biliary Diseases*, Singapore: Springer Nature Singapore, 2022, pp. 279–284.

[13] M. R. Robu, P. Edwards, J. Ramalhinho, *et al.*, “Intelligent viewpoint selection for efficient CT to video registration in laparoscopic liver surgery,” en, *Int. J. Comput. Assist. Radiol. Surg.*, vol. 12, no. 7, pp. 1079–1088, 2017-07.

[14] P. Zhang, H. Luo, W. Zhu, *et al.*, “Real-time navigation for laparoscopic hepatectomy using image fusion of preoperative 3D surgical plan and intraoperative indocyanine green fluorescence imaging,” en, *Surg. Endosc.*, vol. 34, no. 8, pp. 3449–3459, 2020-08.

[15] A. Teatini, J. Pérez de Frutos, B. Eigl, *et al.*, “Influence of sampling accuracy on augmented reality for laparoscopic image-guided surgery,” en, *Minim. Invasive Ther. Allied Technol.*, vol. 30, no. 4, pp. 229–238, 2021-08.

[16] E. Kose, B. Kahramangil, H. Aydin, *et al.*, “A comparison of indocyanine green fluorescence and laparoscopic ultrasound for detection of liver tumors,” en, *HPB (Oxford)*, vol. 22, no. 5, pp. 764–769, 2020-05.

[17] M. A. Choti, “Patient variability in intraoperative ultrasonographic characteristics of colorectal liver metastases,” en, *Arch. Surg.*, vol. 143, no. 1, p. 29, 2008-01.

[18] I. Joo, “The role of intraoperative ultrasonography in the diagnosis and management of focal hepatic lesions,” en, *Ultrasonography*, vol. 34, no. 4, pp. 246–257, 2015-04.

[19] W. Zhu, X. Zeng, H. Hu, *et al.*, “Perioperative and disease-free survival outcomes after hepatectomy for centrally located hepatocellular carcinoma guided by augmented reality and indocyanine green fluorescence imaging: A single-center experience,” en, *J. Am. Coll. Surg.*, vol. 236, no. 2, pp. 328–337, 2023-02.

[20] A. Majlesara, M. Golriz, M. Hafezi, *et al.*, “Indocyanine green fluorescence imaging in hepatobiliary surgery,” en, *Photodiagnosis Photodyn. Ther.*, vol. 17, pp. 208–215, 2017-03.

[21] D. Ntourakis, R. Memeo, L. Soler, J. Marescaux, D. Mutter, and P. Pessaux, “Augmented reality guidance for the resection of missing colorectal liver metastases: An initial experience,” en, *World J. Surg.*, vol. 40, no. 2, pp. 419–426, 2016-02.

[22] J. N. Smit, K. F. D. Kuhlmann, B. R. Thomson, N. F. M. Kok, T. J. M. Ruers, and M. Fusaglia, “Ultrasound guidance in navigated liver surgery: Toward deep-learning enhanced compensation of deformation and organ motion,” en, *Int. J. Comput. Assist. Radiol. Surg.*, vol. 19, no. 1, pp. 1–9, 2023-05.

[23] B. Preim and D. Bartz, *Visualization in medicine* (The Morgan Kaufmann Series in Computer Graphics). Oxford, England: Morgan Kaufmann, 2007-06.

[24] J. Ramalhinho, S. Yoo, T. Dowrick, *et al.*, “The value of augmented reality in surgery — a usability study on laparoscopic liver surgery,” en, *Med. Image Anal.*, vol. 90, no. 102943, p. 102 943, 2023-12.

[25] C. Schneider, M. Allam, D. Stoyanov, D. J. Hawkes, K. Gurusamy, and B. R. Davidson, “Performance of image guided navigation in laparoscopic liver surgery – a systematic review,” en, *Surg. Oncol.*, vol. 38, no. 101637, p. 101 637, 2021-09.

[26] NDigital. “Electromagnetic tracking technology: Aurora 3d guidance comparison.” (2024), [Online]. Available: `https://www.ndigital.com/electromagnetic-tracking-technology/aurora-3d-guidance-comparison/` (visited on 2024-05-02).

[27] N. C. Buchs, F. Volonte, F. Pugin, *et al.*, “Augmented environments for the targeting of hepatic lesions during image-guided robotic liver surgery,” en, *J. Surg. Res.*, vol. 184, no. 2, pp. 825–831, 2013-10.

[28] J. Greeven, *Towards clinical implementation of ultrasound-based navigation for laparoscopic liver resection*, Unpublished thesis, NKI-AvL, 2023.

[29] M. Pruijt, *Augmented reality visualizations in liver surgery: A literature review*, Unpublished article, NKI-AvL, 2024.

[30] G. A. Prevost, B. Eigl, I. Paolucci, *et al.*, “Efficiency, accuracy and clinical applicability of a new image-guided surgery system in 3D laparoscopic liver surgery,” en, *J. Gastrointest. Surg.*, vol. 24, no. 10, pp. 2251–2258, 2020-10.

[31] B. Le Roy, E. Ozgur, B. Koo, E. Buc, and A. Bartoli, “Augmented reality guidance in laparoscopic hepatectomy with deformable semi-automatic computed tomography alignment (with video),” en, *J. Visc. Surg.*, vol. 156, no. 3, pp. 261–262, 2019-06.

[32] W. Zhang, W. Zhu, J. Yang, *et al.*, “Augmented reality navigation for stereoscopic laparoscopic anatomical hepatectomy of primary liver cancer: Preliminary experience,” en, *Front. Oncol.*, vol. 11, p. 663 236, 2021-03.

[33] E. R. Zorzal, J. M. Campos Gomes, M. Sousa, *et al.*, “Laparoscopy with augmented reality adaptations,” en, *J. Biomed. Inform.*, vol. 107, no. 103463, p. 103 463, 2020-07.

[34] C. Hansen, J. Wieferich, F. Ritter, C. Rieder, and H.-O. Peitgen, “Illustrative visualization of 3D planning models for augmented reality in liver surgery,” en, *Int. J. Comput. Assist. Radiol. Surg.*, vol. 5, no. 2, pp. 133–141, 2010-03.

[35] P. Pessaux, M. Diana, L. Soler, T. Piardi, D. Mutter, and J. Marescaux, "Towards cybernetic surgery: Robotic and augmented reality-assisted liver segmentectomy," en, *Langenbecks Arch. Surg.*, vol. 400, no. 3, pp. 381–385, 2015-04.

[36] L. W. Lau, X. Liu, W. Plishker, K. Sharma, R. Shekhar, and T. D. Kane, "Laparoscopic liver resection with augmented reality: A preclinical experience," en, *J. Laparoendosc. Adv. Surg. Tech. A*, vol. 29, no. 1, pp. 88–93, 2019-01.

[37] M. Adballah, Y. Espinel, L. Calvet, *et al.*, "Augmented reality in laparoscopic liver resection evaluated on an ex-vivo animal model with pseudo-tumours," en, *Surg. Endosc.*, vol. 36, no. 1, pp. 833–843, 2022-01.

[38] Y. Ryu, H.-C. O.Li, and S. Kim, "Analyses on characteristics and usage of digital game viewpoint: Why do games use third-person viewpoint more often than first-person viewpoint?" *J. Korea Contents Assoc.*, vol. 15, no. 7, pp. 75–83, 2015-07.

[39] D. Katić, A.-L. Wekerle, J. Görtler, *et al.*, "Context-aware augmented reality in laparoscopic surgery," en, *Comput. Med. Imaging Graph.*, vol. 37, no. 2, pp. 174–182, 2013-03.

[40] L. T. De Paolis and V. De Luca, "Augmented visualization with depth perception cues to improve the surgeon's performance in minimally invasive surgery," en, *Med. Biol. Eng. Comput.*, vol. 57, no. 5, pp. 995–1013, 2019-05.

[41] N. Haouchine, S. Cotin, I. Peterlik, *et al.*, "Impact of soft tissue heterogeneity on augmented reality for liver surgery," en, *IEEE Trans. Vis. Comput. Graph.*, vol. 21, no. 5, pp. 584–597, 2015-05.

[42] M. C. F. Macedo and A. L. Apolinario, "Occlusion handling in augmented reality: Past, present and future," en, *IEEE Trans. Vis. Comput. Graph.*, vol. 29, no. 2, pp. 1590–1609, 2023-02.

[43] S. Thompson, C. Schneider, M. Bosi, *et al.*, "In vivo estimation of target registration errors during augmented reality laparoscopic surgery," en, *Int. J. Comput. Assist. Radiol. Surg.*, vol. 13, no. 6, pp. 865–874, 2018-06.

[44] O. D. Bijlstra, A. Broersen, T. T. M. Oosterveer, *et al.*, "Integration of three-dimensional liver models in a multimodal image-guided robotic liver surgery cockpit," en, *Life (Basel)*, vol. 12, no. 5, p. 667, 2022-04.

[45] Brooke, "SUS: A 'quick and dirty' usability scale," in *Usability Evaluation In Industry*, CRC Press, 1996-06, pp. 207–212.

[46] S. G. Hart and L. E. Staveland, "Development of NASA-TLX (task load index): Results of empirical and theoretical research," in *Advances in Psychology*, ser. Advances in psychology, Elsevier, 1988, pp. 139–183.

[47] F. B. Achterberg, B. G. Sibinga Mulder, R. P. J. Meijer, *et al.*, "Real-time surgical margin assessment using ICG-fluorescence during laparoscopic and robot-assisted resections of colorectal liver metastases," en, *Ann. Transl. Med.*, vol. 8, no. 21, p. 1448, 2020-11.

[48] H. J. M. Handgraaf, L. S. F. Boogerd, D. J. Höppener, *et al.*, "Long-term follow-up after near-infrared fluorescence-guided resection of colorectal liver metastases: A retrospective multicenter analysis," *Eur. J. Surg. Oncol.*, vol. 43, no. 8, pp. 1463–1471, 2017-08.

[49] P. Pessaux, M. Diana, L. Soler, T. Piardi, D. Mutter, and J. Marescaux, "Robotic duodenopancreatectomy assisted with augmented reality and real-time fluorescence guidance," en, *Surg. Endosc.*, vol. 28, no. 8, pp. 2493–2498, 2014-08.

[50] A. Kolagunda, S. Sorensen, S. Mehralivand, *et al.*, "A mixed reality guidance system for robot assisted laparoscopic radical prostatectomy," in *Lecture Notes in Computer Science*, ser. Lecture notes in computer science, Cham: Springer International Publishing, 2018, pp. 164–174.

[51] J. Fischer, D. Bartz, and W. Strasser, "Intuitive and lightweight user interaction for medical augmented reality," in *Proceedings of Vision, Modeling, and Visualization*, 2005-01.

[52] J. Watson, M. Sayed, Z. Qureshi, *et al.*, "Virtual occlusions through implicit depth," in *2023 IEEE/CVF Conference on Computer Vision and Pattern Recognition (CVPR)*, Vancouver, BC, Canada: IEEE, 2023-06.

[53] E. Özgür, B. Koo, B. Le Roy, E. Buc, and A. Bartoli, "Preoperative liver registration for augmented monocular laparoscopy using backward–forward biomechanical simulation," en, *Int. J. Comput. Assist. Radiol. Surg.*, vol. 13, no. 10, pp. 1629–1640, 2018-10.

[54] W. H. Nam, D.-G. Kang, D. Lee, J. Y. Lee, and J. B. Ra, "Automatic registration between 3D intra-operative ultrasound and pre-operative CT images of the liver based on robust edge matching," en, *Phys. Med. Biol.*, vol. 57, no. 1, pp. 69–91, 2012-01.

[55] R. S. Puijk, A. H. Ruarus, L. G. P. H. Vroomen, *et al.*, "Colorectal liver metastases: Surgery versus thermal ablation (COLLISION) - a phase III single-blind prospective randomized controlled trial," en, *BMC Cancer*, vol. 18, no. 1, p. 821, 2018-08.

[56] K. van Duren, *Augmented reality for laparoscopic liver resections*, Unpublished thesis, NKI-AvL, 2022.

[57] T. Yamaguchi, M. Nakamoto, Y. Sato, *et al.*, "Development of a camera model and calibration procedure for oblique-viewing endoscopes," en, *Comput. Aided Surg.*, vol. 9, no. 5, pp. 203–214, 2004.

[58] S. Poorghasem and Y. Bao, "Review of robot-based automated measurement of vibration for civil engineering structures," en, *Measurement (Lond.)*, vol. 207, no. 112382, p. 112 382, 2023-02.

[59] Z. Zhang, "A flexible new technique for camera calibration," *IEEE Trans. Pattern Anal. Mach. Intell.*, vol. 22, no. 11, pp. 1330–1334, 2000.

[60] Artec 3D. "Artec spider - 3d-scanner." (), [Online]. Available: `https://www.artec3d.com/portable-3d-scanners/artec-spider` (visited on 2024-04-30).

[61] X. Liu, H. Su, S. Kang, T. D. Kane, and R. Shekhar, "Application of single-image camera calibration for ultrasound augmented laparoscopic visualization," in *Medical Imaging 2015: Image-Guided Procedures, Robotic Interventions, and Modeling*, R. J. Webster and Z. R. Yaniv, Eds., Orlando, Florida, United States: SPIE, 2015-03.

[62] V. Ferrari, N. Cattari, S. Condino, and F. Cutolo, "Optical rules to mitigate the parallax-related registration error in see-through head-mounted displays for the guidance of manual tasks," en, *Multimodal Technol. Interact.*, vol. 8, no. 1, p. 4, 2024-01.

[63] X. Liu, W. Plishker, G. Zaki, S. Kang, T. D. Kane, and R. Shekhar, "On-demand calibration and evaluation for electromagnetically tracked laparoscope in augmented reality visualization," en, *Int. J. Comput. Assist. Radiol. Surg.*, vol. 11, no. 6, pp. 1163–1171, 2016-06.

[64] C. Wu, B. Jaramaz, and S. G. Narasimhan, "A full geometric and photometric calibration method for oblique-viewing endoscopes," en, *Comput. Aided Surg.*, vol. 15, no. 1-3, pp. 19–31, 2010.

[65] S. Ieiri, M. Uemura, K. Konishi, *et al.*, "Augmented reality navigation system for laparoscopic splenectomy in children based on preoperative CT image using optical tracking device," en, *Pediatr. Surg. Int.*, vol. 28, no. 4, pp. 341–346, 2012-04.

[66] S. De Buck, F. Maes, A. D'Hoore, and P. Suetens, "Evaluation of a novel calibration technique for optically tracked oblique laparoscopes," in *Medical Image Computing and Computer-Assisted Intervention – MICCAI 2007*, ser. Lecture notes in computer science, Berlin, Heidelberg: Springer Berlin Heidelberg, 2007, pp. 467–474.

APPENDIX A: LITERATURE STUDY

Augmented Reality visualizations in liver surgery: A literature review

M.L. Pruijt [a, b]

[a] *Department of Surgical Oncology, Netherlands Cancer Institute – Antoni van Leeuwenhoek (NKI-AVL)*
[b] *MSc student Technical Medicine. Technical University of Delft, Leiden University Medical Center, Erasmus Medical Center, the Netherlands*
Medical supervisors: Prof. Dr. T.J.M. Ruers
Technical supervisors: K.A. Olthof MSc and M. Fusaglia PhD

Abstract

Minimal invasive liver resection offers advantages over open surgery due to patient benefits in recovery and trauma, but it is technically more challenging. Image-guided systems (IGS) based on augmented reality (AR) visualizations are being developed to facilitate these procedures. This review describes the state-of-the-art AR visualizations in liver surgery, its applications, potential benefits and current limitations. Advantages of using AR during liver procedures include enhanced anatomical visualization, more confidence in decision-making for the surgeon, and the elimination of an additional IGS screen. However, challenges such as information overload and a lack of depth perception due to a 2D view and occlusion may impact the intuitiveness and the experience of AR for surgeons. Potential solutions can be found in the field of gaming, sailboat navigation and car navigation by addressing various aspects such as depth cues and information balance. Ultimately, AR has the potential to augment, rather than degrade the surgeon's perception of the surgical scene.

Keywords; Augmented Reality, Liver surgery, Intraoperative, Image-guided surgery, Video assisted surgery

1. Introduction

Colorectal cancer (CRC) is the third most common cancer worldwide, with an estimated incidence of 1.9 million and 0.9 million deaths worldwide in 2020 [1]. Among these patients, colorectal liver metastases (CRLMs) occur in 25-50% of cases [2], emerging as one of the major causes of cancer-related deaths [3]. Surgical intervention is often the best curative option in patients with CRLM and since the first laparoscopic liver resection (LLR) in early 1990s, this has emerged as an expanding option [4, 5]. LLR offers numerous short-term advantages and patient benefits in contrast to open liver resection, such as minimizations in intraoperative bleeding, postoperative complications, hospitalization time, and health care costs [5-7]. However, LLR presents several technical challenges. The two-dimensional (2D) laparoscopic view lacks depth perception of the liver's complex three-dimensional (3D) anatomy and restricts tactile feedback of liver parenchyma [8]. Additionally, LLR faces issues related to operating space, the small field-of-view and suboptimal viewing angles of the scope [9].
Some of these challenges are addressed by robotic liver resection (RLR), such as the incorporation of wristed instruments, tremor abolition, and motion scaling, which enhance dexterity compared to LLR [9]. Nevertheless, both LLR and RLR share limitations in terms of palpating the liver parenchyma and interpreting its 3D anatomical context during surgery. As a result, complex resections are often still performed using open surgery.

Accurate intra-operative tumor localization is crucial to obtain negative resection margins and spare healthy liver parenchyma, bile ducts, and vessels [5]. Intraoperative ultrasound (IOUS) is considered as "gold standard" in the detection of liver tumors and guidance of surgical procedures intraoperatively [10]. The surgeon uses this imaging modality -in addition to diagnostic imaging- to locate the tumor borders, which he/she commonly marks on the liver surface prior to the resection. However, determination of the deep resection borders can be very difficult. In addition, IOUS poses limitations due to its low resolution, reduced sensitivity after ablation and/or chemo therapy, and its 2D representation of the liver's 3D anatomy.

Furthermore, challenges arise when the tumor has an isoechoic appearance, making it difficult to distinguish from the healthy parenchyma [11, 12]. Indocyanine green (ICG) fluorescence may provide additional information, enabling intraoperative visualization of tumor borders and resection boundaries. Nevertheless, fluorescence has a high false-positive rate and is constrained by a limited tissue penetration of 5-10 mm, restricting the visualization of deep-seated tumors [13, 14].

Image-guided surgery (IGS) systems address the aforementioned challenges of LLR and RLR, as they offer a virtual representation of the surgery, displaying surgical instruments in spatial relation to a patient-specific virtual model. These virtual models are manually [15, 16] or automatically [17] delineated from preoperative diagnostic computed tomography (CT) or magnetic resonance imaging (MRI) scans. For the registration process, retroreflective markers or electromagnetic (EM) sensors are typically attached to the surgical instruments and detected by tracking systems. Another tracking method for IGS involves self-localization systems like simultaneous localization and mapping (SLAM) [8, 18]. Additionally, camera calibration is performed to determine the fixed relationships between the intrinsic and extrinsic camera parameters and the tracked sensors, enabling accurate instrument tracking [19]. IGS provides surgeons with real-time diagnostic data, aiding in better lesion localization and visualization of surrounding anatomical structures [18].

In both LLR and RLR, the use of the laparoscopic video camera not only enables the integrating of virtual reality but also allows the implementation of augmented reality (AR) into the workflow. AR involves the real-time superimposition of diagnostic models directly onto the surgical field. Therefore, it also eliminates the necessity of an additional screen displaying the IGS information. However, visualizing AR during liver navigation is challenging, especially in providing surgeons with augmented visualization. AR should not only provide additional anatomical identification but also enhance decision-making, without degrading the surgeons' view [20]. This review describes the state-of-the-art AR visualizations in liver surgery. It examines different AR displays, current visualizations of AR in liver surgery, potential benefits and pitfalls of AR, and future visualization prospects from other applications then medical.

2. Search strategy

A literature search was conducted that included title, abstract and keywords, and incorporates search terms for “liver”, “video assisted” and ”surgery” along with those for “augmented reality” using the Embase (covering the period between 1993 and 2023) and Medline databases (covering the period between 1977 and 2023). The search included 282 articles without duplicates. All articles were screened based on title and abstract and relevant articles were used for this review. To complement the initial search, relevant references from included articles discussing AR in liver surgery or other medical applications were considered. These articles were used to supplement the state-of-the-art approaches of AR in the medical field.

Furthermore, the Scopus and IEEE databases were examined to supplement the review with relevant AR approaches beyond the medical field. These articles were included to delve into current AR techniques and challenges in other fields and to gain future prospects for improvements in AR applications during liver surgery. The search terms included corresponding terms for “information overload” or “occlusion” in conjunction with those for “augmented reality”. A detailed description of the search strategy is stated in Appendix A.

3. AR applications and visualization during liver surgery

This section describes the use of AR in liver surgery. For this purpose, a distinction was made into direct and indirect AR systems, with each category offering its own specific applications.

3.1. Direct AR display

Direct-based AR involves projects virtual models directly onto the surgical field of the patient lying on the OR table. It includes projection-based and optical see-through (OST) AR.

3.1.1. Projection based AR

In both LLR [21-24] and RLR [21, 25], projection-based AR involves projecting diagnostic images directly onto the patient's body surface using a beamer which is installed above the patient to avoid obstruction of the surgeon's field of view (FoV) caused by shadows [25]. This display technique projects a 2D image, making it particularly useful for interactive surgical planning, port positioning of the trocars [21-25] (Figure 1a) or to project anatomical structures onto the liver depending on the surgeon's position during open resections (Figure b-c) [26, 27]. Projection of the anatomy onto the patient's abdomen allows the surgeon to place the robotic or laparoscopic instruments in the desired direction [21, 24, 25]. Proper port placement is crucial to avoid potential collision of instrument shafts, ensuring maximum access, adequate surgeon dexterity, and visualization of critical areas [23]. In addition, young surgeons could use the AR projection as teaching approach [21]. However, a significant drawback of projection-based AR is that the projection on the surface of the patient could lead to depth perceptual issues [21, 23].

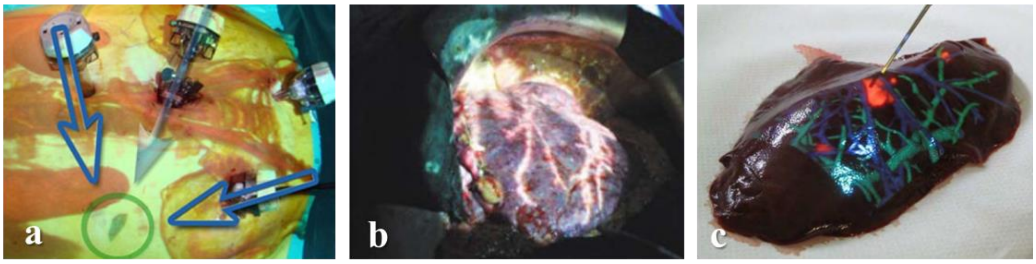

Figure 1. Projection-based augmented reality during image-guided liver surgery (a) 2-Dimensional image projection on the patients' body for port placement [22]. (b-c) Projection of anatomical structures onto liver surface during open resection [27, 28].

3.1.2. Optical see-through AR

Optical see-through (OST) is a type AR display that project virtual models directly onto the real-world through transparent displays. A deprecated OST involves overlaying virtual models onto the real world through semi-transparent half-silvered mirrors on which the reflection is superimposed [28] (Figure 2a). The mirror may be incorporated into the eye lenses or be placed in front of the surgical scene. However, this approach is only used for open liver surgery and limited by a reduced depth perception [29, 30].

A more common display form of OST is a head-mounted display (HMD). It relies on HMDs like glasses or a HoloLens to present the augmented content and can elevate the user's sensory experience and allows hands-free interaction with the virtual model. An application of OST HMD integrated the laparoscopic screen into the surgeon's FoV, effectively alleviating discomfort and fatigue during prolonged procedures (Figure 2b) [31]. This application, however, does not provide any additional information as other IGS systems. Saito et al. [32] discussed a HoloLens technology to overlay virtual content directly onto the user's real-world view, creating a hologram (Figure 2c). This visualization is useful because the surgeon has the possibility of moving around the augmented object, thus looking at the augmented model from different perspectives. Nevertheless, the physical burden caused by the weight of the HMD necessitates further technical improvements of the device before its application during surgery.

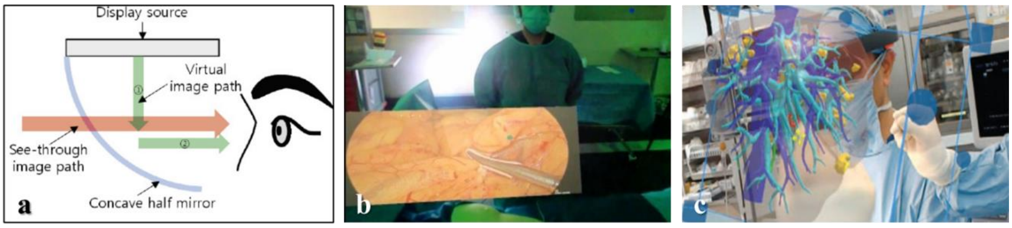

Figure 2. Optical see through (OST) Augmented Reality. (a) Overlaying virtual models onto the surgical field through semi-transparent half-silvered mirrors on which the reflection is superimposed [31]. (b) Using Head Mounted Displays to integrate the laparoscopic screen into the surgeon's field of view [20]. (c) Using a HoloLens to display a Hologram [32].

3.2. *Indirect AR display*

Indirect, or also video-based AR, overlays virtual models onto surgical scenes captured through a video camera (commonly the laparoscopic video camera). Video-based AR is used in open navigation procedures using a smartphone or tablet, also referred as video-see-through AR [33] (Figure 3a). Additionally, this display technique is used in LLR [34-38] and RLR [19, 24, 39] onto the external OR monitor (Figure 3b) [15]. An advantage of this display technique is that the monitor is already implemented into the workflow and all surgeons and assistants share the same perspective [15, 16].

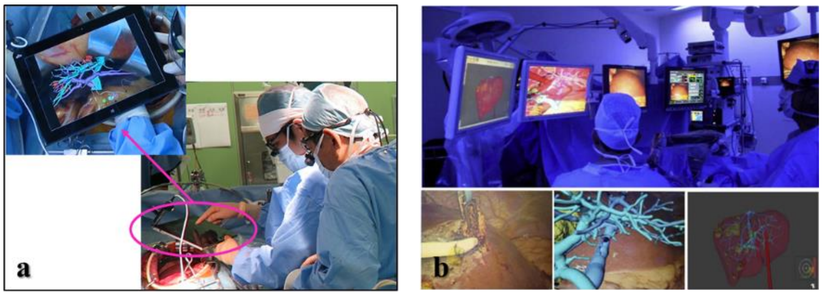

Figure 3. Video-based Augmented Reality (AR) display. (a) Video-see-through AR display using a tablet during open resections [33]. (b) Image-guided surgery using a video-based AR display. AR is displayed on a screen positioned in front of the surgeon and assistants [15].

There are several applications for the visualization of these AR overlays. Nearly all virtual models are presented in a semi-transparent display, using different colors to distinguish various structures such as arteries, veins, and tumors [34]. Many articles incorporate the entire liver model for their AR overlay (Figure 4a) [15, 16, 36, 39, 40], while others choose to project vessels at interest for the resection, the target lesion, and/or liver segments encountered during the resection (Figure 4b and c) [19, 34, 41]. The projection of an entire liver model is limited by information overload in the visualization, a lack of depth perception, and complexity of the AR accuracy in the entire overlay [39]. Focusing on partial liver model visualization provides a more targeted and less overwhelming representation.

Examples of different AR visualizations are provided in Figure 4. In Zhang et al. [34], AR was used for intraoperative navigation of the important vessels (Figure 4b). However, the virtual portal vein occluded the surgical instruments, leading to a lack of depth perception in the visualization.

Özgür et al. [41] compensated for liver motions, by using biomechanical constraints to deform the virtual model. While the model was accurately aligned with the real liver, the virtual liver lacked sufficient transparency, leading to occlusion of the real liver (Figure 4c). Additionally, Le Roy et al. [37] visualized a deformed liver model and augmented one target vessel and two lesions onto the liver (Figure 4d). This liver model created some information balance and avoids occlusion through full transparency but has limited depth perception. The performance of this AR visualization was tested in comparison with IOUS, showing more accurate resection margins with less variability than IOUS, especially in liver zones that were challenging to access with tumors situated deeply in the liver parenchyma [38].

To distinguish between superficial and deep-seated vessels in LLR, Thompson et al. [36] implemented saliency in their AR view. This allows more transparent rendering in deep vessels and less transparent rendering in vessels closer to the liver surface (Figure 4e). This visualization enhances depth perception and interpretation of the augmented overlay.

In a different approach, Prevost et al. [35] implemented an augmented window view during LLR including an adjustable radius (Figure 4f). In this visualization, the liver model is not completely occluded, resulting in enhanced depth perception an reduced visual clutter in the augmented view.

Moreover, real-time augmentation of the IOUS scan onto the LLR view to compensate for liver deformations without a diagnostic model was visualized by Lau et al. [42] (Figure 4g). The IOUS imaging guided surgeons in making real-time adjustments to resection depth without screen-switching between the US and the laparoscopic camera view.

In addition, augmentation of the virtual delineation of resection margins aids in planning for RLR (Figure 4h) [24]. However, the visualization is cluttered due to the entire model overlay. This augmented margin information was also projected during LLR without the entire liver model (Figure 4i).

Furthermore, the distanced between robotic [19] or laparoscopic [43] instruments and the tumor can be augmented onto the laparoscopic camera view (Figure 4j). This AR view has the potential to enhance the surgeon's orientation of the anatomy and improve depth perception.

Another LLR study addressed the limited depth perception of the AR view by applying textures with distance-encoding silhouettes (vessel contours) and surfaces (stroke width) for AR visualization [44]. This reduced visible complexity and enhanced depth perception of the vessels (Figure 4k-l). Furthermore, they presented a method for the illustrative visualization of resection surfaces (Figure 4k), but this sows a higher complexity due to over-information of the visualization.

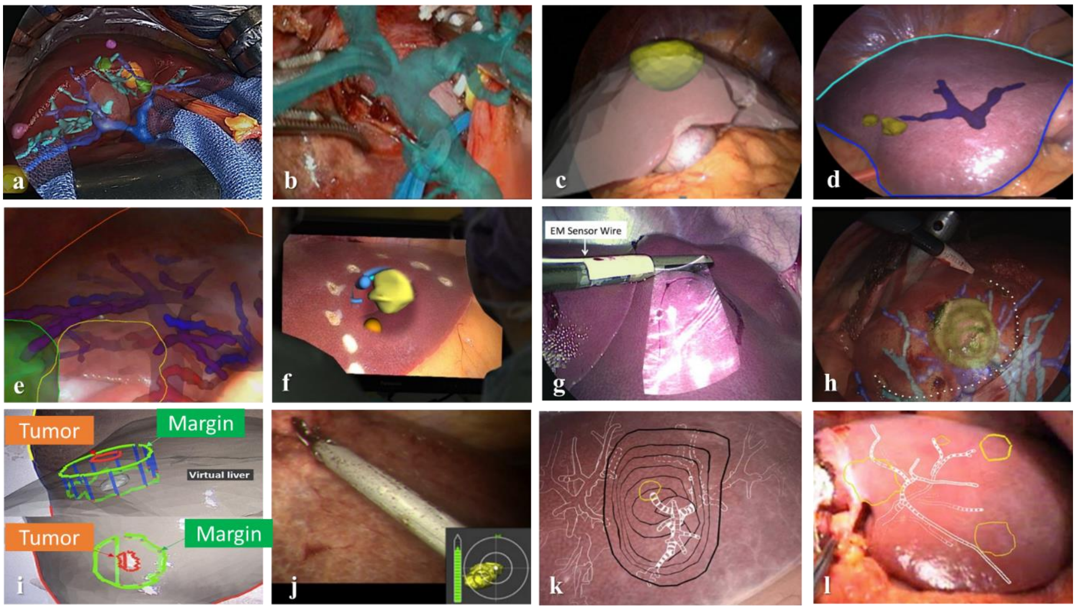

Figure 4. Intraoperative Augmented reality (AR) visualizations. (a) Entire liver model overlay creates visual clutter. Portal vein in deep blue, hepatic veins in light blue, and tumors in varying colors [16]. (b) Targeted visualization of the portal vein (light blue). Occluded instruments visible [34]. (c) Lesion (yellow) and deformable liver which occludes the real liver [41]. (d) Full-transparant deformable liver model and its target lesions (yellow) and vessels (purple). Limited depth perception [37]. (e) Transparency differences to visualize depth perception. Veins in blue and purple, arteries in red, tumor in green and gallbladder (yellow outline) [36]. (f) Window visualization to reduce visual clutter and create depth perception. Target lesion in yellow [35]. (g) Overlay of the Intraoperative laparoscopic Ultrasound image to the probe tip [42]. (h) Visualization of a margin planning. Visual clutter due over-information of all virtual structures [25]. (i) Visualization of lesion (red sketch) and margin (green sketch) onto the liver's surface [38]. (j) Visualization of tumor- instrument distance. A color bar ranging from green to red to alert the surgeon when the tumor is close- or not [19]. (k) Visualization of resection surfaces results in visual clutter. Distance to the liver surface is depicted through stroke thickness of the vessels, called distance-encoding surface. Some branches are faded based on a distance threshold [44]. (l) Distance-encoding surface and silhouettes [44].

4. General potential benefits of AR in liver surgery

AR enhances anatomical visualization during navigated liver resections [19, 24, 34, 39, 41, 45, 46]. It serves as a valuable navigation tool for resecting disappearing [35], deeply seated [37] or small liver lesions, broadening surgical options for previously undetectable lesions [11, 12, 16].

Moreover, AR demonstrates improved surgeon comfort and confidence during surgical procedures [20], facilitates decision-making, and improves situation awareness by providing a clearer understanding of anatomical structures [34, 42]. This minimizes the risk of damaging healthy surrounding tissues and blood vessels, resulting in less blood loss [34].

Furthermore, the implementation of AR aims to reduce screen-switching for surgeons [31] and improves tactile feedback of liver parenchyma during intraoperative IGS [47, 48]. However, reduced morbidity and improvements in oncological outcomes for the patients are not evaluated yet [39]. Future clinical studies are needed to evaluate the benefits of AR for reducing postoperative morbidity and mortality and improving long-term clinical outcomes.

5. Current limitations to AR in liver surgery

At this moment, AR in liver surgery is not standard of care. This is due to the challenges in obtaining a sufficiently high accuracy for AR navigation in a deformable organ, but also due to current limitations of the AR visualization.

5.1. Accuracy challenges

Accurate alignment of the virtual model with the laparoscopic view of the liver poses a significant challenge. For effective AR as a support tool for surgical decisions, precise localization of tumors in the AR visualization is important. Currently, the AR overlay may result in incorrect decisions, posing a risk of inadvertent damage to healthy tissue due to potentially misleading situational awareness.

Accurate registration of the virtual model onto the camera view is constrained by the laparoscopic screen size, which captures a small amount of information about reality. Surface reconstruction techniques attempt to reconstruct the 2D view in 3D. However, laparoscopic views composed of (2D) pixels that consists three values (Red-Green-Blue), while virtual models are derived from a MRI or CT scans, composed of (3D) voxels that consists a single intensity value. As a result, this leads to partial 3D information after surface reconstruction of the laparoscopic view, restricting accurate surface reconstruction [8, 34].

5.2. Pitfalls in AR visualization

It is a challenge to visualize the AR overlay effectively. Errors in visualization may impact the intuitiveness and the experience of AR for surgeons. Important pitfalls include information overload and a lack of depth perception due to a 2D view and the occlusion problem.

5.2.1. *Information overload*

In AR-assisted liver surgeries, the projection of comprehensive liver models and their structures often results to information overload and visual clutter. This can result in ineffective localization of the anatomy. Visual clutter occurs when the AR view is overwhelmed by excessive or disorganized information (Figure 4a). Finding a balance between excessive and insufficient data is needed for effective AR [49].

5.2.2. *Lack of depth perception*

One of the main challenges of AR in liver surgeries is the lack of depth perception [43]. Whilst in projection-based systems, the AR is displayed in a 3D environment, in laparoscopy, AR is displayed in a 2D monitor and thus perception of depth has to be modeled in a different way. For example, in 3D holograms, the viewer has the possibility of moving around the augmented object, thus looking at the augmented information from different perspectives. In laparoscopy, the only available view is the laparoscopic one, which is almost static and from a single perspective viewpoint. Therefore, the visualization of structures which are far away from the perspective view are more difficult to be accurately perceived.

Additionally, the virtual model seems occluded on top of the real objects in the laparoscopic view, even when it should be located behind them. This limits the immersion and spatial comprehension of the objects on the screen [45]. Being occlusion handling a long-standing and important problem in AR, Macedo et al. [50] conducted a comprehensive review about this. They addressed two key aspects in their review: *the order problem* and *the x-ray vision problem*. Clear understanding of the order of the real and virtual models in the augmented scene can enhance knowledge of, for instance, the positioning of instruments and the virtual liver in the laparoscopic scene [20, 45]. X-ray vision in occlusion handling means that the real world is visualized behind the virtual model, allowing see-through visualization of occluded real objects. In MIS, this means the visualization of the real liver through the overlaid virtual model.

5.3. *Human interaction*

Many AR techniques need varying degrees of human interaction to use the AR system [16]. This may include manual landmark identification for registration [15, 16, 37, 51], enabling or disabling of 3D models, or changing transparency of the augmented model. While the manual process may negatively impact the surgical workflow time, the efficiency varies with the degree of interaction (semi-automatic) [52], the surgeon's experience, the involvement of computer scientists and the intuitiveness of the UI [24].

6. Future prospects

Enhancements in AR accuracy and visualization are necessary before AR can become the standard of care.

6.1. *Improved accuracy*

To handle the issue of partial surface reconstruction during surface reconstruction approaches, active surface reconstruction techniques can be employed. These techniques handle the visual complexity and the lack of texture in the camera view, though they have not yet applied in laparoscopic liver procedures. One example of these active techniques is Shape-from-Polarization (SfP), which utilizes polarized light sources to enhance surface reconstruction. SfP proves advantageous in homogeneous lighting of texture-less surfaces [53, 54]. Additionally, Time-of-Flight technology transmits light and measures the time until it is reflected back to provide real-time depth information [55]. Lastly, structured light techniques may compensate for the lack of texture by projecting light patterns onto the scene, particularly useful in reconstructing dynamic scenes [56]. Although these techniques requires specialized equipment, they potentially improve accuracy in laparoscopic liver settings. As the depth maps produced by these techniques are generated from the laparoscope perspective, they share the same point of view of the AR and therefore can be immediately used for enhancing the perception of depth.

Nevertheless, there is a need for human interaction between the virtual model and the surgeon to achieve the most accurate AR overlay. This would enable real-time interaction with the virtual model and all surgical instruments during surgical procedures. This interaction is partially presented in VR games and enhances the user's immersive experience, but is not implemented in AR yet [57].

6.2. *Visualization*

6.2.1. *Information balance*

Information balance can be achieved through visualization windows and the display of target structures, but also by projecting resection lines onto the liver surface (Figure 4h-i) [38]. Automating the detection of tumor margins, similar to how AR navigation in the automotive sector automatically detects and visualizes car routes onto the road would be useful. Car navigation uses digital road map data and GPS to track the real-time position and route of the car. This route is then augmented onto the windshield (Figure 5a). Similar AR technologies have been adopted by the civil aviation industry and for sailboat navigation (Figure 5b) [58]. Sailboat navigation shares similarities with laparoscopic navigation, particularly in the context of real-time decision-making and therefore research in these AR visualizations could be valuable also in medical domain [59].

As an alternative approach to reduce visual clutter, Fischer et al. [60] demonstrated an AR application in which the surgeon can manually sketch the resection plan directly on the patient’s skull (Figure 5c). This augmented operation plan may also be useful during liver surgery.

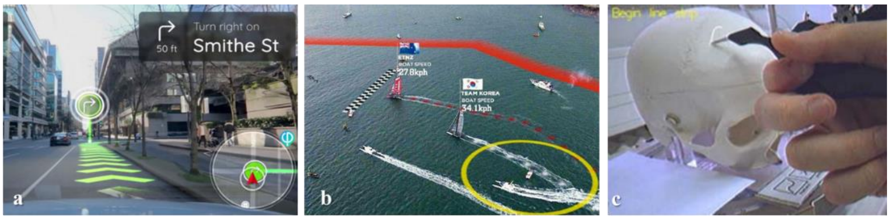

Figure 5. Potential improvements in Augmented reality (AR) visualization from other applications. (a) AR path overlay in car navigation [59]. (b) Augmented detection of sailors onto the water surface [59]. (c) Interactive resection plan [61].

Finally, information overload can be reduced by employing activation-on-demand, permitting AR activation at critical moments to minimize disruptions and prevent decisions solely based on AR. This is commonly employed in AR-integrated RAS of prostatectomy, where surgeons use an HMD [61] or a foot pedal to activate AR visualization on the surgeon console. Moreover, an intuitive UI including simple controls allowing toggling structures on- and off would benefit the surgeon.

6.2.2. Enhanced depth perception

Different advanced AR visualization methods have been proposed to address better depth perception.

6.2.2.1. Occlusion handling

To tackle the “order problem” in AR visualizations, binary masks or depth maps may be implemented.
Fischer et al. [62] described an approach of using binary masks from diagnostic scans for object segmentation. Their AR system visually indicates whether the instrument should be displayed in front of or behind the skull (Figure 6a-b). A more data-driven approach using binary masks, involves deep learning or CNN to detect surgical instruments in the laparoscopic scene [63, 64]. This visualization enhances spatial awareness and depth perception. However, binary masks do not visualize depth information of all objects within the scene.

Depth-maps approaches in AR include 1) stereo vision and 2) multi-view stereo techniques for accurate depth perception using two or more cameras. Furthermore, they encompass 3) active techniques such as Light Detection and Ranging (LiDAR), ToF and structured light sensors to provide real-time depth data. These approaches enhance occlusion handling and provide a detailed understanding of the real scene [50, 65].

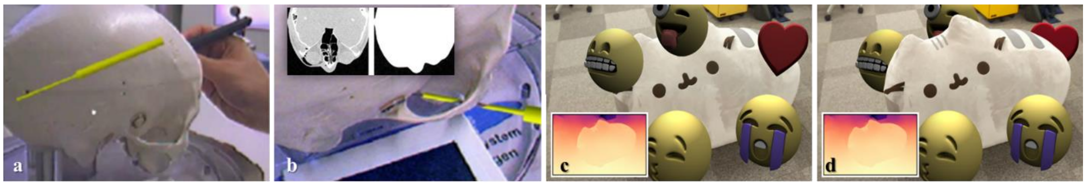

Figure 6. Occlusion handling to improve the interpretation of the object position in the scene. (a) Surgical instrument is supposed to be occluded behind the skull, but is overlaid on top of it. (b) Detail of the cheek bone correctly occludes part of the tool, because a binary mask is segmented from the diagnostic scan [63]. (c) Virtual smiley models occlude the real cat. (d) Shape-for Motion technique generates depth maps for occlusion handing in different layers. Two smileys are positioned behind the real cat, and two are in front [67].

Moreover, there are depth-maps approaches with a single camera such as 4) spherical vision and 5) monocular Shape-for Motion (SfM) approaches. SfM methods are already used on smartphones, addressing occlusion in AR applications using real-time depth maps [66] (Figure 6c-d). Furthermore, the realism of AR visualization including depth perception can be implemented with localized-based depth (Figure 7a-b), surface-based depth (Figure 7c), and dense-based depth (Figure 7d) [67].

In contrast to depth-based approaches, an occlusion mask can be estimated without implementing a depth map [65]. A multi-layer perceptron can predict per pixel in the real scene if it is in front or behind a virtual target's depth map. This technique outperforms Apple's ARKit Lidar approach and conventional regression approaches in visualizing edge fidelity.

Figure 7. Depth maps to solve the order problem (a-b) Location-based depth visualization. Left Reflection and right collision checking. (c) Surface-based depth. Color balloons explode on surfaces and wrap around objects upon contact, creating a dynamic visual display. (d) Dense-based depth. Background is adaptively blurred out according to the distance to the focal point [68].

X-ray vision

Various strategies to solve the "x-ray vision problem" have been proposed by Macedo et al. [50] have already been implemented in liver surgery. These strategies include: 1) semi- transparency to ensure smooth transitions between visible and occluded structures, 2) virtual windows to restrict the display of occluded objects (Figure 4f), and 3) saliency to create a visually balanced transparency in the augmented view (Figure 4e) [35, 36]. Others include the implementation of 4) edge extraction (figure 8a-b) [68] and 5) perspective lines [69] (figure 8c). During liver AR, edge extraction may enhance depth perception of virtual tumors and vessels. Perspective lines may be useful to create a sense of depth perception in the surficial or deep-seated tumors. Moreover, 6) spatial manipulation techniques, such as distortion (Figure 8d-e), warping, or curvature (Figure 8f), are used to enable see-through visualization of the occluded view [70]. All techniques are often combined with semi-transparency [71] (Figure 8f). Unfortunately, since humans do not have X-ray vision capability, no ground truth is available for assessing X-ray vision techniques using an accuracy metric [50].

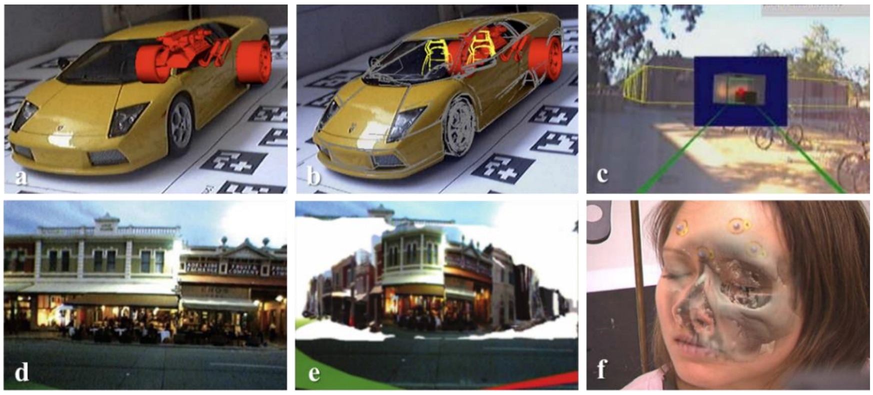

Figure 8. X-ray vision techniques for occluded objects. (a) The virtual red wheel of the car is visualized in the foreground. (b) Edge extraction to create more depth perception of the virtual red wheel [69] (c) Virtual perspective lines from the camera towards the occluded content to provide more depth perception [69]. (d) The original image undergoes (e) distortion (spatial manipulation) to visualize the occluded houses beyond the frame [71]. (f) The virtual model is curved to follow the structure of the face [72].

6.2.2.2. Other visual depth cues

AR in liver surgery not only faces challenges with occlusion, but also limits other crucial depth cues to provide better depth perception [72]. Ray tracing, also implemented in the gaming industry, can provide real-time interaction between virtual and real objects [73, 74]. Shadows within the AR view may improve depth perception and shape of the objects (Figure 9a) [71, 73]. Size perceptions can also contribute to the creation of depth, however it may create a depth illusion. By implementing reflection due virtual mirrors into the AR scene this depth illusion can be elevated [73, 75] (Figure 9b). The movement of these virtual mirrors introduces motion parallax, further enhancing the perceptual depth within the visual field [75]. Furthermore, motion parallax can be implemented in HMDs, causing objects at different distances appear to move at different speeds as your head moves, contributing to a more realistic perception of depth and immersion. However, this visualization may also lead to inaccuracies in real-world due HMD conditions [71, 76]. Moreover, texture gradients may be added as additional depth cues to improve the realism of the visualization (figure 4k-I and 9c-d) [77]. However, this can result in visual clutter in the laparoscopic view, so it may not useful for this approach.

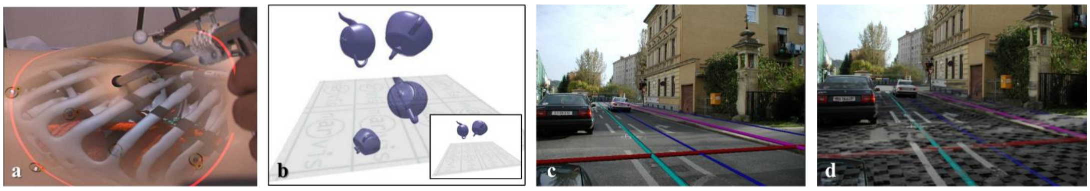

Figure 9. Depth cues to improve depth perception. (a) Relative shadows. Bichlmeier et al. [72]. (b) Size perspective resulting in depth illusion. Virtual mirror creates reflections to improve depth perception. Through the virtual mirror, it is visible that the small teapot is in front of the big teapot. Bichlmeier et al. [76] (c-d) Texture gradients improve the realism of the visualization including underground pipes. Zollman et al. [78].

7. Conclusion

In conclusion, the current state of AR is suboptimal but has the potential to enhance anatomical visualization by superimposing diagnostic imaging information directly onto the patient's anatomy, thereby improving decision-making for surgeons. Challenges such as vascular injury, imprecise tumor localization, and excessive resection of normal liver tissue could be potentially mitigated by AR. This review describes the current state-of-the-art AR visualizations in liver surgery, including various display methods and their visualizations, benefits, challenges and future prospects to improve the visualization of AR. AR should augment rather than degrade the surgeon's perception of the surgical scene. Therefore, it is recommended to improve registration accuracy, balance the augmented information, and enhance depth perception of the anatomical structures. Conducting preclinical and clinical studies to test various AR visualization approaches would be useful to determine which visualization yields the best outcomes. Only then, AR can be an implemented step in the surgical workflow, offering significant enhancements that translate into improved patient care. Ultimately, the successful implementation of AR in surgery holds promise as a transformative technique for the future of liver surgery.

Appendix

Appendix A. Search strategy

1. **Arts Interview AVL-NKI**: The challenges of AR in the current workflow during laparoscopic liver surgeries at AVL-NKI were identified. These AR challenges were incorporated during the article screening process. Relevant literature was evaluated, emphasizing solutions and insights that address the issues revealed in the Arts' interview.
2. **Medline and Embase search for articles AR in (laparoscopic) liver surgery:** state-of-the-art description (Tables A2.1. and 2.2.).

Table A2.1. General information included articles

Database	Platform	Years of coverage	Records	Records after duplicates removed
Medline ALL	Ovid	1977 – Dec 2023	184	170
Embase	Embase.com	1993 – Dec 2023	258	112
Total			442	**282**

Table A2.2. Search strings Medline and Embase database

Database	Search string
Medline ALL	(Augmented Reality / OR virtual reality/ OR Virtual Reality / OR Exergaming / OR (((augment* OR virtual* OR mixed OR extended) ADJ3 realit*) OR exergam*).ab,ti,kw. OR (ar OR vr OR xr OR augment* OR virtual*).ti.) AND (* Liver/su OR (Liver/su AND (Robotic Surgical Procedures/ OR Video-Assisted Surgery/ OR Laparoscopy/ OR Surgery, Computer-Assisted/ OR Surgical Navigation Systems/)) OR (((robot* OR video* OR laparoscop* OR mapping* OR navigation* OR guided* OR guidance* OR imaging* OR image*) ADJ6 (liver* OR hepat*) ADJ6 (surg* OR operat* OR intrasurg* OR intraoperat* OR resect*)) OR ((laparoscop*) ADJ6 (liver* OR hepat*))).ab,ti,kw. OR (((liver* OR hepat*) AND (surg* OR operat* OR intrasurg* OR intraoperat* OR resect*)) OR ((laparoscop*) AND (liver* OR hepat*)) OR hepatectom*).ti.) AND english.la. NOT (exp animals/ NOT humans/)
Embase	('augmented reality'/de OR 'augmented reality system'/de OR 'virtual reality'/de OR ' virtual reality system'/de OR 'mixed reality'/de OR 'extended reality'/de OR exergaming/de OR (((augment* OR virtual* OR mixed OR extended) NEAR/3 realit*) OR exergam*):ab,ti,kw OR (ar OR vr OR xr OR augment* OR virtual*):ti) AND ('liver surgery'/exp/mj OR ('liver surgery'/exp AND ('laparoscopic surgery'/exp OR 'robot assisted surgery'/exp OR 'video assisted surgery'/exp OR laparoscopy/de OR 'computer assisted surgery'/de OR 'surgical navigation system'/de)) OR (((robot* OR video* OR laparoscop* OR mapping* OR navigation* OR guided* OR guidance* OR imaging* OR image*) NEAR/6 (liver* OR hepat*) NEAR/6 (surg* OR operat* OR intrasurg* OR intraoperat* OR resect*)) OR ((laparoscop*) NEAR/6 (liver* OR hepat*))):Ab,ti,kw OR (((liver* OR hepat*) AND (surg* OR operat* OR intrasurg* OR intraoperat* OR resect*)) OR ((laparoscop*) AND (liver* OR hepat*)) OR hepatectom*):ti) NOT [conference abstract]/lim AND [english]/lim NOT ([animals]/lim NOT [humans]/lim)

3. **To complement the information obtained in the initial search, relevant references from the included articles discussing AR in liver surgery or other medical applications were considered.** These articles were used to supplement the state-of-the-art approaches of AR in the medical field.
4. **Complement Search to other Applications:**
   Furthermore, the Scopus and IEEE databases were examined to supplement the review with relevant XR approaches (VR, AR, and MR) beyond the medical field, such as Gaming industry. These articles were included to delve into current AR techniques and challenges in other fields and to gain future prospects for improvements in AR applications during liver surgery. The search terms included corresponding terms for “information overload” or “occlusion” in conjunction with those for “extended reality” (Table A4.1. and 4.2.).

Table A4.1. General information included articles

Database searched	Platform	Years of coverage
Scopus	Scopus.com	2000-2024
IEEE	ieeexplore.ieee.org	2000-2024

Table A4.2. Search strings Scopus and IEEE database

Databases searched	Search string
Scopus and IEEE	("information overload" OR "visual clutter") AND ("Extended reality" OR "augmented reality" OR "Mixed reality") ("occlusion" AND ("Extended reality" OR "augmented reality" OR "Mixed reality")) ("depth cues" AND ("Extended reality" OR "augmented reality" OR "Mixed reality"))

References

[1] Y. Xi and P. Xu, "Global colorectal cancer burden in 2020 and projections to 2040," (in eng), *Transl Oncol*, vol. 14, no. 10, p. 101174, Oct 2021, doi: 10.1016/j.tranon.2021.101174.

[2] E. De Raffele *et al.*, "Simultaneous colorectal and parenchymal-sparing liver resection for advanced colorectal carcinoma with synchronous liver metastases: Between conventional and mini-invasive approaches," (in eng), *World J Gastroenterol*, vol. 26, no. 42, pp. 6529-6555, Nov 14 2020, doi: 10.3748/wjg.v26.i42.6529.

[3] U. Testa, E. Pelosi, and G. Castelli, "Colorectal cancer: genetic abnormalities, tumor progression, tumor heterogeneity, clonal evolution and tumor-initiating cells," (in eng), *Med Sci (Basel)*, vol. 6, no. 2, Apr 13 2018, doi: 10.3390/medsci6020031.

[4] D. L. Aghayan *et al.*, "Evolution of laparoscopic liver surgery: 20-year experience of a Norwegian high-volume referral center," (in eng), *Surg Endosc*, vol. 36, no. 5, pp. 2818-2826, May 2022, doi: 10.1007/s00464-021-08570-3.

[5] M. Nicolás *et al.*, "Laparoscopic vs open liver resection for metastatic colorectal cancer: analysis of surgical margin status and survival," *Langenbeck's Archives of Surgery*, vol. 407, no. 3, pp. 1113-1119, 2022/05/01 2022, doi: 10.1007/s00423-021-02396-2.

[6] K. T. Nguyen, J. W. Marsh, A. Tsung, J. J. Steel, T. C. Gamblin, and D. A. Geller, "Comparative benefits of laparoscopic vs open hepatic resection: a critical appraisal," (in eng), *Arch Surg*, vol. 146, no. 3, pp. 348-56, Mar 2011, doi: 10.1001/archsurg.2010.248.

[7] R. Ciria, D. Cherqui, D. A. Geller, J. Briceno, and G. Wakabayashi, "Comparative Short-term Benefits of Laparoscopic Liver Resection: 9000 Cases and Climbing," (in eng), *Ann Surg*, vol. 263, no. 4, pp. 761-77, Apr 2016, doi: 10.1097/sla.0000000000001413.

[8] P. Zhang *et al.*, "Real-time navigation for laparoscopic hepatectomy using image fusion of preoperative 3D surgical plan and intraoperative indocyanine green fluorescence imaging," (in eng), *Surg Endosc*, vol. 34, no. 8, pp. 3449-3459, Aug 2020, doi: 10.1007/s00464-019-07121-1.

[9] K. Moorthy *et al.*, "Dexterity enhancement with robotic surgery," (in eng), *Surg Endosc*, vol. 18, no. 5, pp. 790-5, May 2004, doi: 10.1007/s00464-003-8922-2.

[10] E. Kose *et al.*, "A comparison of indocyanine green fluorescence and laparoscopic ultrasound for detection of liver tumors," (in eng), *HPB (Oxford)*, vol. 22, no. 5, pp. 764-769, May 2020, doi: 10.1016/j.hpb.2019.10.005.

[11] M. A. Choti *et al.*, "Patient variability in intraoperative ultrasonographic characteristics of colorectal liver metastases," (in eng), *Arch Surg*, vol. 143, no. 1, pp. 29-34; discussion 35, Jan 2008, doi: 10.1001/archsurg.2007.5.

[12] I. Joo, "The role of intraoperative ultrasonography in the diagnosis and management of focal hepatic lesions," (in eng), *Ultrasonography*, vol. 34, no. 4, pp. 246-57, Oct 2015, doi: 10.14366/usg.15014.

[13] W. Zhu *et al.*, "Perioperative and Disease-Free Survival Outcomes after Hepatectomy for Centrally Located Hepatocellular Carcinoma Guided by Augmented Reality and Indocyanine Green Fluorescence Imaging: A Single-Center Experience," *J Am Coll Surg*, vol. 236, no. 2, pp. 328-337, 2023, doi: 10.1097/xcs.0000000000000472.

[14] A. Majlesara *et al.*, "Indocyanine green fluorescence imaging in hepatobiliary surgery," (in eng), *Photodiagnosis Photodyn Ther*, vol. 17, pp. 208-215, Mar 2017, doi: 10.1016/j.pdpdt.2016.12.005.

[15] C. Conrad, M. Fusaglia, M. Peterhans, H. Lu, S. Weber, and B. Gayet, "Augmented Reality Navigation Surgery Facilitates Laparoscopic Rescue of Failed Portal Vein Embolization," (in English), *J Am Coll Surg*, Article vol. 223, no. 4, pp. e31-e34, 2016, doi: 10.1016/j.jamcollsurg.2016.06.392.

[16] D. Ntourakis, R. Memeo, L. Soler, J. Marescaux, D. Mutter, and P. Pessaux, "Augmented Reality Guidance for the Resection of Missing Colorectal Liver Metastases: An Initial Experience," *World J Surg,* vol. 40, no. 2, pp. 419-426, 2016, doi: 10.1007/s00268-015-3229-8.

[17] M. R. Robu *et al.*, "Intelligent viewpoint selection for efficient CT to video registration in laparoscopic liver surgery," *Int. j. comput. assist. radiol. surg.,* vol. 12, no. 7, pp. 1079-1088, 2017, doi: 10.1007/s11548-017-1584-7.

[18] B. Preim and D. Bartz, *Visualization in Medicine: Theory, Algorithms, and Applications*. Morgan Kaufmann Publishers Inc., 2007.

[19] N. C. Buchs *et al.*, "Augmented environments for the targeting of hepatic lesions during image-guided robotic liver surgery," *J Surg Res,* vol. 184, no. 2, pp. 825-831, 2013, doi: 10.1016/j.jss.2013.04.032.

[20] J. Ramalhinho *et al.*, "The value of Augmented Reality in surgery - A usability study on laparoscopic liver surgery," *Med Image Anal,* vol. 90, p. 102943, 2023, doi: 10.1016/j.media.2023.102943.

[21] F. Volonte, F. Pugin, P. Bucher, M. Sugimoto, O. Ratib, and P. Morel, "Augmented reality and image overlay navigation with OsiriX in laparoscopic and robotic surgery: not only a matter of fashion," *J Hepatobiliary Pancreat Sci,* vol. 18, no. 4, pp. 506-509, 2011, doi: 10.1007/s00534-011-0385-6.

[22] M. Sugimoto *et al.*, "Image overlay navigation by markerless surface registration in gastrointestinal, hepatobiliary and pancreatic surgery," *J Hepatobiliary Pancreat Sci,* vol. 17, no. 5, pp. 629-636, 2010, doi: 10.1007/s00534-009-0199-y.

[23] M. Feuerstein, T. Mussack, S. M. Heining, and N. Navab, "Intraoperative laparoscope augmentation for port placement and resection planning in minimally invasive liver resection," *IEEE Trans Med Imaging,* vol. 27, no. 3, pp. 355-369, 2008, doi: 10.1109/tmi.2007.907327.

[24] J. Hallet *et al.*, "Trans-thoracic minimally invasive liver resection guided by augmented reality," *J Am Coll Surg,* vol. 220, no. 5, pp. e55-60, 2015, doi: 10.1016/j.jamcollsurg.2014.12.053.

[25] P. Pessaux, M. Diana, L. Soler, T. Piardi, D. Mutter, and J. Marescaux, "Towards cybernetic surgery: robotic and augmented reality-assisted liver segmentectomy," *Langenbecks Arch Surg,* vol. 400, no. 3, pp. 381-385, 2015, doi: 10.1007/s00423-014-1256-9.

[26] M. Riechmann, L. A. Kahrs, C. Ulmer, J. Raczkowsky, W. Lamade, and H. Wörn, "Visualisierungskonzept für die projektorbasierte Erweiterte Realität in der Leberchirurgie," 2006.

[27] K. A. Gavaghan, M. Peterhans, T. Oliveira-Santos, and S. Weber, "A portable image overlay projection device for computer-aided open liver surgery," *IEEE Trans Biomed Eng,* vol. 58, no. 6, pp. 1855-1864, 2011, doi: 10.1109/tbme.2011.2126572.

[28] J. Dai, W. Qi, Z. Qiu, and C. Li, "The application and prospection of augmented reality in hepato-pancreato-biliary surgery," *Biosci. trends,* vol. 17, no. 3, pp. 193-202, 2023, doi: 10.5582/bst.2023.01086.

[29] T. Okamoto *et al.*, "Utility of augmented reality system in hepatobiliary surgery," *J Hepatobiliary Pancreat Sci,* vol. 20, no. 2, pp. 249-253, 2013, doi: 10.1007/s00534-012-0504-z.

[30] S.-g. Park, "Augmented and Mixed Reality Optical See-Through Combiners Based on Plastic Optics," *Information Display,* vol. 37, 2021, doi: 10.1002/msid.1226

[31] E. R. Zorzal *et al.*, "Laparoscopy with augmented reality adaptations," (in eng), *J Biomed Inform,* vol. 107, p. 103463, Jul 2020, doi: 10.1016/j.jbi.2020.103463.

[32] Y. Saito *et al.*, "Intraoperative 3D Hologram Support With Mixed Reality Techniques in Liver Surgery," *Ann Surg,* vol. 271, no. 1, pp. e4-e7, 2020, doi: 10.1097/sla.0000000000003552.

[33] J. Yasuda *et al.*, "Novel navigation system by augmented reality technology using a tablet PC for hepatobiliary and pancreatic surgery," *Int J Med Robot,* vol. 14, no. 5, p. e1921, 2018, doi: 10.1002/rcs.1921.

[34] W. Zhang *et al.*, "Augmented Reality Navigation for Stereoscopic Laparoscopic Anatomical Hepatectomy of Primary Liver Cancer: Preliminary Experience," *Front. oncol.*, vol. 11, p. 663236, 2021, doi: 10.3389/fonc.2021.663236.

[35] G. A. Prevost *et al.*, "Efficiency, Accuracy and Clinical Applicability of a New Image-Guided Surgery System in 3D Laparoscopic Liver Surgery," *J Gastrointest Surg*, vol. 24, no. 10, pp. 2251-2258, 2020, doi: 10.1007/s11605-019-04395-7.

[36] S. Thompson *et al.*, "In vivo estimation of target registration errors during augmented reality laparoscopic surgery," *Int. j. comput. assist. radiol. surg.*, vol. 13, no. 6, pp. 865-874, 2018, doi: 10.1007/s11548-018-1761-3.

[37] B. Le Roy, E. Ozgur, B. Koo, E. Buc, and A. Bartoli, "Augmented reality guidance in laparoscopic hepatectomy with deformable semi-automatic computed tomography alignment (with video)," *J Visc Surg*, vol. 156, no. 3, pp. 261-262, 2019, doi: 10.1016/j.jviscsurg.2019.01.009.

[38] M. Adballah *et al.*, "Augmented reality in laparoscopic liver resection evaluated on an ex-vivo animal model with pseudo-tumours," (in English), *Surg. Endosc.*, Article vol. 36, no. 1, pp. 833-843, Jan 2022, doi: 10.1007/s00464-021-08798-z.

[39] F. Giannone, E. Felli, Z. Cherkaoui, P. Mascagni, and P. Pessaux, "Augmented Reality and Image-Guided Robotic Liver Surgery," 2021, doi: 10.3390/cancers13246268.

[40] L. Soler, S. Nicolau, P. Pessaux, D. Mutter, and J. Marescaux, "Real-time 3D image reconstruction guidance in liver resection surgery," *Hepatobiliary surg. nutr.*, vol. 3, no. 2, pp. 73-81, 2014, doi: 10.3978/j.issn.2304-3881.2014.02.03.

[41] E. Ozgur, B. Koo, B. Le Roy, E. Buc, and A. Bartoli, "Preoperative liver registration for augmented monocular laparoscopy using backward-forward biomechanical simulation," *Int. j. comput. assist. radiol. surg.*, vol. 13, no. 10, pp. 1629-1640, 2018, doi: 10.1007/s11548-018-1842-3.

[42] L. W. Lau, X. Y. Liu, W. Plishker, K. Sharma, R. Shekhar, and T. D. Kane, "Laparoscopic Liver Resection with Augmented Reality: A Preclinical Experience," (in English), *J. Laparoendosc. Adv. Surg. Tech.*, Article vol. 29, no. 1, pp. 88-93, Jan 2019, doi: 10.1089/lap.2018.0183.

[43] L. T. De Paolis and V. De Luca, "Augmented visualization with depth perception cues to improve the surgeon's performance in minimally invasive surgery," (in eng), *Med Biol Eng Comput*, vol. 57, no. 5, pp. 995-1013, May 2019, doi: 10.1007/s11517-018-1929-6.

[44] C. Hansen, J. Wieferich, F. Ritter, C. Rieder, and H. O. Peitgen, "Illustrative visualization of 3D planning models for augmented reality in liver surgery," *Int. j. comput. assist. radiol. surg.*, vol. 5, no. 2, pp. 133-141, 2010, doi: 10.1007/s11548-009-0365-3.

[45] N. Haouchine *et al.*, "Impact of Soft Tissue Heterogeneity on Augmented Reality for Liver Surgery," *IEEE trans. vis. comput. graph.*, vol. 21, no. 5, pp. 584-597, 2015, doi: 10.1109/tvcg.2014.2377772.

[46] C. Schneider, M. Allam, D. Stoyanov, D. J. Hawkes, K. Gurusamy, and B. R. Davidson, "Performance of image guided navigation in laparoscopic liver surgery – A systematic review," (in English), *Surg Oncol*, Review vol. 38, 2021, doi: 10.1016/j.suronc.2021.101637.

[47] B. Acidi, M. Ghallab, S. Cotin, E. Vibert, and N. Golse, "Augmented reality in liver surgery," *J Visc Surg*, vol. 160, no. 2, pp. 118-126, 2023, doi: 10.1016/j.jviscsurg.2023.01.008.

[48] F. Giannone, E. Felli, Z. Cherkaoui, P. Mascagni, and P. Pessaux, "Augmented Reality and Image-Guided Robotic Liver Surgery," (in eng), *Cancers (Basel)*, vol. 13, no. 24, Dec 14 2021, doi: 10.3390/cancers13246268.

[49] D. Katic *et al.*, "Context-aware Augmented Reality in laparoscopic surgery," *Comput Med Imaging Graph*, vol. 37, no. 2, pp. 174-182, 2013, doi: 10.1016/j.compmedimag.2013.03.003.

[50] M. C. F. Macedo and A. L. Apolinário, "Occlusion Handling in Augmented Reality: Past, Present and Future," *Ieee Transactions on Visualization and Computer Graphics*, vol. 29, no. 2, pp. 1590-1609, 2023, doi: 10.1109/TVCG.2021.3117866.

[51] J. N. Smit *et al.*, "Ultrasound-based navigation for open liver surgery using active liver tracking," (in eng), *Int J Comput Assist Radiol Surg*, vol. 17, no. 10, pp. 1765-1773, Oct 2022, doi: 10.1007/s11548-022-02659-3.

[52] C. Schneider *et al.*, "Comparison of manual and semi-automatic registration in augmented reality image-guided liver surgery: a clinical feasibility study," *Surg Endosc*, vol. 34, no. 10, pp. 4702-4711, 2020, doi: 10.1007/s00464-020-07807-x.

[53] S. E. M. Herrera, A. C. Malti, O. Morel, and A. Bartoli, "Shape-from-Polarization in laparoscopy," *2013 IEEE 10th International Symposium on Biomedical Imaging*, pp. 1412-1415, 2013.

[54] B. Shi, J. Yang, J. Chen, R. Zhang, and R. Chen, "Recent Progress in Shape from Polarization," pp. 177-203, 2020 2020, doi: 10.1007/978-3-030-51866-0_6.

[55] J. Penne *et al.*, "Time-of-Flight 3-D Endoscopy," vol. 12, pp. 467-74, 2009, doi: 10.1007/978-3-642-04268-3_58.

[56] Y. Wang, J. I. Laughner, I. R. Efimov, and S. Zhang, "3D absolute shape measurement of live rabbit hearts with a superfast two-frequency phase-shifting technique," *Optics express*, vol. 21, no. 5, pp. 5822-5832, 2013, doi: 10.1364/OE.21.005822.

[57] P. Z. A. Protopsaltis *et al.*, "MAGES 4.0: Accelerating the world's transition to VR training and democratizing the authoring of the medical metaverse," (in eng), *IEEE Comput Graph Appl*, vol. Pp, Feb 6 2023, doi: 10.1109/mcg.2023.3242686.

[58] "Cojoc-Wisernig E,"Marine Visualization System: An Augmented Reality Approach," Master's Thesis, Computer Science, University of Bucharest, [Online]. Available: http://hdl.handle.net/1828/12060," p. 186, Aug. 28, 2020.

[59] F. Laera, V. M. Manghisi, A. Evangelista, A. E. Uva, M. M. Foglia, and M. Fiorentino, "Evaluating an augmented reality interface for sailing navigation: a comparative study with a immersive virtual reality simulator," *Virtual Reality*, vol. 27, no. 2, pp. 929-940, 2023/06/01 2023, doi: 10.1007/s10055-022-00706-7.

[60] J. Fischer, D. Bartz, and W. Straßer, "Intuitive and lightweight user interaction for medical augmented reality," *Proc. of Vision, Modeling, and Visualization*, 01/01 2005.

[61] A. Kolagunda *et al.*, "A Mixed Reality Guidance System for Robot Assisted Laparoscopic Radical Prostatectomy: First International Workshop, OR 2.0 2018, 5th International Workshop, CARE 2018, 7th International Workshop, CLIP 2018, Third International Workshop, ISIC 2018, Held in Conjunction with MICCAI 2018, Granada, Spain, September 16 and 20, 2018, Proceedings," pp. 164-174, 2018, doi: 10.1007/978-3-030-01201-4_18.

[62] J. Fischer, D. Bartz, and W. Straßer, "Occlusion handling for medical augmented reality using a volumetric phantom model," pp. 174-177, 2004, doi: 10.1145/1077534.1077570.

[63] P. Mascagni *et al.*, "Computer vision in surgery: from potential to clinical value," (in eng), *NPJ Digit Med*, vol. 5, no. 1, p. 163, Oct 28 2022, doi: 10.1038/s41746-022-00707-5.

[64] L. Barba-Guaman, J. E. Naranjo, and A. Ortiz, "Object detection in rural roads using Tensorflow API," in *2020 International Conference of Digital Transformation and Innovation Technology (Incodtrin)*, 28-30 Oct. 2020 2020, pp. 84-88, doi: 10.1109/Incodtrin51881.2020.00028.

[65] J. Watson *et al.*, "Virtual Occlusions Through Implicit Depth," pp. 9053-9064, 2023, doi: 10.1109/CVPR52729.2023.00874.

[66] A. Holynski and J. Kopf, "Fast depth densification for occlusion-aware augmented reality," *ACM Trans. Graph.*, vol. 37, no. 6, p. Article 194, 2018, doi: 10.1145/3272127.3275083.

[67] R. Du *et al.*, "DepthLab: Real-time 3D Interaction with Depth Maps for Mobile Augmented Reality," pp. 829-843, 2020, doi: 10.1145/3379337.3415881.

[68] D. Kalkofen, E. Mendez, and D. Schmalstieg, "Interactive Focus and Context Visualization for Augmented Reality," in *2007 6th IEEE and ACM International Symposium on Mixed and Augmented Reality*, 13-16 Nov. 2007 2007, pp. 191-201, doi: 10.1109/ISMAR.2007.4538846.

[69] R. Bane and T. Hollerer, "Interactive Tools for Virtual X-Ray Vision in Mobile Augmented Reality," pp. 231–239, 2004, doi: 10.1109/ismar.2004.36.

[70] C. Sandor *et al.*, "Egocentric Space-Distorting Visualizations for Rapid Environment Exploration in Mobile Mixed Reality," pp. 47-50, 2010, doi: 10.1109/VR.2010.5444815.

[71] C. Bichlmeier, F. Wimmer, S. M. Heining, and N. Navab, "Contextual Anatomic Mimesis Hybrid In-Situ Visualization Method for Improving Multi-Sensory Depth Perception in Medical Augmented Reality," *2007 6th IEEE and ACM International Symposium on Mixed and Augmented Reality,* pp. 129-138, 2007, doi: 10.1109/ISMAR.2007.4538837.

[72] R. Khoshabeh, J. Juang, M. Talamini, and T. Nguyen, "Multiview Glasses-Free 3-D Laparoscopy," *IEEE transactions on bio-medical engineering,* vol. 59, pp. 2859-65, 08/07 2012, doi: 10.1109/TBME.2012.2212192.

[73] A. L. D. Santos, D. Lemos, J. E. F. Lindoso, and V. Teichrieb, "Real Time Ray Tracing for Augmented Reality," in *2012 14th Symposium on Virtual and Augmented Reality*, 28-31 May 2012 2012, pp. 131-140, doi: 10.1109/SVR.2012.8.

[74] R. Weitzman, A. Mizrahi, R. Perlman, E. Haviv, O. Pyshchenko, and T. Stephenson, "Real Time Ray Tracing in AR," p. Article 27, 2023, doi: 10.1145/3587421.3595455.

[75] C. Bichlmeier, S. M. Heining, M. Feuerstein, and N. Navab, "The virtual mirror: a new interaction paradigm for augmented reality environments," (in eng), *IEEE Trans Med Imaging,* vol. 28, no. 9, pp. 1498-510, Sep 2009, doi: 10.1109/tmi.2009.2018622.

[76] J. A. Jones, J. E. Zwaan, G. Singh, E. Kolstad, and S. R. Ellis, "The Effects of Virtual Reality, Augmented Reality, and Motion Parallax on Egocentric Depth Perception," pp. 9-14, 2008, doi: 10.1145/1394281.1394283.

[77] S. Zollmann, D. Kalkofen, E. Mendez, and G. Reitmayr, "Image-based ghostings for single layer occlusions in augmented reality," in *2010 IEEE International Symposium on Mixed and Augmented Reality*, 13-16 Oct. 2010 2010, pp. 19-26, doi: 10.1109/ISMAR.2010.5643546.

APPENDIX B: QUALITATIVE SURVEY

B.1 Survey Phase 1

Onderzoek naar de gebruikerservaring van Augmented Reality visualisaties tijdens het gebruik van navigatietechnologie tijdens een operatie

2024

No.	**Visualisatie voorbeeld 1**
AR1	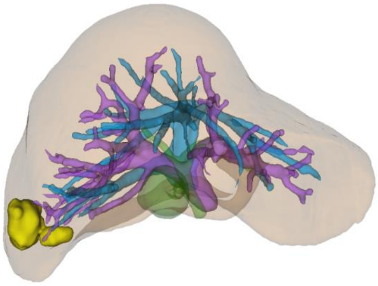

		Sterk mee oneens				Sterk mee eens
1	**Ik vond de AR visualisatie makkelijk te interpreteren zonder uitgebreide uitleg**	☐	☐	☐	☐	☐
		1	2	3	4	5
2	**Ik vond de AR ervaring goed**	☐	☐	☐	☐	☐
		1	2	3	4	5
3	**Ik vond de AR-visualisatie effectief (aanvullend) in het:**					
	- *Bepalen waar de leverstructuren en tumor zich bevinden;*	☐	☐	☐	☐	☐
		1	2	3	4	5
	- *Bepalen van de tumormarges om tumor weefsel zo nauwkeurig mogelijk te verwijderen;*	☐	☐	☐	☐	☐
		1	2	3	4	5
	- *Bepalen van het resectieplan om zo veel mogelijk gezond weefsel te besparen;*	☐	☐	☐	☐	☐
		1	2	3	4	5
4	**Ik vond dat de AR-visualisatie een duidelijke diepte perceptie weergaf**	☐	☐	☐	☐	☐
	Dit betekent dat de AR-visualisatie: - *Duidelijk de volgorde van structuren dichtbij of veraf weergaf (denk aan virtuele modellen, de lever en instrumenten);* - *Met gebruik van schaduwen, semi-transparantie en andere diepte visualisaties perceptie van diepte creëerde;*	1	2	3	4	5
5	**Ik vond dat de AR-visualisatie de juiste balans gaf tussen te veel en te weinig gegevens**	☐	☐	☐	☐	☐
	Dit betekent dat de AR overzichtelijk geprojecteerd was op het laparoscopische beeld zonder de chirurg te veel af te leiden.	1	2	3	4	5

6. Mocht u eventuele extra opmerkingen of suggesties hebben over de AR-visualisatie zelf of het proces eromheen, kunt u deze hieronder beschrijven.

………

………

B.2 Survey Phase 2

Ingevuld door (naam arts): ______________________________ Datum: ___-___- 2024

Klasse 1 - Anatomische 3D modellen

1a. Kruis de Augmented Reality visualisatie(s) aan waarvan u denkt dat u het in de toekomst het liefst zou gebruiken tijdens lever chirurgie (Meerdere antwoorden mogelijk):

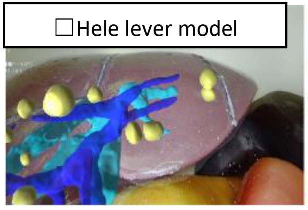
☐Hele lever model

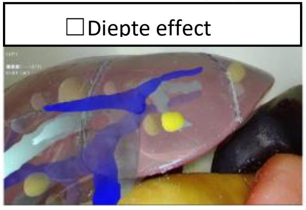
☐Diepte effect


☐Doel vaten en tumor

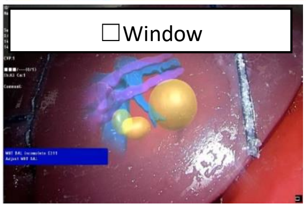
☐Window


☐Gaten in het lever oppervlakte bij doel laesie

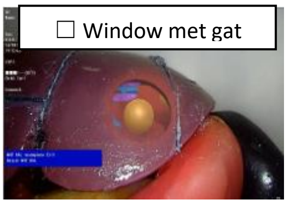
☐ Window met gat

1b. Voor welke applicatie(s) zou u deze aangekruiste visualisatie(s) gebruiken? (Meerdere antwoorden mogelijk)
☐ (Wig/ segment/ hemi) resectie ☐ Ablatie

1c. Welke lever structuren zou u belangrijk vinden om met AR weer te geven op het laparoscopische beeld? Geef een score van 1 (niet belangrijk) tot 3 (heel belangrijk) per anatomische structuur:
Lever oppervlak: ___a. hepatica: ___ v. hepatica: ___ v. porta: ___ galblaas: ___ galwegen: ___ tumor(en): ___

1d. Zou u het fijn vinden om aanvullend ook het resectieplan te visualiseren? ☐Ja/☐ Nee, Score (1-3): ___

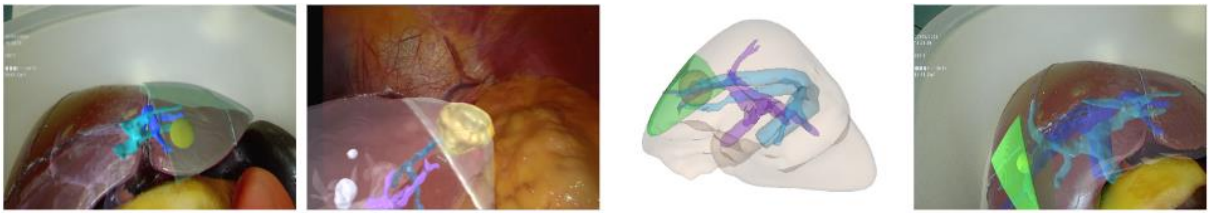

Klasse 2 - Instrument interactie

2a. Virtueel resectieplan: Met deze tool kunt u door met de chirurgische "pointer" over het lever oppervlak te bewegen een virtueel resectieplan tekenen. Zou u de volgende tool gebruiken tijdens lever resecties? ☐Ja/☐ Nee

2b. Real time echo beeld in laparoscopische beeld: Zou u de volgende visualisatie gebruiken tijdens lever chirurgie?
☐Ja/☐ Nee. Indien ja, kruis aan welke visualisatie(s) u zou gebruiken:


☐Alleen echo

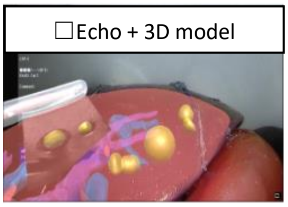
☐Echo + 3D model


☐Echo in de hoek

Thesis Maaike Pruijt, Chirurgische oncologie NKI-AvL, "Evaluating surgeon experience to improve Augmented Reality in liver surgery"

2c. Voor welke applicatie(s) zou u deze aangekruiste echo visualisatie(s) gebruiken? (Meerdere antwoorden mogelijk)
☐ (Wig/ segment/ hemi) resectie ☐ Ablatie

Klasse 3 – Virtual Reality

3a. Virtueel zijaanzicht lever: Diepteperceptie is een probleem bij AR-visualisatie. In het linker voorbeeldplaatje hieronder lijkt het alsof de tumor wordt aanraakt, maar in werkelijkheid (zie zij-aanzicht) ben je verder van de tumor verwijderd. Het schakelen naar een virtueel zijaanzicht van de lever zou extra informatie kunnen geven over de diepte.

Zou u de volgende visualisatie gebruiken tijdens lever chirurgie? ☐Ja/☐ Nee. Indien ja, ☐ Met of ☐ zonder afstand (in mm) informatie in de hoek?

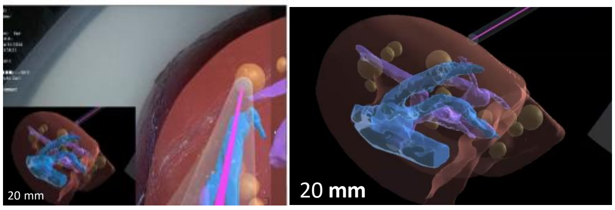

3b. Voor welke applicatie(s) zou u de visualisatie gebruiken? (Meerdere antwoorden mogelijk)
☐ (Wig/ segment/ hemi) resectie ☐ Ablatie

3c. Target view: Een dergelijke visualisatie toont door middel van een bullseye de afstand tussen de tumor (geel) en het uiteinde van de "pointer". De bullseye kleurt groen wanneer de afstand minder dan 5 mm is. In het centrum van de tumor bevindt zich een rood bolletje, zodat je de pointer nauwkeurig kunt centreren en richten.

Zou u de volgende visualisatie tool gebruiken tijdens open/laparoscopische ablaties? ☐Ja/☐ Nee

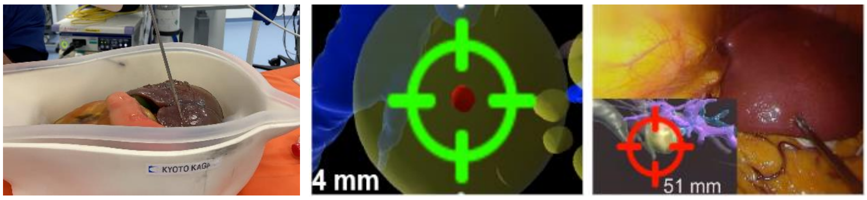

4. Open opmerkingen/aanvullingen/ aanbevelingen/ tips:

____

____

____

____

____

____

Appendix C: Unity 3D C# scripts

C.1 Depth shader

```
Shader "Custom/Final_transparency_depth_shader"
{
    Properties
    {
        _Color ("Main Color", Color) = (1, 1, 1, 1)
        _Transparency ("Transparency", Range(0, 1)) = 1.0 // added for transparency
        _Exponent ("Transparency Exponent", Range(1, 10)) = 2.0 // Exponent for transparency calculation
    }
    SubShader
    {
        Tags { "Queue" = "Transparent" }
        Blend SrcAlpha OneMinusSrcAlpha // added for transparency, alpha blending
        ZWrite On // added for transparency, right depth perception
        Pass
        {
            CGPROGRAM
            #pragma vertex vert
            #pragma fragment frag
            #include "UnityCG.cginc" // Include Unity's general shader functions and macros

            // Define input values vertex shader function
            struct appdata_t
            {
                float4 vertex : POSITION;
                float4 texcoord : TEXCOORD0;
            };

            struct v2f
            {
                float4 pos : POSITION;
                float4 screenPos : TEXCOORD0;
            };

            sampler2D _CameraDepthTexture;
            float _Transparency; // added for transparency
            float _Exponent; // Exponent for transparency calculation
            float4 _Color;

            // Vertex-shader function
            v2f vert (appdata_t v)
            {
                v2f o;
                // Transform vertex position from object space to clip space
                o.pos = UnityObjectToClipPos(v.vertex);
                // Calculate screen position for the current vertex
                o.screenPos = ComputeScreenPos(o.pos);
                return o;
            }

            // Fragment-shader function
            fixed4 frag (v2f i) : SV_Target
            {
                // Calculate the projected screen coordinates
                UNITY_PROJ_COORD(i.screenPos);
                // Read the depth value of the depth texture at the screen position
                float textureDepth = tex2Dproj(_CameraDepthTexture, UNITY_PROJ_COORD(i.screenPos)).r;
                // Calculate the current pixel depth from the screen position
                float currentPixelDepth = (i.screenPos.z / i.screenPos.w);
                // Calculate the difference in depth between the texture and the current pixel
                float depthDelta = abs(textureDepth - currentPixelDepth);

                // Apply exponent to depthDelta to control transparency range
                float transparency = pow(depthDelta, _Exponent);
                depthDelta = 1.0 - depthDelta;

                // Interpolate the color based on the depth delta (inverted)
                float3 finalColor = lerp(_Color.rgb, float3(0, 0, 0), depthDelta);

                // Apply overall transparency and return the final color
                return float4(finalColor, _Color.a * _Transparency * transparency);
            }
            ENDCG
        }
    }
    FallBack "Diffuse"}
```

C.2 Virtual painter to draw resection plan

```
using UnityEditor;
using UnityEngine;

public class Resectionplan_generator : MonoBehaviour
{
    private LineRenderer lineRenderer;
    public bool draw = false; // This variable is used to control the “draw” Button.When set to true, the line can be drawn
    [HideInInspector] public bool removeDrawing = false; // This variable is used to control the “remove drawing” button. When set to true, the line
will be completely removed.

    void Start()
    // Default settings Line
    {
        lineRenderer = GetComponent<LineRenderer>();
        // Start position of the line on the same position of the pointer. Start drawing without line.
        lineRenderer.positionCount = 0;
        // Width line
        lineRenderer.startWidth = 5f;
        lineRenderer.endWidth = 5f;
        // Tiled texture mode
                    lineRenderer.textureMode = LineTextureMode.Tile;
    }
    void Update()
    {
        if (draw && !removeDrawing)
        // if draw is true and removeDrawing is false, call the DrawLineToPoint() method to draw the line based on the object's current position
        {
            DrawLineToPoint(transform.position);
        }
        else if (removeDrawing)
        // If removeDrawing is true (button), call the RemoveDrawing() method to reset the drawing
        {
            RemoveDrawing();
        }
    }

    void DrawLineToPoint(Vector3 point)
    {
    // This method calculates a new position for the line based on the current position of the pointer. End position line = Position object + poisition
in the forward direction of the object
        Vector3 tipPosition = transform.position + transform.forward;
        lineRenderer.positionCount++;
        // New position is added to the LineRenderer
        lineRenderer.SetPosition(lineRenderer.positionCount - 1, tipPosition);
    }

    // This method removes the drawing by resetting the position count of the LineRenderer
    void RemoveDrawing()
    {
        lineRenderer.positionCount = 0;
    }
}
// This method generates a button to remove the drawing
[CustomEditor(typeof(Resectionplan_generator))]
public class UserInterface : Editor
{
    public override void OnInspectorGUI()
    {
        DrawDefaultInspector();
        Resectionplan_generator generator = (Resectionplan_generator)target;
        // Add a button to reset drawing
        if (GUILayout.Button("Reset drawing"))
        {
            generator.removeDrawing = true;
            generator.draw = false;
        }

        // If drawing is enabled again, reset removeDrawing to false
        if (generator.draw)
        {
            generator.removeDrawing = false;
        }

    }
}
```

C.3 Target view

```
using System;
using UnityEngine;


public class DistanceMeasure : MonoBehaviour
{
    //public TextMesh Text;
    [SerializeField] private TextMesh Distance_display;
    [SerializeField] private GameObject Target;
    [SerializeField] private LineRenderer Line;

    public float hitdistance = 8000.0f;

    private Camera camera_object;


    void Start()
    {
        // Automate camera setup
        SetupCamera();
        // Automate Target image setup
        SetupTargetImage();
        // Automate Canvas setup including distance text
        SetupCanvas();
    }

    void FixedUpdate()
    {
        RaycastHit hit;

        if (Physics.Raycast(transform.position, -transform.forward, out hit, hitdistance))
        {

            if (hit.collider.name == "Lesions_Model")
            {
                Line.enabled = true;
                Line.SetPosition(0, transform.position);
                Line.SetPosition(1, hit.point);
                // Add distance in display 2
                Distance_display.text =  Math.Round(hit.distance, 1) + " mm";
                Distance_display.color = Color.white;
                // Call method to update target image color based on the target- to pointer distance
                SetTargetColor(hit.distance);
                return;
            }
        }
        //Line.enabled = true;
        Distance_display.text = " ";
    }

    void SetupCamera()
    // Method to automatically add a camera to pointer object (incl. automated settings)
    {
        GameObject cameraObject = new GameObject("Camera_object");
        camera_object = cameraObject.AddComponent<Camera>();
        // Set the parent of the camera to be the current object's transform
        cameraObject.transform.position = transform.position;
        cameraObject.transform.parent = transform;
        // Rotate the camera 180 degrees around its vertical axis to make it look outward
        camera_object.transform.Rotate(0f, 180f, 0f);
        // Set the camera background to a solid black color
        camera_object.backgroundColor = Color.black;
        camera_object.clearFlags = CameraClearFlags.SolidColor;
        // Perspective camera view, depth of 16 mm, and FOV of 60 mm
        camera_object.orthographic = false;
        camera_object.depth = 16;
        camera_object.fieldOfView = 60f;
        // Set the camera display to display 2 and show view in the right corner of the screen
        camera_object.targetDisplay = 1;
        camera_object.rect = new Rect(0.08f, 0.66f, 0.3f, 0.3f);
        // Show the lesions, target image and distance text in the camera view
        camera_object.cullingMask = LayerMask.GetMask("Lesion", "Target Image", "Distance text", "Liver", "3D Model");
    }
```

```
    void SetupTargetImage()
    // Method to automatically add an image in FOV pointer object (incl. automated settings)
    {
        // Create new GameObject
        GameObject targetImage = new GameObject("Target Image");
        // Set the parent of the target image to be the current object's transform
        targetImage.transform.parent = transform;
        // Add Target image layer to the image
        targetImage.layer = LayerMask.NameToLayer("Target Image");
        // Adjust the position of the image in the z-direction by -0.6 units to ensure the image appears correctly within the FOV of the camera.
        targetImage.transform.localPosition = new Vector3(0f, 0f, -0.6f);
        // This quaternion corresponds to "no rotation"
        targetImage.transform.rotation = Quaternion.identity;
        // Automatically assign target image in code component of the Unity inspector
        Target = targetImage;
        // Load a sprite named "UI Elements/Target" from the Resources folder and assign it to a new GameObject's SpriteRenderer component
        SpriteRenderer spriteRenderer = targetImage.AddComponent<SpriteRenderer>();
        Sprite targetSprite = Resources.Load<Sprite>("UI Elements/Target");
        if (targetSprite != null)
        {
            spriteRenderer.sprite = targetSprite;
        }
    }

    void SetupCanvas()
    // Method to automatically add a canvas showing the distance in FOV pointer object (incl. automated settings)
    {
        GameObject canvasObject = new GameObject("Distance_display");
        Canvas canvas = canvasObject.AddComponent<Canvas>();
        canvas.transform.position = transform.position;
        canvas.transform.parent = transform;
        canvasObject.layer = LayerMask.NameToLayer("Distance text");
        canvas.renderMode = RenderMode.WorldSpace;            //ScreenSpaceCamera;
        canvas.worldCamera = camera_object;
        // Add textmesh and automate fontsize, color and charactersize settings
        TextMesh textMesh = canvasObject.AddComponent<TextMesh>();
        textMesh.fontSize = 300;
        textMesh.text = "";
        textMesh.characterSize = 2;
        textMesh.color = Color.white;
        // Show text in left corner of the canvas
        RectTransform rectTransform = textMesh.GetComponent<RectTransform>();
        rectTransform.Rotate(new Vector3(0f, 180f, 0f));
        rectTransform.localPosition = new Vector3(425f, -160f, -420f);
        // Automatically assign distance display in code component of the Unity inspector
        Distance_display = textMesh;
    }

    void SetTargetColor(float distance)
    // Method to set the color of the target image based on distance
    {
        // In SpriteRenderer the color of the image is defined
        SpriteRenderer spriteRenderer = Target.GetComponent<SpriteRenderer>();
        if (spriteRenderer != null)
        {
            if (distance < 5f)
            {
                spriteRenderer.color = Color.green;
            }
            else
            {
                spriteRenderer.color = Color.red;
            }
        }
    }
}
```